INFORMATION TO USERS

This manuscript has been reproduced from the microfilm master. UMI films the text directly from the original or copy submitted. Thus, some thesis and dissertation copies are in typewriter face, while others may be from any type of computer printer.

The quality of this reproduction is dependent upon the quality of the copy submitted. Broken or indistinct print, colored or poor quality illustrations and photographs, print bleedthrough, substandard margins, and improper alignment can adversely affect reproduction.

In the unlikely event that the author did not send UMI a complete manuscript and there are missing pages, these will be noted. Also, if unauthorized copyright material had to be removed, a note will indicate the deletion.

Oversize materials (e.g., maps, drawings, charts) are reproduced by sectioning the original, beginning at the upper left-hand corner and continuing from left to right in equal sections with small overlaps.

Photographs included in the original manuscript have been reproduced xerographically in this copy. Higher quality 6" x 9" black and white photographic prints are available for any photographs or illustrations appearing in this copy for an additional charge. Contact UMI directly to order.

Bell & Howell Information and Learning
300 North Zeeb Road, Ann Arbor, MI 48106-1346 USA
800-521-0600

UMI®

Université d'Ottawa • University of Ottawa

Advanced Demodulation Techniques for Digital Audio Broadcast Signals over Fast Fading Channels

by Douglas Taylor

A thesis submitted to the
School of Graduate Studies and Research
in partial fulfillment of the requirements for the degree of

Master of Applied Science
in Electrical Engineering

Ottawa-Carleton Institute for Electrical and Computer Engineering
School of Information Technology and Engineering
Department of Electrical and Computer Engineering
Faculty of Engineering
University of Ottawa

July, 1999

Abstract

The Canadian digital audio broadcast (DAB) system uses a multicarrier modulation technique known as coded orthogonal frequency division multiplexing (COFDM). Several modes of operation are available. Mode IV, which has the longest symbol duration, allows transmitting antennas to be spaced more widely than other modes of operation providing a saving in broadcast infrastructure. However, the longer symbol duration also causes partial loss of coherence in subsequent symbol epochs that can cause a noticeable degradation in audio quality at velocities exceeding 92 km/hr in a typical urban propagation environment. This thesis identifies several advanced demodulation techniques that can be used in a receiver that will operate at higher vehicle velocities. One of these techniques, an iterative decision directed linear predictive receiver, has not been previously discussed in the literature. Simulation results indicate that the maximum vehicle velocity can be increased to 144 km/hr using this new receiver design.

Acknowledgements

I would like to express my thanks to my thesis supervisor Dr. Jean-Yves Chouinard, for his guidance and support during the course of this research. Louis Thibault and Minh Le of the Communications Research Center also made many contributions for which I am grateful. I am also thankful to these same individuals and the organizations they represent for providing me with the opportunity to learn a great deal over the past 12 months. A year ago I knew virtually nothing about mobile communications.

John Lodge and his group kindly provided a demonstration version of their codec software free of charge. I also want to thank Louis for lending me his computer.

Table of Contents

List of Figures

List of Tables

List of Acronyms

AWGN	Additive White Gaussian Noise
BER	Bit Error Rate
CD	Compact Disk
CDD	Conventional Differential Detector
COFDM	Coded Orthogonal Frequency Division Multiplexing
CPM	Continuous Phase Modulation
CRC	Cyclic Redundancy Code
DAB	Digital Audio Broadcast
DFT	Discrete Fourier Transform
DPSK	Differential Phase Shift Keying
DSP	Digital Signal Processing
ETSI	European Telecommunications Standards Institute
FCS	Frame Check Sequence
FIC	Fast Information Channel
FIR	Finite Impulse Response
FFT	Fast Fourier Transform
ICI	Intercarrier Interference
IDFT	Inverse Discrete Fourier Transform
IFFT	Inverse Fast Fourier Transform
ISI	Intersymbol Interference
LMS	Least Mean Squares
LP	Linear Predictive, Linear Prediction
MAP	Maximum A-posteriori Probability
MIPS	Mega-Instructions Per Second
ML	Maximum Likelihood
MLSD	Maximum Likelihood Sequence Detection
OFDM	Orthogonal Frequency Division Multiplexing
OQAM	Offset Quadrature Amplitude Modulation
PAM	Pulse Amplitude Modulation
PSD	Power Spectral Density

PSK	Phase Shift Keying
QPSK	Quaternary Phase Shift Keying
RCPC	Rate Compatible Punctured Convolutional
RLS	Recursive Least Squares
RMS	Root Mean Square
RF	Radio Frequency
SIHO	Soft-input Hard-output
SISO	Soft-input Soft-output
SNR	Signal to Noise Ratio
SOVA	Soft Output Viterbi Algorithm
WSSUS	Wide Sense Stationary Uncorrelated Scattering

List of Symbols

$\mathbf{a}$	Vector of linear predictor coefficients
$a_{n,k}$	Symbol transmitted in the n^{th} symbol interval and the k^{th} subcarrier prior to differential encoding
$c_{n,k}$	Symbol transmitted in the n^{th} symbol interval and the k^{th} subcarrier
Δf_c	Channel coherence bandwidth
Δt_c	Channel coherence time
E_U	Energy per symbol in the useful symbol interval
E_S	Energy per symbol
E_b/N_0	Signal to noise ratio. E_b is the energy per information bit over the entire useful symbol interval. N_0 is the PSD of the AWGN.
f_c	RF carrier frequency
f_d	Channel Doppler spread
$f_d T_S$	Normalized Doppler spread
f_S	The inverse of the symbol duration. This is the subcarrier spacing when no guard interval is used.
f_U	The inverse of the useful symbol duration. This is the subcarrier spacing when a guard interval is used.
Γ_n	Maximum likelihood metric for sequence of length n
$h(\tau, t)$	Input delay spread function
$H(f, t)$	Time variant transfer function
$H_{n,k}$	Gain for n^{th} symbol interval and k^{th} subchannel
$\tilde{H}_{n,k}$	Computed noisy channel gain for n^{th} symbol interval and k^{th} subchannel
$\hat{H}_{n,k}$	Linear prediction of channel gain for n^{th} symbol interval and k^{th} subchannel
L	Linear predictor order
M	Number of paths in channel model
N	Number of OFDM subcarriers, number of previous samples used for subchannel gain estimate
$\hat{N}$	Size of DFT used in modulation and demodulation.
$\mathbf{R}$	Correlation matrix
σ^2_{ICI}	Variance of interchannel interference component at DFT output

$s(t)$	Transmitted signal
σ_w^2	Variance of white noise component at DFT output
$r(t)$	Received signal
$R_H(\Delta t)$	Spaced-time correlation function
$R_h(\tau)$	Multipath intensity profile
$R_H(\Delta f)$	Spaced-frequency correlation function
$R_H(\Delta f, \Delta t)$	Spaced-frequency, spaced-time correlation function
$R_H(\Delta k, \Delta n)$	Correlation between discrete channel gain spaced by Δk subchannels and Δn symbol intervals
$S(\tau, \nu)$	Channel scattering function
T_G	The OFDM guard interval
τ_m	Channel delay spread
T_S	The OFDM symbol interval
T_U	The OFDM useful symbol interval
$U(\tau, \nu)$	Delay Doppler spread function
$y_{n,k}$	Demodulated value at DFT output corresponding to n^{th} symbol interval and k^{th} subcarrier

Notation

The superscripts H and T are used to represent matrix conjugate transpose and transpose respectively. The notation $\langle x(t) | y(t) \rangle$ means the inner product of the functions $x(t)$ and $y(t)$. Matrices are represented using upper case bold type: $\mathbf{R}$. $M\times 1$ matrices (column vectors) are represented by lower case bold type: $\mathbf{a}$. The function denoted with upper case $X(f)$ is the Fourier transform of $x(t)$. Similarly $X(k)$ is the discrete Fourier transform of $x(n)$. Random variables are denoted with upper case letters. Random processes are represented using the same notation as deterministic signals. The expectation operator on the random variable X is represented by $E\{X\}$.

1

Introduction

1.1 Advanced Demodulation Techniques for Digital Audio Broadcasting

1.1.1 COFDM and digital audio broadcasting

Digital audio broadcasting (DAB) services are intended to supplement and eventually replace existing amplitude and frequency modulated broadcast services. The chief advantage of the proposed digital technology is an improvement in sound quality to the level currently available on an audio compact disk (CD). In addition, there is the potential for transmission of data services along with the audio signal.

In Canada, the DAB service will conform to the European Telecommunication Standards Institute (ETSI) ETS 300 401 standard [8]. This standard is based on a modulation scheme termed Coded Orthogonal Frequency Division Multiplexing (COFDM). Not surprisingly, this refers to an Orthogonal Frequency Division Multiplexing (OFDM) scheme where the data are error protected by means of convolutional encoding prior to modulation. OFDM itself is a multicarrier modulation technique that uses a rectangular pulse shape. Multicarrier modulation is

a term that refers to a number of schemes where data are modulated onto many synchronized carriers closely spaced in frequency. These are usually referred to as subchannels or subcarriers.

An advantage of multicarrier modulation is that the many subcarriers allow transmission of high data rates using a relatively long symbol interval. This considerably simplifies the symbol synchronization and equalization problem in dispersive channels [3]. In fact, the DAB specification has been designed so that no channel equalization is normally required. For OFDM transmission over an ideal channel with no dispersion, the orthogonality of the adjacent subchannel is ensured when the subcarriers are spaced by the inverse of the symbol duration. In dispersive channels, the symbol interval is lengthened somewhat to provide a guard interval. As long as the guard interval is longer than the duration of the channel impulse response, the OFDM signal can be demodulated without any equalization and there will be no intersymbol interference. A crucial feature of OFDM with a guard interval is that it allows multiple transmitters to be interspersed throughout a broadcast region. The multiple signals arriving from these transmitters will appear to the receiver as a single signal transmitted over a channel with a long impulse response. For this reason, the DAB specification calls for a rather long guard interval.

Four transmission modes with different subcarrier spacing and symbol duration are defined by the DAB specification. These four modes are designed primarily for optimality at different radio frequency bands. Mode IV operation, the main focus of this thesis, uses symbol intervals of 0.623 ms and subcarrier spacing of 2 kHz.

1.1.2 COFDM over wireless mobile channels

Wireless channels are affected by multipath propagation caused by scattering of the RF signal from many objects [33], [45]. The signal reaches the receiver by many paths having different attenuation and phase shift. Furthermore, as the receiver moves, the number, length and attenuation of the scattering paths changes with time. The nature of these scattering interactions is usually so complex that the wireless channel cannot be characterized deterministically but must be treated as a random time varying system.

The superposition of the randomly changing multiple paths at the receiver causes the modulus and phase of the received signal to vary randomly. When the modulus of the signal is very low, a condition referred to as a fade, the channel background noise may be larger than the signal, resulting in bit errors. Also, if the phase of the received signal is changing rapidly enough that it is not relatively constant over many subsequent symbol intervals, a condition referred to as fast fading, coherent detection of the signal becomes difficult. To counteract this effect, the COFDM signal used in DAB is differentially encoded prior to transmission. However, a bit error rate (BER) floor is associated with differential demodulation of these signals in fast fading conditions. Rather than continuing to decrease as the signal to noise ratio increases, the BER asymptotically approaches an error rate floor. For example, a conventional differential detector (CDD) operating in a vehicle traveling at highway speeds in a typical urban environment would achieve a BER no lower than about 0.08 regardless of how high the signal to noise ratio.

Another effect of the mobile channel is to induce a Doppler frequency shift on the received signal. This shift will not be constant for all of the OFDM subcarriers and consequently may cause some of the energy from a given subcarrier to spill over into the adjacent subchannel resulting in interchannel interference.

The COFDM system is designed to compensate for these mobile channel effects. The convolutional encoding introduces redundancy in the transmitted signal. This redundancy is interleaved in time and frequency so that it is unlikely that all of the information about any single bit will be lost in a fade. This is a necessary condition for effective decoding using the Viterbi algorithm. To combat the BER floor encountered by the differential demodulation it is necessary to select an operating mode that has a symbol duration short enough so that the signal phase is relatively constant over subsequent symbol intervals. At the frequency designated for operation in Canada, mode II fulfills this requirement.

However, the DAB guard interval is specified to be one fifth of the symbol duration in all operating modes. Thus selecting a short symbol interval has the undesired effect of also reducing the duration of the guard interval mentioned in the previous section. This means that there must be more lower power transmitter antennas to cover a given area. For mode II, typical broadcast tower spacing is 10-12 km for urban areas and 20-25 km for rural areas. Mode IV has a symbol

interval (and consequently also a guard interval) that is twice that of mode II. Broadcast tower spacing can be twice the distance for mode II allowing a significant saving in infrastructure. Unfortunately, this long symbol duration increases the BER at high vehicle velocities so that in a typical urban propagation environment, differential detection based DAB receivers suffer degraded performance at highway velocities. This is clearly unsatisfactory and motivates the study of advanced demodulation techniques to combat this effect.

1.1.3 Advanced demodulation techniques for DAB

It has been demonstrated that CD quality sound can be achieved when the BER in the compressed audio signal is less than 10^{-4} [12]. The design criteria for a DAB receiver is to have a decoded BER less than this value for a signal to noise ratio E_b/N_0 in the range of 15 to 20 dB.

The BER floor that results from differential demodulation of signals transmitted over fast fading channels is a well-known phenomenon and several techniques to mitigate this effect have been studied. All of these techniques exploit known or estimated statistical properties of the channel to obtain a decision procedure that is superior to a CDD. Four possible techniques are analyzed in this thesis:

- a decision directed linear predictive demodulation technique. This technique feeds back L symbol decisions and uses these to form the minimum mean squared error prediction of the subchannel gain for the current symbol epoch. This estimate is then used to demodulate the current symbol.

- a maximum likelihood sequence detection (MLSD) technique. This technique is related to the linear predictive technique because an approximation allows the maximum likelihood metric to be updated recursively by the Euclidean distance between the actual received signal and the linear prediction of the received signal. This linear prediction is based on the previous L symbols. The receiver can then use per-survivor processing to search efficiently for the sequence that minimizes the accumulated Euclidean distance over all possible symbol sequences.

- a technique based on a series expansion of the random process describing the time varying channel and processing by a filter bank matched to each of the series terms

- a maximum a-posteriori probability technique that can be used in an iterative soft decision feedback manner similar to turbo decoding of serial concatenated codes

The second and fourth techniques are judged to be promising to make mode IV operation feasible. The third technique listed above is shown to be unsuitable for OFDM demodulation because it introduces an unacceptably high intercarrier interference (ICI) component.

The first technique on its own is not adequate to provide a sufficiently low BER for mode IV operation. This is a consequence of errors in the decisions that are fed back to form the linear prediction of the channel gain. If the error rate in these fed back decisions could be reduced by some means, the linear predictive (LP) detector would be adequate to meet the BER criteria. The convolutional encoding of the compressed audio program data provides such a means. The errors in the decisions can be corrected using Viterbi decoding, then the corrected sequence can be re-encoded and used in a second iteration of the LP detector. This process can be repeated any number of times and if the channel conditions are not too extreme it will converge at a BER close to what could be achieved with no errors in the fed back decisions.

This iterative scheme has not, to our knowledge, been previously applied to the problem of demodulating COFDM signals in fast fading conditions. A Matlab simulation was written to evaluate the performance of this receiver design. The simulation results indicate that this iterative decision feedback LP receiver can achieve the BER objective in the required range of E_b/N_0 at vehicle velocities up to 144 km/hr.

It is always of interest to evaluate the practicality of any new receiver design and the potential widespread application makes it even more so in this case. An estimation of the processing speed and memory (i.e. memory and computational complexities) required for the receiver indicates that implementation of the receiver algorithm on a DSP microcomputer would require execution at a speed around 1100 MIPS and about 5 Mbytes of memory.

1.2 Thesis Organization

Chapter 2 of this thesis is devoted to an in-depth discussion of the COFDM modulation technique and its application to digital audio broadcasting.

Chapter 3 of this thesis presents a detailed discussion of modeling and analysis techniques used for mobile wireless channels. These are then applied to a COFDM signal and the limitations of a CDD based receiver are demonstrated.

Chapter 4 an analysis of four advanced demodulation techniques that could potentially be applied to the COFDM signal used in DAB. This chapter also discusses how the decision directed linear predictive detector can be applied in an iterative manner to largely eliminate the performance deterioration resulting from incorrect decisions in the fed back symbol sequence.

Chapter 5 is entirely devoted to presenting the results of simulations on the iterative decision directed linear predictive receiver operating with the multiptath channel model developed in chapter 3.

Chapter 6 discusses practical issues related to implementation of the iterative decision directed linear predictive receiver. A discussion of receiver timing as it pertains to processing delay is followed by an estimate of the receiver memory and computational complexity.

The thesis concludes with chapter 7 providing a summary as well as a discussion of the research contributions and recommendations for further study.

2

Coded Orthogonal Frequency Division Multiplexing

When digital data must be transmitted at a high rate over a wideband channel, they can be interleaved over several symbol streams and each stream can be modulated onto a carrier at a different frequency. If the carriers are synchronized, they can be spaced closely together without any co-channel interference. This type of transmission scheme is referred to as multicarrier modulation [3]. A number of schemes for realizing this type of modulation have been developed [4], [30], [44]. The data transmission technique referred to as Orthogonal Frequency Division Multiplexing (OFDM) is a type of multicarrier modulation.

Coded Orthogonal Frequency Division Multiplexing (COFDM) [22], [36] is an OFDM multicarrier modulation technique that is suitable for use over mobile wireless channels. Prior to being modulated onto the multiple carriers, the data are encoded using some type of error correcting code and interleaved across time and frequency. COFDM has been proposed for use in digital television broadcast [7] and also cellular mobile telephony [29]. The digital audio broadcasting standard [8] currently in use in Europe and soon to be introduced in Canada is a COFDM based system.

2.1 ORTHOGONAL FREQUENCY DIVISION MULTIPLEXING

2.1.1 OFDM basics

A double sideband pulse amplitude modulated (PAM) signal modulated on to a sinusoidal carrier at frequency f_c is represented by

$$s(t) = \mathrm{Re}\left\{ s_l(t) e^{j2\pi f_c t} \right\} \tag{2.1}$$

where the signal $s_l(t)$ is the lowpass equivalent of the transmitted signal and is given by

$$s_l(t) = \sqrt{\frac{2E_S}{T_S}} \sum_n c_n p(t - nT_S) \tag{2.2}$$

The function $p(t)$ is a unit magnitude rectangular pulse that is zero outside the interval $[0,T_S]$ and T_S is the symbol duration. The variable c_n represents the complex valued symbol being transmitted in the n^{th} symbol interval and E_s is the energy per transmitted symbol. Two sequences of symbols $c_{n,0}$ and $c_{n,1}$ modulated onto two carriers offset by Δf can be represented by the following lowpass equivalents.

$$\begin{aligned} s_{l,0}(t) &= \sqrt{\frac{2E_S}{T_S}} \sum_n c_{n,0} p(t - nT_S) \\ s_{l,1}(t) &= \sqrt{\frac{2E_S}{T_S}} \sum_n c_{n,1} e^{j2\pi\Delta f (t - nT_S)} e^{j\theta_n} p(t - nT_S) \end{aligned} \tag{2.3}$$

where θ_n is an arbitrary phase shift. In the signal space representation, the inner product $\langle x(t) | y(t) \rangle$ can be defined as

$$\langle x(t) | y(t) \rangle = \int x(t) y^*(t) dt \tag{2.4}$$

and therefore

$$\begin{aligned} \langle s_{l,0}(t) | s_{l,1}(t) \rangle &= \frac{2E_s}{T_s} \sum_n c_{n,0} c_{n,1}^* e^{-j\theta_n} \int_{nT_s}^{(n+1)T_s} e^{-j2\pi\Delta f (t - nT_s)} dt \\ &= \frac{2E_s}{T_s} \sum_n c_{n,0} c_{n,1}^* e^{-j\theta_n} \frac{1 - e^{-j2\pi\Delta f T_s}}{j2\pi\Delta f} \end{aligned} \tag{2.5}$$

It can be seen that under the condition $\Delta f=k/T_S$, k being an integer, (2.4) evaluates to zero so the two signals are orthogonal. This suggests a multicarrier modulation scheme where N symbol sequences designated $\{c_{n,k}\}$, k=0, 1, 2, ..., N-1 are modulated onto N carriers separated by $\Delta f=1/T_S$. Equation (2.4) indicates that if the symbol intervals for each data stream are synchronized, the signals on each carrier will be orthogonal. This scheme for multicarrier modulation is referred to as OFDM. The signals on the individual OFDM carriers are orthogonal and can thus be separated by a correlation receiver. It is common to refer to the individual carriers as *subcarriers* or *subchannels*. The lowpass equivalent of an OFDM signal referenced to a carrier frequency f_c centered in the range of N subcarriers is

$$s_l(t)=\sqrt{\frac{2E_S}{T_S}}\sum_n \sum_{k=1-N/2}^{N/2} c_{n,k}e^{j2\pi k(t-nT_S)/T_S}\,p(t-nT_S), \qquad \text{for } N \text{ even} \tag{2.6}$$

where $c_{n,k}$ represents the symbol in the n^{th} symbol interval on the k^{th} subcarrier.

2.1.2 OFDM susceptibility to intersymbol and interchannel interference

One can interpret the OFDM signal as being an expansion over an orthonormal basis defined by

$$\begin{aligned} s(t) &= \sqrt{2E_S}\sum_{n,k} c_{n,k}x_{n,k}(t) \\ x_{n,k}(t) &= \frac{p(t-nT_S)}{\sqrt{T_S}}e^{j2\pi kf_S(t-nT_S)}, \quad f_ST_S=1 \end{aligned} \tag{2.7}$$

The subscript l which has been used to designate a lowpass equivalent signal is not used in (2.6). From this point forward, all signals are to be interpreted as lowpass equivalents unless otherwise indicated. The information symbols may be obtained from $s(t)$ by projecting on to this set of basis functions.

$$\hat{c}_{n,k}=\langle s(t)|x_{n,k}(t)\rangle=\left\langle \sum_{m,l} c_{m,l}x_{m,l}(t)\middle| x_{n,k}(t)\right\rangle=\sum_{m,l} c_{m,l}\langle x_{m,l}(t)|x_{n,k}(t)\rangle=c_{n,k} \tag{2.8}$$

This is what is commonly referred to as a correlation receiver because the inner product operation is essentially a correlation in the time domain. When the signal passes through a linear channel the received signal consists of a weighted sum of the channel responses to the individual basis functions. In general, these responses will be distorted in such a way as to loose their

orthogonality. Even with no such distortion, there can be a loss of orthogonality due to imperfect receiver synchronization in time and errors in the carrier frequency estimate. This loss of orthogonality causes intersymbol interference (ISI) and interchannel interference (ICI).

To alleviate this effect, OFDM signals are transmitted with a guard interval. The total duration of the OFDM symbol interval is made longer than the inverse of the frequency separation.

$$s(t) = \sqrt{\frac{2E_U}{T_U}} \sum_n \sum_{k=1-N/2}^{N/2} c_{n,k} e^{j2\pi k f_U (t-nT_S)} p_S(t-nT_S), \quad \text{where } f_U T_U = 1, N \text{ even} \tag{2.9}$$

The symbol interval T_S now consists of a guard interval T_G followed by a useful symbol interval T_U. E_U refers to the energy per symbol in the useful symbol interval. The function $p_S(t)$ is a unit pulse function that is zero outside the interval $[-T_G, T_U]$. One can analyze what happens when the transmit signal $s(t)$ is passed through a linear time invariant channel and then detected by correlating with the following set of orthonormal functions.

$$x_{n,k}(t) = \frac{p_U(t-nT_S+\delta)}{\sqrt{T_U}} e^{j2\pi k f_U (t-nT_S+\delta)}, \quad f_U T_U = 1 \tag{2.10}$$

where δ represents a timing error in the receiver and $p_U(t)$ is a unit pulse function that is zero outside the interval $[0, T_U]$. The duration of the impulse response plus the receiver error is assumed to be less than the guard interval. The received signal $r(t)$ is the convolution of the transmit signal with the channel impulse response.

$$r(t) = \int_{-\infty}^{\infty} h(\tau) s(t-\tau) d\tau \tag{2.11}$$

The functions in the above integrand are plotted in figure 2-1 for $t = nT_S$. From this, it is apparent that the above integral for $t \in [nT_S-\delta, nT_S+T_U]$ is equal to

$$r_n(t) = \sqrt{\frac{2E_U}{T_U}} \sum_{k=1-N/2}^{N/2} c_{n,k} \int_0^{T_G} h(\tau) e^{j2\pi k f_U [(t-\tau)-nT_S]} d\tau \tag{2.12}$$

which evaluates to

$$r_n(t) = \sqrt{\frac{2E_U}{T_U}} \sum_{k=1-N/2}^{N/2} H(kf_U) c_{n,k} e^{j2\pi k f_U (t-nT_S)} \tag{2.13}$$

where $H(f)$, the channel transfer function, is the Fourier transform of the channel impulse response. The receiver decision variables are retrieved by projecting the received signal on to the set of functions $\{x_{n,k}(t)\}$ from (2.10).

$$y_{n,k} = \left\langle r(t) \middle| x_{n,k}(t) \right\rangle \tag{2.14}$$

The interval where $x_{n,k}(t)$ is non-zero is contained completely within the interval where $r_n(t)$ is defined so one may write

$$y_{n,k} = \frac{\sqrt{2E_U}}{T_U} \int_{nT_S-\delta}^{nT_S-T_U-\delta} \sum_l H(lf_U) c_{n,l} e^{j2\pi l f_U (t-nT_S)} e^{-j2\pi k f_U (t-nT_S+\delta)} dt \tag{2.15}$$

which is equal to

$$y_{n,k} = \sqrt{2E_U} e^{-j2\pi k f_U \delta} H(kf_U) c_{n,k} \tag{2.16}$$

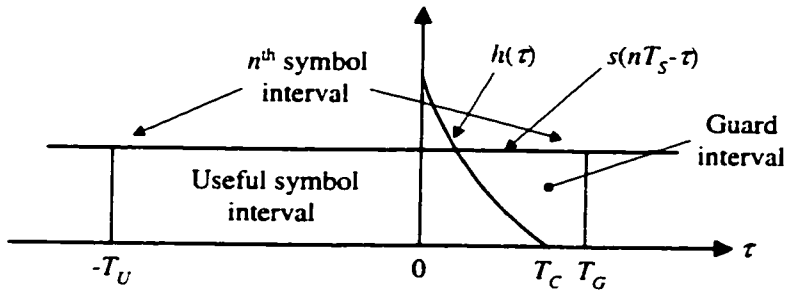

Figure 2-1 Graphical representation of integrand factors in the convolution of the channel impulse response with the OFDM signal.

The demodulated symbol is equal to the transmitted signal multiplied by a complex constant equal to the channel transfer function $H(f)$ evaluated at kf_U and phase shifted by a linear term which is proportional to the timing error δ. There is no contribution from the transmitted symbols in any other symbol interval or any other subcarrier. One can conclude that as long as the duration of the guard interval is greater than the duration of the channel impulse response plus the timing error, i.e.

$$T_C \leq T_G - \delta \tag{2.17}$$

there will be no ISI or ICI. The converse has not been demonstrated but it can be demonstrated that if condition (2.17) is not fulfilled, than there will be both ICI and ISI.

Expression (2.15) for the received signal reduces to (2.16) because the limits of integration are over an integer number of cycles of a complex exponential and thus are zero when $l \neq k$. This simple expression in the integrand of (2.15) occurs as a result of the signal transmitted in the guard interval, commonly referred to as a cyclic prefix. Without the cyclic prefix signal, the integral in (2.15) would not reduce to zero when $l \neq k$ and there would be ICI terms in the received variable $y_{n,k}$. The cyclic prefix causes the total energy transmitted per symbol to be larger than the energy in the useful symbol interval.

$$E_S = \frac{T_S}{T_U} E_U \tag{2.18}$$

The receiver however only uses the useful interval for detection. Therefore, in an additive noise channel, it will perform as if the energy per symbol was only E_U rather than E_S. This results in an effective loss of $10 \log_{10}(E_S/E_U)$ dB in SNR performance.

2.1.2 Use of DFT for modulation and demodulation

Let the OFDM signal (2.8) be sampled at $\hat{N}$ equally spaced instants over the n^{th} useful symbol interval where $\hat{N}$ is a power 2 of that is larger than N.

$$s\left(nT_S + \frac{mT_U}{\hat{N}}\right) \equiv s_n[m] = \sqrt{\frac{2E_U}{T_U}} \sum_{k=1-N/2}^{N/2} c_{n,k} e^{j2\pi \frac{km}{\hat{N}}}, \quad m = 0, 1, \cdots, \hat{N}-1 \tag{2.19}$$

Define a rearranged symbol sequence $\tilde{c}_{n,k}$ as:

$$\tilde{c}_{n,k} = \begin{cases} c_{n,k}, & 0 \le k \le N/2 \\ c_{n,k-\hat{N}}, & \hat{N} - N/2 + 1 \le k \le \hat{N} - 1 \\ 0, & \text{otherwise} \end{cases} \tag{2.20}$$

The negative indexed $c_{n,k}$ values, have been placed at the end of the rearranged sequence and zeros have been padded in between. Equation (2.19) becomes

$$s_n[m] = \sqrt{\frac{2E_U}{T_U}} \sum_{k=0}^{\hat{N}-1} \tilde{c}_{n,k} e^{j2\pi \frac{km}{\hat{N}}}, \quad m = 0, 1, \cdots, \hat{N}-1 \tag{2.21}$$

This is the expression for an $\hat{N}$-point inverse discrete Fourier transform (IDFT) except for a missing multiplicative factor of $1/\hat{N}$. One familiar with the periodic properties of the IDFT could obtain (2.21) from (2.19) by inspection. A sampled version of the OFDM signal in the n^{th} useful symbol interval can thus be obtained by passing the modified sequence $\tilde{c}_{n,k}$ through an IDFT. Since we have chosen $\hat{N}$ to be a power of 2, the inverse fast Fourier transform (IFFT) can be used to generate the sampled signal in a computationally efficient manner. The sampled version of the cyclic prefix signal for symbol interval n is simply generated by taking the last $\lfloor T_G \hat{N} / T_U \rfloor$ values of $s_n[m]$. The sampled signals can then be passed through a digital-to-analog converter to generate the transmitted OFDM signal.

At the receiver, the signal (2.13) can again be sampled at $\hat{N}$ equally spaced instants over the interval $[nT_S-\delta, nT_S+T_U-\delta]$ to obtain

$$r(nT_S + \frac{mT_U}{\hat{N}} - \delta) \equiv r_n[m] = \sqrt{\frac{2E_U}{T_U}} \sum_{k=1-N/2}^{N/2} H(kf_U) e^{-j2\pi k f_U \delta} c_{n,k} e^{j2\pi \frac{km}{\hat{N}}}, \quad m = 0, 1, \cdots, \hat{N}-1 \tag{2.22}$$

Once again define

$$\tilde{H}(kf_U) = \begin{cases} H(kf_U) e^{-j2\pi k f_U \delta} & 0 \le k \le N/2 \\ H((k-\hat{N})f_U) e^{-j2\pi(k-\hat{N})f_U \delta} & \hat{N} - N/2 + 1 \le k \le \hat{N} - 1 \\ 0 & \text{otherwise} \end{cases} \tag{2.23}$$

and rearrange the above terms to obtain

$$r_n[m] = \sqrt{\frac{2E_U}{T_U}} \sum_{k=0}^{\hat{N}-1} \tilde{H}(kf_U) \tilde{c}_{n,k} e^{j2\pi \frac{km}{\hat{N}}}, \quad m = 0, 1, \cdots, \hat{N}-1 \tag{2.24}$$

This is simply the IDFT of the modified sequence $\tilde{H}(kf_U)\tilde{c}_{n,k}$ so one can retrieve this sequence using the DFT:

$$\sqrt{\frac{2E_U}{T_U}}\tilde{H}(kf_U)\tilde{c}_{n,k} = \frac{1}{\hat{N}}\sum_{m=0}^{\hat{N}-1} r_n[m]e^{-j2\pi\frac{km}{\hat{N}}}, \quad k = 0,1,\cdots,\hat{N}-1 \tag{2.25}$$

Finally, the complex symbols are obtained after rearranging the sequence according to the inverse of (2.23):

$$y_{n,k} = \sqrt{\frac{2E_U}{T_U}}H(kf_U)e^{-j2\pi kf_U\delta}c_{n,k} \tag{2.26}$$

The detected symbols are equal to the transmitted symbols multiplied by a constant gain factor and a channel gain factor, and phase shifted by a linear term. This result is analogous to that obtained using the correlation detector in the previous section.

2.1.3 OFDM over an AWGN channel

The system block diagram shown in figure 2-2 depicts OFDM transmission over a linear, time invariant additive white Gaussian noise (AWGN) channel. Since the sampling and DFT are linear operations, one may calculate the DFT of the sampled noise process and add it to (2.24) to obtain the signal plus noise DFT output. The signal is sampled at a frequency $\hat{N}/T_U$ so it should be passed through an ideal anti-aliasing filter with bandwidth $\hat{N}/2T_U$ prior to sampling. Assume that $\hat{N}$ is large enough so that the information signal is not affected by the anti-aliasing filter. The complex low pass equivalent of a real noise process with power spectral density $N_0/2$ has a power spectral density of $2N_0$. After passing the signal through the filter and sampling one obtains discrete, zero mean, white, complex Gaussian random process n_m with variance $\sigma_n^2 = 2\hat{N}N_0/T_U$. If one takes $\hat{N}$ of these from the n^{th} symbol interval and passes them through a DFT one obtains (see appendix A) $\hat{N}$ independent zero mean complex Gaussian random variables $v_{n,k}$ with variance $\sigma_v^2 = 2N_0/T_U$. The combined signal at the DFT output is then

$$y'_{n,k} = \sqrt{\frac{2E_U}{T_U}}H(kf_U)e^{-j2\pi kf_U\delta}c_{n,k} + v_{n,k} \tag{2.27}$$

The system of figure 2-2 can thus be treated as consisting of N discrete AWGN channels with a sample frequency of $1/T_S$. To further simplify, the outputs can be normalized resulting in

$$y_{n,k} = H(kf_U)e^{-j2\pi kf_U\delta}c_{n,k} + w_{n,k} \tag{2.28}$$

and the variance the $w_{n,k}$ is $\sigma_w^2 = N_0 / E_U$.

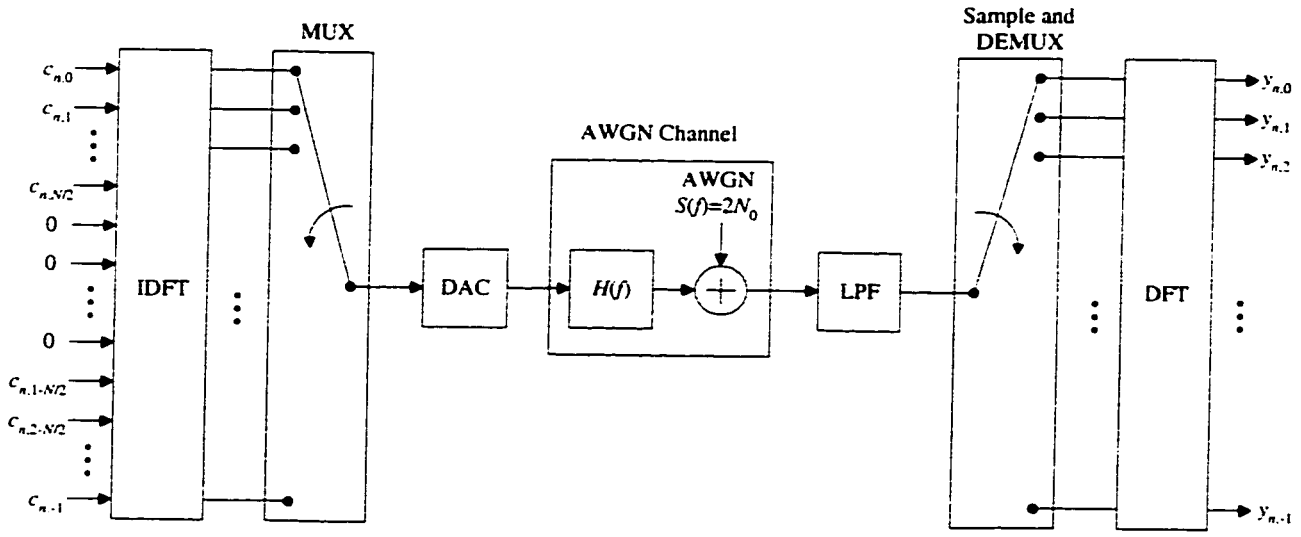

Figure 2-2 Block diagram depicting OFDM transmission over AWGN channel

2.1.4 Other multicarrier modulation techniques

As discussed briefly above, the OFDM signal with no guard interval can be considered as an expansion of the transmitted signal over an orthonormal basis as defined in (2.6). Each member of this basis consists of a rectangular pulse of duration T_S which is time and frequency shifted to obtain a basis that spans all of $L^2(R)$, the set of square integrable functions. Another basis which can be used for multicarrier modulation is obtained by using a sinc($f_S t$) shaped signaling pulse having a rectangular spectrum whose frequency shifted versions do not overlap at all. This can be considered as the dual of the OFDM system.

It is well known that abrupt cutoffs in either the time or frequency domain generally impose constraints on transmitter and receiver design that are difficult to meet. These constraints are mitigated somewhat by the use of a guard interval as discussed above, but this requires a waste of transmitted power and transmission capacity. It is therefore natural to look for an orthonormal basis whose members can be obtained as time and frequency shifted versions of a lowpass pulse having time and frequency domain characteristics that roll off gradually. In fact such bases do

exist [22] but they require that the symbol length be related to the frequency spacing by $f_S T_S = 1/2$. In this case, the inner product for the signal space is redefined as

$$\langle x(t) | y(t) \rangle_R = \mathrm{Re}\left\{ \int x(t) y^*(t) dt \right\} \tag{2.29}$$

and the basis functions are defined as

$$x_{n,k}(t) = j^{n+k} e^{j2\pi k f_S t} x(t - nT_S) \tag{2.30}$$

The most common multicarrier scheme requires that the following condition is met for orthogonality of the basis functions.

$$\begin{array}{ll} X(f) = 0 & |f| \geq f_S \\ |X(f)|^2 + |X(f - f_S)|^2 = 1/f_S & 0 \leq f < f_S \\ |X(f)|^2 + |X(f + f_S)|^2 = 1/f_S & -f_S < f < 0 \end{array} \tag{2.31}$$

where $X(f)$ represents the Fourier transform of the signaling pulse $x(t)$ which must be an even function. The signaling pulse is defined here to be centered at $t = 0$ as opposed to starting at zero as in the previous section. An example of such a pulse spectrum is the half cycle cosine function which has the spectrum

$$X(f) = \begin{cases} \dfrac{1}{\sqrt{f_S}} \cos \dfrac{\pi f}{2 f_S} & |f| \leq f_S \\ 0 & \text{otherwise} \end{cases} \tag{2.32}$$

and the time domain representation

$$x(t) = \frac{4\sqrt{f_S} \cos(2\pi f_S t)}{\pi(1 - 16 f_S^2 t^2)} \tag{2.33}$$

Using this scheme, an information sequence may be transmitted using the signal

$$s(t) = \sqrt{2E_S} \sum_{n,k} c_{n,k} x_{n,k}(t) \tag{2.34}$$

In the conventional OFDM scheme transmitted symbols were allowed to take complex values and could be retrieved by performing the inner product operation as defined in (2.4). However, with the modified definition of inner product given by (2.29), only the real portion of a complex transmitted signal can be retrieved using a correlation receiver. Consequently the transmitted

symbols must now be real numbers. One is still able to transmit the same amount of information in a given bandwidth because of the modified relation between the subcarrier spacing f_S and the symbol interval T_S.

The actual signal transmitted can be obtained from the lowpass equivalent representation (2.34)

$$\frac{s_{RF}(t)}{\sqrt{2E_S}} = \sum_{k\,\text{even}}\left[\sum_{n\,\text{even}} c'_{n,k}\,x(t-nT_S)\cos 2\pi(f_c+kf_S)t + \sum_{n\,\text{odd}} c'_{n,k}\,x(t-nT_S)\sin 2\pi(f_c+kf_S)t\right] + \sum_{k\,\text{odd}}\left[\sum_{n\,\text{odd}} c'_{n,k}\,x(t-nT_S)\cos 2\pi(f_c+kf_S)t + \sum_{n\,\text{even}} c'_{n,k}\,x(t-nT_S)\sin 2\pi(f_c+kf_S)t\right] \tag{2.35}$$

The signal on each subcarrier is an offset quadrature amplitude modulated (OQAM) signal [28]. The modified information sequence $c'_{n,k}$ has some of the signs changed from the original sequence.

$$c'_{n,k} = \begin{cases} c_{n,k}(-1)^{\frac{n+k}{2}} & ,\text{for } n+k \text{ even} \\ c_{n,k}(-1)^{\frac{n+k+1}{2}} & ,\text{for } n+k \text{ odd} \end{cases} \tag{2.36}$$

As in the case of OFDM, there are efficient digital signal processing techniques that can be used to generate the signal [31], [32]. Other pulse shapes that will ensure the orthogonality of the basis functions (2.30) are discussed in [22].

2.2 COFDM System

2.2.1 System description

Coded Orthogonal Frequency Domain Multiplexing (COFDM) refers to an OFDM system with some form of error control coding used on the symbols $c_{n,k}$ prior to transmission. A block diagram of a COFDM system is shown in figure 2-3. This is a simplified version of the scheme used in the European and Canadian Digital Audio Broadcasting (DAB) standard discussed in more detail in the section 2.2.2. This block diagram is the basis for most of the analysis and simulation discussed in this thesis.

The sequence of binary information symbols is encoded using a convolutional code. For our simulations we have used a rate 1/2 convolutional code with constraint length K=7 as depicted in

figure 2-4. Here constraint length is defined to be number of memory elements in the encoder plus one. The two interleaved outputs of the encoder are a modulo 2 convolution of the input sequence with the generator sequences $g_0^{(0)}$ and $g_0^{(1)}$. It is common to specify encoders by writing the generator sequences in right justified octal format resulting in $g_0^{(0)} = 133$ and $g_0^{(1)} = 171$ for our code.

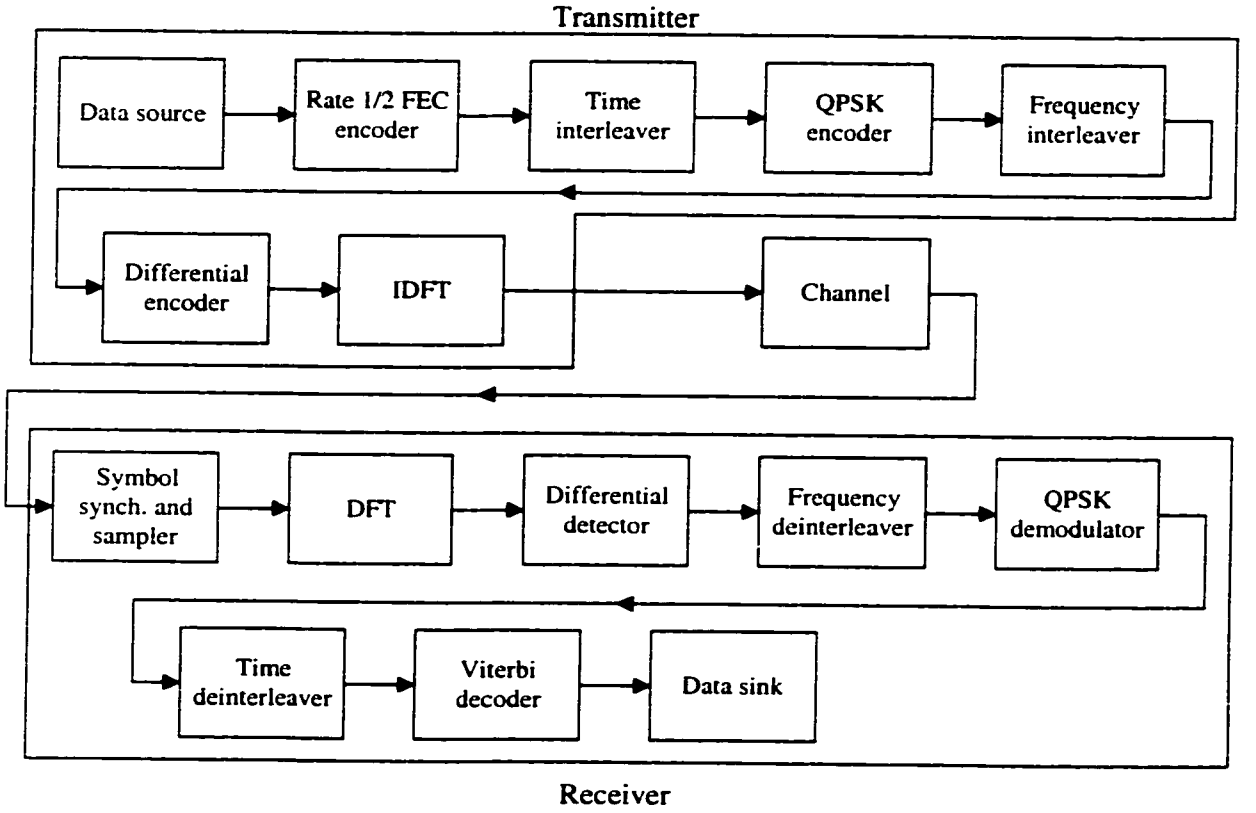

Figure 2-3 COFDM system block diagram.

The next block is the time interleaver which rearranges the sequence of the coded bits by delaying a bit by n frames where a frame is 59,136 bits long. The delay n is determined by bit reversing a binary representation of its position in the coded sequence modulo 16. Figure 2-5 shows a diagram of how the bits are delayed according to this formula. For example, the binary representation of position 4 is 0100. A bit reversal of this gives 0010: a delay of 2 frames. Thus the bit in position 4 of frame i is placed in position 4 of frame i+2 in the interleaved sequence.

The bit in position 20 of frame i would also be delayed by 2 frames since 20 modulo 16 is equal to 4.

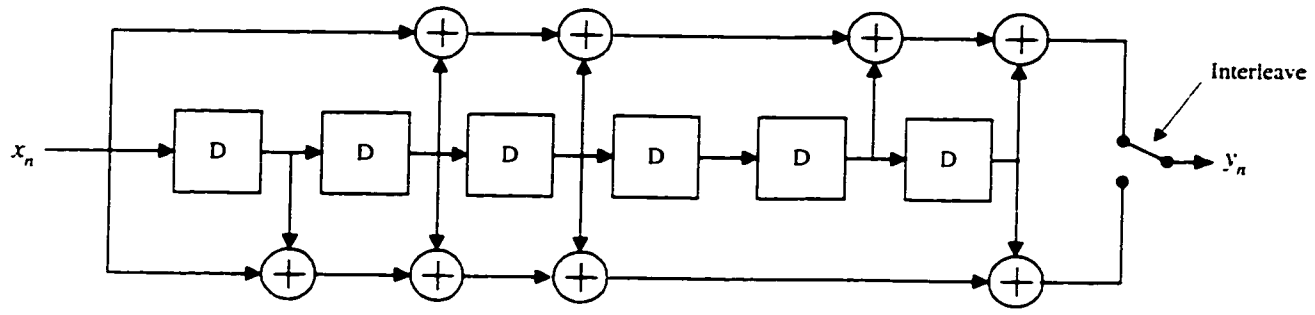

Figure 2-4 Rate 1/2 convolutional encoder used for COFDM simulations. The symbol D represents a delay element.

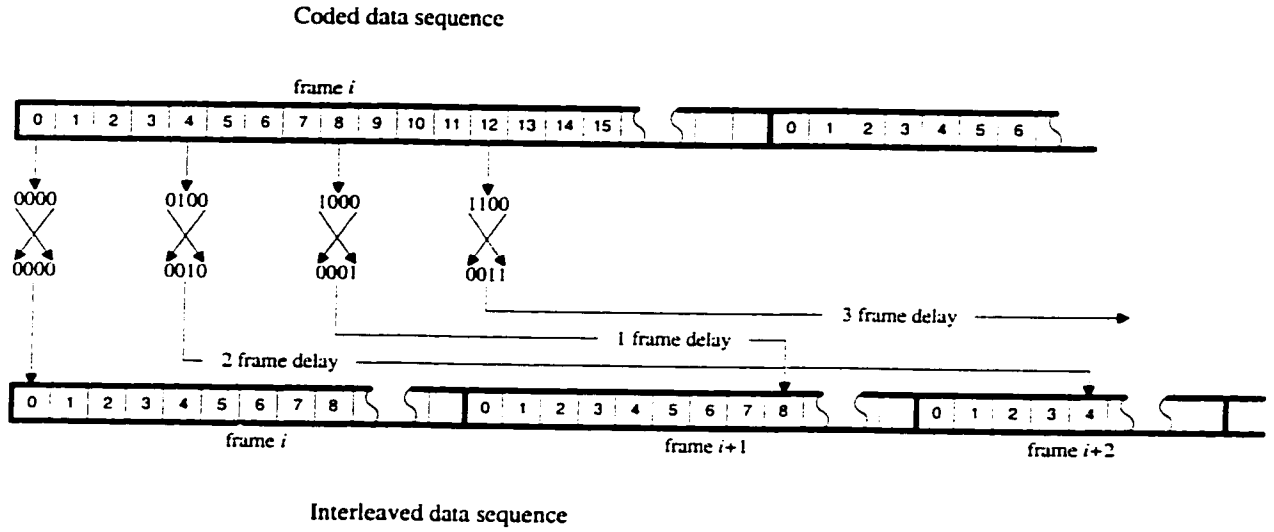

Figure 2-5 Time interleaving scheme for COFDM system used in DAB specification.

This interleaving scheme means that one frame of coded data is dispersed throughout the subsequent 15 frames of the interleaved sequence. Also a single frame of interleaved data contains bits from the previous 15 frames of the coded sequence. Thus an n frame long sequence of coded data will result in an n+15 frame long sequence of time interleaved data. When simulating the COFDM system, the first frame of interleaved data requires the coded bit sequence from 15 previous non-interleaved frames. When the simulation starts, these 15 frames are not available. The second frame of interleaved data requires bits from the first coded frame and 14 other previous frames which are not available and so on. The first 15 frames of

interleaved data will thus have some positions for which data are not available. There needs to be some means to initialize the time interleaved sequence when simulating the COFDM system. This can be done simply by entering random bit values in positions where coded bits are not available. A similar situation occurs in the last 15 frames of time interleaved data.

The time interleaved bit sequence is mapped to complex 4-PSK symbols which will be assigned to the OFDM subcarriers. Let b_i represent the i^{th} bit in the time interleaved sequence.

$$a_{n,\pi(k)} = \frac{1}{\sqrt{2}}\left(1 - 2b_{2nN+k} + j(1 - 2b_{(2n+1)N+k})\right) \tag{2.37}$$

where $a_{n,k}$ is the symbol corresponding to the n^{th} symbol interval and the k^{th} subcarrier, N is the number of subcarriers, and $\pi(k)$ represents a permutation of the integers k=0, 1, ..., N-1. This permutation accomplishes the frequency interleaving portion of the system. The permutation used for DAB is rather lengthy to specify and the reader is referred to [8] for the details.

Prior to modulation onto the OFDM subcarriers, the symbols $a_{n,k}$ are differentially encoded. We have used two differential encoding schemes for simulations.

$$c_{n,k} = a_{n,k} c_{n-1,k} e^{-j\pi/4} \tag{2.38}$$

and

$$c_{n,k} = a_{n,k} c_{n-1,k} \tag{2.39}$$

The second scheme is called $\pi/4$-shift 4-DPSK and is the technique actually used in the DAB standard. The two schemes differ in that (2.38) produces symbols $c_{n,k} \in \{1, j, -1, -j\}$ that form a 4-PSK constellation while (2.39) produces symbols $c_{n,k} \in \{e^{jm\pi/4}\}$ m=-3, -2, ..., 4 that form an 8-PSK constellation. This has no effect on differential detection of the symbol sequence but does have ramifications for some of the other detection techniques that will be discussed.

The symbols $c_{n,k}$ are OFDM modulated using the IDFT approach and transmitted across the channel. The channel model is a lowpass equivalent channel so there are no RF carrier modulation and demodulation blocks in the system baseband representation. A block that performs symbol synchronization and sampling is shown. In the simulations and analysis that follow, it is assumed that the symbol synchronization function has been realized perfectly. After

the FFT retrieves the symbols on the individual subcarriers, the receiver performs differential detection:

$$\hat{a}_{n,k} = y_{n,k} y^{*}_{n-1,k} e^{j\pi/4} \tag{2.40}$$

for ordinary 4-DPSK and

$$\hat{a}_{n,k} = y_{n,k} y^{*}_{n-1,k} \tag{2.41}$$

for $\pi/4$-shift 4-DPSK. The de-interleaving functions are the inverse of the corresponding transmitter functions except they are operating on the real and imaginary parts of the differential detector output rather than on binary digits. The final block in the receiver is a Viterbi decoder which performs maximum likelihood decoding of the convolutional code.

2.2.2 Application to digital audio broadcasting

The digital audio broadcast (DAB) standard [8] adopted for use in Europe and Canada is a COFDM system. Four modes of transmission referred to as modes I to IV, are defined in this specification. The fundamental difference in these modes is the spacing of the subcarriers and the related symbol duration. Since all modes must operate in a fixed allocated bandwidth, this implies that the number of subcarriers varies between modes and the overall symbol rate is the same for all modes. A list of transmission parameters for the four modes is provided in table 2-1. Mode I is currently not being considered for use in Canada. This thesis considers only mode IV because it has the longest symbol interval of the remaining modes and is thus the most vulnerable to errors caused by fast fading (as will be discussed in the next chapter).

The standard groups data into transmission frames which are 48 ms in duration for mode IV. At the start of each frame there is a null symbol when no signal is transmitted followed by a phase reference symbol when known symbols are transmitted on each OFDM subcarrier. These symbols are used for receiver synchronization purposes. The data transmission capability of the DAB standard is large enough to allow the transmission of several audio broadcasting programs. Following the synchronization symbols, there are three symbol periods that are used for fast information channel data. These data contain information about the multiplexing configuration of the audio data in the remainder of the frame. To allow the receiver fast access to this information, the time interleaving discussed above is not performed on these frames. Note that in

the simulations discussed in chapter 5, we will consider a COFDM system that does not include the fast information symbols.

Parameter	Symbol	Value			
		Mode I	Mode II	Mode III	Mode IV
Number of subcarriers	N	1536	384	192	768
Frame duration [ms]	T_F	96	24	24	48
Symbol duration [μs]	T_S	1246	312	156	623
Useful symbol duration [μs]	T_U	1000	250	125	500
Guard interval duration [μs]	T_G	246	62	31	123
Subcarrier spacing [Hz]	f_U	1000	4000	8000	2000
Number of OFDM symbols per frame	L	77	77	154	77
RF carrier frequency [GHz]	f_c	1.5			

Table 2-1 DAB transmission parameters.

The discussion of the time interleaving in the previous section has specified the delay applied to a coded bit in terms of frames. The transmission frame length for the DAB system varies for the different modes so the time interleaving delay is actually specified in logical frames which are the same duration for all of the modes. In our COFDM simulation, we break the data into 24 ms-long logical frames and base the interleaving delay on these rather than on the 48 ms transmission frames. This provides the required maximum interleaver delay of 16×24 = 384 ms.

The DAB standard allows for varying degrees of error protection on the individual audio programs that are transmitted by means of rate compatible punctured convolutional (RCPC) codes [13], [14]. This is a scheme where a low rate "mother code" is punctured to obtain a desired higher coding rate. In the DAB standard, the mother code is a rate 1/4 convolutional code which is punctured to obtain rates up to 3/4. Our simulations of the COFDM system use a rate 1/2 code to be representative of an intermediate level of error protection. The DAB standard calls for each individual audio program data to be coded separately. In our COFDM system

simulations the data in a transmission frame are treated as one long block that is encoded in a continuous stream.

2.3 SUMMARY

The basic principles of the OFDM multicarrier modulation technique have been discussed in some detail. OFDM is basically a PAM system where the pulses are rectangular windowed complex sinusoids. By spacing the frequency of the sinusoids by the inverse of the pulse length, the orthogonality of the pulses is ensured. Two important aspects of OFDM were discussed in detail. It has been demonstrated that the guard interval with the cyclic prefix eliminates ISI and ICI when the duration of the channel impulse response is less than the duration of the guard interval. Also the use of the IDFT and DFT to synthesize and demodulate the OFDM signal was discussed.

When an OFDM signal passes through a linear time invariant AWGN channel it is possible to treat each subcarrier as an independent AWGN channel. This occurs because uncorrelated Gaussian noise samples at the input to a DFT remain uncorrelated at the output. The sequence of decision variables appearing at any DFT output tap will be equal to the data symbol sequence at the corresponding IDFT input tap multiplied by a channel gain factor and corrupted by an equivalent white Gaussian noise sequence.

The COFDM system that is employed for DAB is simply an OFDM modulation system where the information sequence is convolutionally encoded and interleaved prior to being 4-DPSK encoded and modulated on the OFDM subcarriers. The aspects of the COFDM system that are important for the computer simulations detailed in chapter 5 have been discussed.

For DAB applications it is obviously important to know how the COFDM system performs over wireless mobile channels. The next step in the analysis of the problem is the analysis of COFDM transmission over this type of channel. This is the topic of the next chapter.

3

Frequency Selective Fast Fading Channel Model

Wireless transmission of radio frequency (RF) modulated data signals between a fixed transmitter and a mobile receiver is subject to two fundamental physical effects [28], [33], [45]. The first, multipath propagation, arises because there are many paths for the RF signal to follow between the transmitter and the receiver. These paths have different delay, phase shift and attenuation and the received signal is a superposition of these multipath signals. The moving receiver gives rise to a second effect known as Doppler shift: the frequency of the received RF signal shifts by an amount that depends on the vehicle speed and the incident angle relative to the direction of movement.

Since the receiver is moving the length, attenuation, incident direction and number of propagation paths change with time. This requires one to model a mobile channel as a time varying linear system. Also the RF propagation environment is generally complex enough that a deterministic characterization is not possible. Thus mobile channels are usually modeled as randomly time varying linear systems. This chapter discusses the theory relating to randomly time varying linear systems. Following this, a model for multipath propagation over a mobile wireless channel is developed and the theory is applied to this model.

Multipath propagation gives rise to a characteristic of wireless channels known as fading. The signal varies in strength with time and position due to the random superposition of sinusoidal signals. Channels can be characterized according to the probability density function of the signal strength and the rate of change of signal strength. This channel characterization will be discussed.

An important aspect of digital communication is known as diversity combining. In diversity combining, redundant information is transmitted over uncorrelated paths and then combined at the receiver to improve BER. The COFDM system has features that attempt to enhance performance over a mobile channel by taking advantage of uncorrelated avenues of transmission that exist at different frequencies and times.

The final section of this chapter is devoted to developing a discrete time statistical model for OFDM propagation over a time varying multipath channel. This results in an expression very similar to (2.26). This model is then applied to calculate the theoretical BER for a conventional differential detector (CDD) operating on the COFDM signal. This model will also be the basis for much of the analysis in chapter 4.

3.1 Statistical Characterization of Linear Time Varying Channels

3.1.1 Linear time varying systems

A linear time varying system can be represented by its impulse response $h(\tau, t)$ which gives the channel response at observation time t to an impulse at excitation time τ seconds in the past. Bello [2] called this the *input delay spread function*. Since the analysis is based on processing lowpass equivalent signals, this function takes complex values. The response to an input $x(t)$ can be written as a convolution

$$y(t) = \int x(t-\tau)h(\tau,t)d\tau \tag{3.1}$$

It is important to realize that there is some delay between the time of transmission of an impulse and the first response at the receiver so that in actual fact the function $h(\tau, t)$ will be identically zero in some region $\tau \in (-\infty, \tau_p)$. However channels are almost always characterized as if this excess delay did not exist and the $h(\tau, t)$ is shifted appropriately so that it is zero only for $\tau < 0$.

Alternate channel characterizations can be obtained by Fourier transforming the input delay spread function in one or both variables. A summary of these appears in table 3-1. Here the notation $\Im_\tau\{\bullet\}$ is used to represent the Fourier transform with respect to the variable τ. For single variable functions the capitalized $Y(f)$ means the Fourier transform of $y(t)$.

Name	Notation	Interpretation	Output
Input delay spread function	$h(\tau, t)$	The response at time t to an impulse at time $t-\tau$	$y(t) = \int x(t-\tau)h(\tau,t)d\tau$
Time-variant transfer function	$H(f,t) = \Im_\tau\{h(\tau,t)\}$	The system transfer function at time t	$y(t) = \int X(f)H(f,t)e^{j2\pi ft}df$
Delay-Doppler spread function	$U(\tau,\nu) = \Im_t\{h(\tau,t)\}$		$y(t) = \iint x(t-\tau)U(\tau,\nu)e^{j2\pi\nu t}d\tau d\nu$
Output Doppler-spread function	$G(f,\nu) = \Im_t\{H(f,t)\}$	The response at frequency $f+\nu$ to a complex sinusoid at frequency f	$Y(f) = \int Y(f-\nu)G(f-\nu,\nu)d\nu$

Table 3-1 Characterization of a linear time varying system.

3.1.2 Random linear time varying systems

For mobile channels it is usually necessary to treat the channel impulse response $h(\tau, t)$ as a sample function of a random process. One is often concerned with a second order characterization of this random process. For this, the autocorrelation function of the process is defined as

$$R_h(\tau_1,\tau_2,t_1,t_2) = E\{h(\tau_1,t_1)h^*(\tau_2,t_2)\} \tag{3.2}$$

In general, this is a function of four variables and is thus difficult to conceptualize. However, it is generally accepted that it is valid to make two approximations when dealing with time varying channels in a multipath environment. The first is called the uncorrelated scattering assumption which says that there is no correlation between the complex scattering amplitude at different values of the delay parameter τ. The second is that the process is wide sense stationary in the time variable t meaning that the correlation function only depends on the time difference

$\Delta t = t_1 - t_2$. Together these constitute the wide sense stationary uncorrelated scattering (WSSUS) assumption which is employed in most modeling of wireless communication channels. In this case, the correlation function reduces to

$$R_h(\tau,\Delta t) = E\{h(\tau,t+\Delta t)h^*(\tau,t)\} \tag{3.3}$$

In the case where we have an input signal $x(t)$ passing through a random time varying channel, the output will be a sample function of a random process $y(t)$ given by

$$y(t) = \int x(t-\tau)h(\tau,t)d\tau \tag{3.4}$$

The autocorrelation function of the output of a WSSUS channel is given by

$$R_y(t+\Delta t,t) = E\{y(t+\Delta t)y^*(t)\} = \int x(t+\Delta t-\tau)x^*(t-\tau)R_h(\tau,\Delta t)d\tau \tag{3.5}$$

Using this it can be shown that if the system is excited with an impulse function $x(t) = \delta(t-t_1)$, then the autocorrelation of the output process will be

$$R_y(t) = R_h(t-t_1) \tag{3.6}$$

where

$$R_h(\tau) \equiv R_h(\tau,0) \tag{3.7}$$

It is seen that the output is a non-stationary random process whose mean power is spread over time by the channel. The function $R_h(\tau)$ is called the *multipath intensity profile* or *delay spread profile*. The duration of time where this function is non-zero or greater than some predetermined threshold value is called the *multipath spread* or *delay spread* of the channel and is designated by τ_m.

As with deterministic time varying channels, it is possible to characterize the random channel by Fourier transforming the channel function $h(\tau, t)$. In analogy with table 3-1 the *time variant transfer function* $H(f, t)$ for a random channel is defined to be the Fourier transform of $h(\tau, t)$ with respect to the variable τ. The time variant transfer function is a sample function of a random process and the *spaced-frequency, spaced-time correlation function* which for a WSSUS channel is only a function of Δf and Δt may be defined as follows

$$R_H(\Delta f, \Delta t) = E\{H(f+\Delta f, t+\Delta t)H^*(f,t)\} \tag{3.8}$$

Also $R_H(\Delta f,\Delta t)$ is the Fourier transform of $R_h(\tau, \Delta t)$ with respect to the variable τ. If two complex sinusoid functions $x_1(t) = e^{j2\pi f_1 t}$ and $x_2(t) = e^{j2\pi f_2 t}$ are input to the channel described by $R_H(\Delta f, \Delta t)$ then one may calculate the cross correlation between the corresponding output processes to be

$$E\{y_1(t+\Delta t), y_2(t)\} = e^{j2\pi\Delta f t} e^{j2\pi f_1 \Delta t} R_H(\Delta f, \Delta t), \quad \Delta f = f_1 - f_2 \tag{3.9}$$

Therefore the function $R_H(\Delta f, \Delta t)$ gives a measure of the correlation between channel outputs corresponding to inputs separated by Δf. If this function is zero for a region $|\Delta f| > \Delta f_c$ then the responses, $y_1(t)$ and $y_2(t)$, to inputs separated by more than Δf will be uncorrelated. Conversely for $|\Delta f| < \Delta f_c$, the two output processes will maintain some level of coherence. Thus the parameter Δf_c is referred to as the *coherence bandwidth* of the channel. The *spaced-frequency correlation function* is defined as $R_H(\Delta f) \equiv R_H(\Delta f, 0)$. This is the Fourier transform of the channel delay spread profile. This Fourier transform relationship means that Δf_c is proportional to the inverse of τ_m.

Returning now to equation (3.5) one can see that if the function $R_h(\tau, \Delta t)$ is zero for $|\Delta t| > \Delta t_c$ then $R_y(t+\Delta t, t)$ will also be zero in this same range and there will be no correlation between samples of the output signal separated in time by more than Δt_c. Furthermore, when the input to the channel is $x_1(t) = e^{j2\pi f_1 t}$, the autocorrelation of the output is

$$R_{y_1}(\Delta t) = e^{j2\pi f_1 \Delta t} R_H(\Delta t) \tag{3.10}$$

where

$$R_H(\Delta t) \equiv R_H(0, \Delta t) = \int R_h(\tau, \Delta t) d\tau \tag{3.11}$$

is called the *spaced-time correlation function*. Because of the relation (3.11) the function $R_H(\Delta t)$ is non-zero in the interval $|\Delta t| < \Delta t_c$. From (3.10) then one sees that channel response to a sinusoidal input maintains some degree of coherence over an interval of time that is less than Δt_c. For this reason the parameter Δt_c is referred to as the *coherence time* of the channel.

A third characterization of a time varying channel is obtained by Fourier transforming $h(\tau, t)$ with respect to t obtaining the *delay-Doppler spread function* $U(\tau, \nu)$. For a WSSUS channel, this process is uncorrelated at different values of τ and ν. The correlation function given by

$$S(\tau,\nu) = E\{U(\tau+\Delta\tau,\nu+\Delta\nu)U^*(\tau,\nu)\} \tag{3.12}$$

is referred to as the *channel scattering function* and this can be shown to be the Fourier transform of the channel correlation function $R_h(\tau, \Delta t)$ with respect to the variable Δt. If the function $x_1(t) = e^{j2\pi f_1 t}$ is input to the channel it can be shown that the power spectral density of the output random process is given by

$$S_{y_1}(\nu) = S(\nu - f_1) \tag{3.13}$$

where

$$S(\nu) \equiv \int S(\tau,\nu)d\tau = \Im_{\Delta t}\{R_H(\Delta t)\} \tag{3.14}$$

This is called the *Doppler spread function* of the channel. The effect of the random channel is to spread the mean power spectrum of the input cissoid (complex sinusoidal) around the frequency f_1. The Doppler spread f_d of the channel defines the region $|\nu| < f_d$ where $S(\nu)$ is non-zero or non-negligible. Because of the Fourier transform relation (3.14), the Doppler spread of the channel is proportional to the inverse of the coherence time Δt_c.

Since the delay spread profile $R_h(\tau)$ is equal to $R_h(\tau, 0)$ and the channel scattering function is the Fourier transform of $R_h(\tau, \Delta t)$ with respect to Δt, one deduces that

$$R_h(\tau) = \int S(\tau,\nu)d\nu \tag{3.15}$$

Therefore integrating the channel scattering function over the variable ν produces the delay spread profile which gives an indication of how the power from a function that is perfectly localized time (a delta function) is spread over time by the channel. Integrating the channel scattering function over the variable τ produces the Doppler spread which gives an indication of how the power from a function that is perfectly localized in frequency (a cissoid) is spread over frequency by the channel. The channel scattering function thus provides a good indication of the

time and frequency spreading effects of the channel and in practice is often used to characterize a time varying WSSUS channel.

3.2 Time Varying Multipath Channel Model

3.2.1 Multipath propagation for narrowband signals

To proceed with the analysis of DAB it is necessary to develop a model allowing the calculation of the channel statistics discussed in the previous section for a broadcast channel. That is, a channel consisting of multipath RF propagation between a fixed transmitting antenna and a receiver antenna on a moving vehicle. To do this, assume that RF propagation takes place over M paths as depicted in figure 3-1.

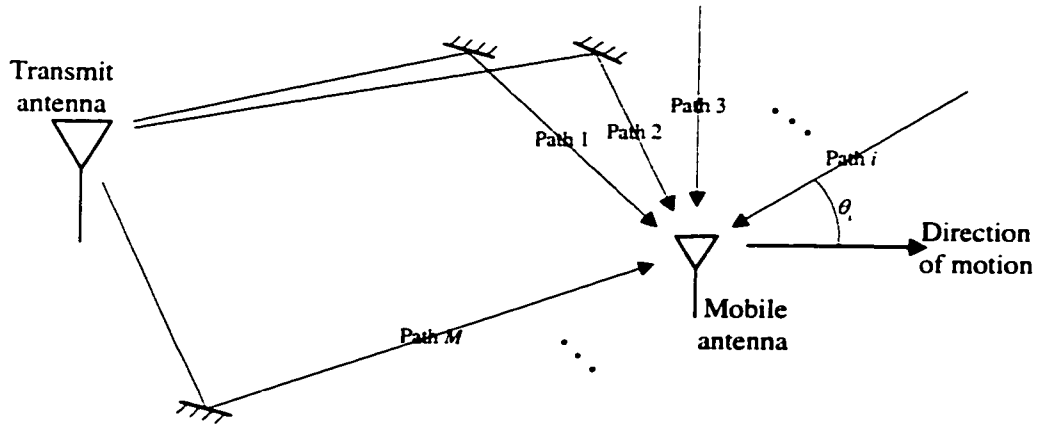

Figure 3-1 Multipath propagation between fixed transmit antenna and mobile receive antenna.

The transmitted signal is represented as

$$s(t) = \mathrm{Re}\{s_l(t)e^{j2\pi f_c t}\} \tag{3.16}$$

It is assumed that the bandwidth of the lowpass equivalent signal $s_l(t)$ is several orders of magnitude lower than the carrier frequency. This is valid for DAB in Canada as the signal bandwidth is about 1.5 MHz and the carrier is 1.5 GHz. Under this condition, the lowpass equivalent received signal from any particular path can be approximated as [33]

$$r_l(t) = \alpha_i s_l(t-\tau_i) e^{-j2\pi(f_c+f_{d,i})\tau_i} e^{j2\pi f_{d,i}t} \tag{3.17}$$

where the parameters α_i, $f_{d,i}$ and τ_i represent the complex attenuation, the Doppler shift and the propagation delay for the i^{th} path. Referring to equation (3.1) one can see that the time varying channel impulse response corresponding to this received signal is

$$h_i(\tau,t) = a_i e^{-j2\pi(f_c+f_{d,i})\tau_i} e^{j2\pi f_{d,i}t} \delta(\tau-\tau_i) \tag{3.18}$$

To model the multipath channel, the parameters a_i, $f_{d,i}$ and τ_i will be treated as random variables and then the number of paths M will be made large enough that the central limit theorem can be invoked. The statistical characteristics of the channel will depend on the assumptions that are made about the statistics of these random variables.

The first assumption is that the carrier frequency f_c is sufficiently large that the phase shift $\phi_i = 2\pi(f_c + f_{d,i})\tau_i$ in (3.18) goes through so many rotations over the range of τ_i that it can be treated as uniformly distributed between $-\pi$ and π. The random channel function is expressed as the summation of the contribution from each path

$$h(\tau,t) = \sum_{i=1}^{M} h_i(\tau,t) = \sum_{i=1}^{M} A_i e^{-j\Phi_i} e^{j2\pi F_i t} \delta(\tau - T_i) \tag{3.19}$$

where A_i, Φ_i, F_i, and T_i are independent random variables representing the complex attenuation, the phase shift, the Doppler shift, and the delay associated with path i. This means that

$$E\{h_i(\tau_1,t_1)\} = E\{A_i\}E\{e^{-j\Phi_i}\}E\{e^{jF_i t_1}\}E\{\delta(\tau_1 - F_i)\} \tag{3.20}$$

and since Φ_i is uniformly distributed, $E\{e^{-j\Phi_i}\} = 0$ and consequently

$$E\{h_i(\tau_1,t_1)\} = 0 \tag{3.21}$$

Now assume further that the random variables A_i, Φ_i, F_i, and T_i are independent for different paths. This means that the random variables $h_i(\tau_1,t_1)$, being functions of independent random variables, are themselves independent random variables. Now, let σ_i^2 represent the variance of the random variable $h_i(\tau_1,t_1)$. One can invoke the central limit theorem which says that as M becomes large, the scaled random variable

$$\frac{1}{\sigma}h(\tau_1,t_1), \quad \sigma^2=\sigma_1^2+\sigma_2^2+\cdots+\sigma_M^2 \tag{3.22}$$

will approach a normally distributed random variable with variance 1. Let us then calculate the autocorrelation function for the random process $h(\tau,t)$

$$\begin{aligned} R_h(\tau_1,\tau_2,t_1,t_2) &= E\{h(\tau_1,t_1)h^*(\tau_2,t_2)\} \\ &= E\left\{\sum_{i=1}^{M}h_i(\tau_1,t_1)\sum_{k=1}^{M}h_k^*(\tau_2,t_2)\right\} \\ &= \sum_{i=1}^{M}\sum_{k=1}^{M}E\{h_i(\tau_1,t_1)h_k^*(\tau_2,t_2)\} \end{aligned}$$

The expectation in the above double summation is equal to zero for $i\neq k$ since the $h_i(\tau_1,t_1)$ and $h_k(\tau_2,t_2)$ are independent zero mean random variables for $i\neq k$. The result is that

$$\begin{aligned} R_h(\tau_1,\tau_2,t_1,t_2) &= \sum_{i=1}^{M}E\{h_i(\tau_1,t_1)h_i^*(\tau_2,t_2)\} \\ &= \sum_{i=1}^{M}R_{h_i}(\tau_1,\tau_2,t_1,t_2) \end{aligned} \tag{3.23}$$

The conclusion is that for a sufficiently large M, the aggregate random process will be a zero mean complex Gaussian process with autocorrelation function given by the sum of the autocorrelation functions of the individual processes. At this point it should be noted that the autocorrelation function (3.23) does not contain information about the correlation between the real and imaginary parts of the complex process. This is discussed further in appendix B.

3.2.2 Multipath channel model

The multipath channel will be modeled using (3.19) where each path is assumed to have equal non-random attenuation $a_i=1/\sqrt{M}$, the delays are exponentially distributed and the direction of path incidence on the mobile unit is assumed uniformly distributed. The resulting channel model [5], [36] is depicted in figure 3-2.

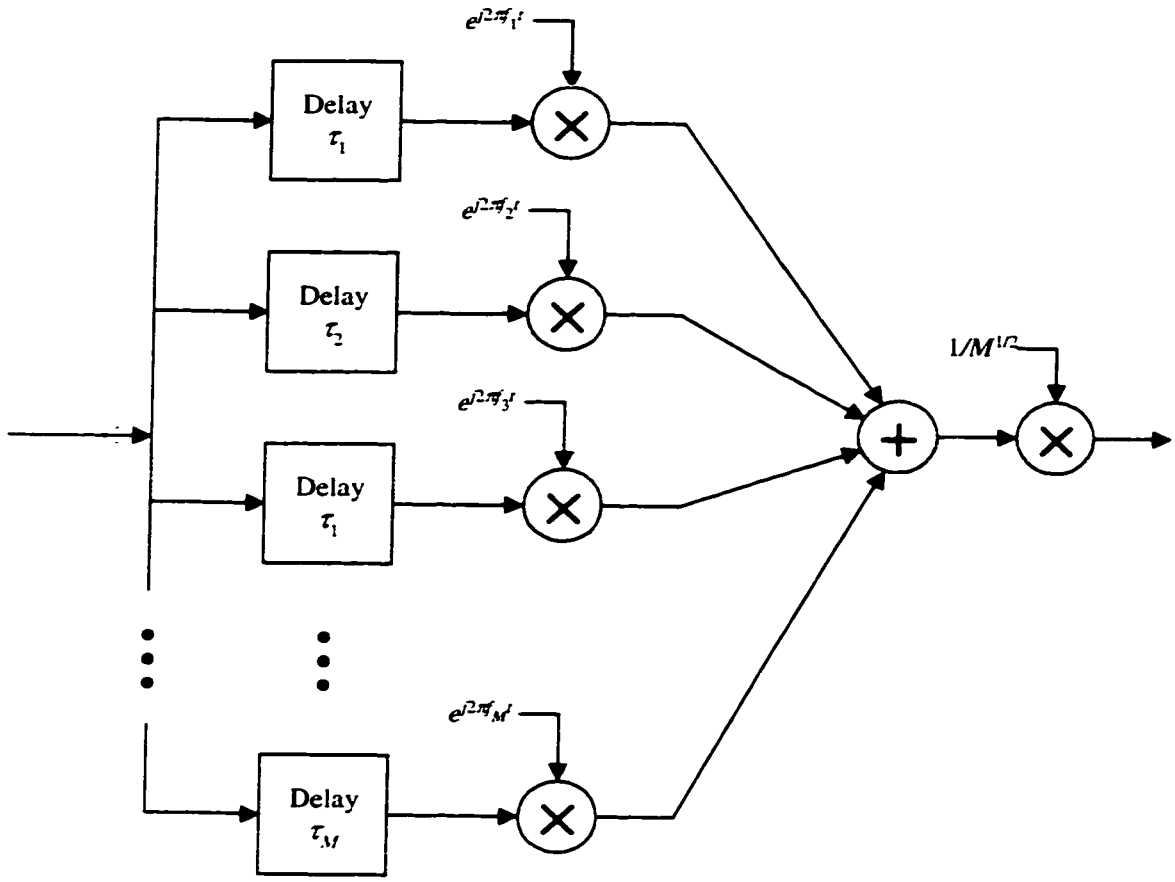

Figure 3-2 M path wireless channel model.

Let the random variable Θ_i represent the angle of incidence of the i^{th} path measured in relation to the direction of vehicle movement. This means that the Doppler shift is given by

$$F_i = f_d \cos\Theta_i \tag{3.24}$$

The maximum Doppler shift f_d is given by $f_d=f_c v/c$ where f_c is the carrier frequency, v is the vehicle velocity and c is the speed of light.

If Θ_i is uniformly distributed between $-\pi$ and π, the density function for F_i will be

$$f_{F_i}(f) = \begin{cases} \dfrac{1}{\pi\sqrt{f_d^2 - f^2}}, & |f| \le f_d \\ 0 & \text{otherwise} \end{cases} \tag{3.25}$$

The density function for the delay is

$$f_{T_i}(t) = \begin{cases} \frac{1}{\sigma_d} e^{-t/\sigma_d}, & t \geq 0 \\ 0, & \text{otherwise} \end{cases} \tag{3.26}$$

where σ_d is the mean delay spread. Equation (3.19) will be Fourier transformed with respect to the variable τ to obtain the time variant transfer function and then the spaced-frequency, spaced-time correlation function for the channel model will be evaluated.

$$H(f,t) = \sum_{i=1}^{M} H_i(f,t) = \frac{1}{\sqrt{M}} \sum_{i=1}^{M} e^{-j\Phi_i} e^{j2\pi F_i t} e^{-j2\pi f T_i} \tag{3.27}$$

For sufficiently large M, this channel function is a zero mean Gaussian random process. The correlation function may be calculated as the sum of the individual process correlation functions

$$R_{H_i}(\Delta f, \Delta t) = \frac{1}{M} E\{e^{j2\pi F_i \Delta t} e^{-j2\pi \Delta f T_i}\} = \frac{1}{M} \frac{J_0(2\pi f_d \Delta t)}{1 + j2\pi \Delta f \sigma_d} \tag{3.28}$$

where $J_0(x)$ represents an order zero Bessel function of the first kind. The summation merely removes the $1/M$ factor so that

$$R_H(\Delta f, \Delta t) = \frac{J_0(2\pi f_d \Delta t)}{1 + j2\pi \Delta f \sigma_d} \tag{3.29}$$

The details of the above calculation are shown in appendix B. The function (3.29) may be Fourier transformed in both variables to obtain the channel scattering function.

$$S(\tau, f) = \frac{1}{\sigma_d \pi} e^{-\tau/\sigma_d} \frac{1}{\sqrt{f_d^2 - f^2}} \tag{3.30}$$

The delay spread profile for the channel has the same shape as the probability density function for the path delays and the Doppler spread function has the same shape as the probability density function for the path Doppler shifts.

The M path channel model discussed here will be used for computer simulations discussed in chapter 5. The correlation functions discussed up to this point are ensemble averages. When performing a computer simulation, one must use a particular realization of the model random process. For any particular realization of a random process it is possible to define a time-frequency averaged autocorrelation function as

$$\hat{R}_H(\Delta f, \Delta t) = \lim_{F,T\to\infty} \frac{1}{4FT} \int_{-T}^{T} \int_{-F}^{F} H(f+\Delta f, t+\Delta t) H^*(f,t)\, df dt \tag{3.31}$$

For the channel model under consideration, this function evaluates to

$$\hat{R}_H(\Delta f, \Delta t) = \frac{1}{M} \sum_{i=1}^{M} e^{j2\pi f_i \Delta t} e^{-j2\pi \Delta f \tau_i} \tag{3.32}$$

where f_i and τ_i, i=1, 2, ..., M are the observations of the random variables F_i and T_i which correspond to a particular realization of the random process. The quantity under the summation sign in the above is an independent observation of the random variable $e^{j2\pi F_i \Delta t} e^{-j2\pi \Delta f T_i}$. The sum of any M independent observations of a random variable converges to M times the expected value of that random variable for sufficiently large M. Therefore for large M, (3.32) will converge to

$$\hat{R}_H(\Delta f, \Delta t) = E\{e^{j2\pi F_i \Delta t} e^{-j2\pi \Delta f T_i}\} = \frac{J_0(2\pi f_d \Delta t)}{1 + j2\pi \Delta f \sigma} \tag{3.33}$$

which is equal to the ensemble averaged correlation function (3.29). Figure 3-3 is a plot of the time averaged spaced time correlation function for three realizations of an M=40 path channel model. Each realization is a plot of (3.32) for Δf=0 and f_i drawn independently from the density function (3.25). The ensemble averaged function which is (3.29) for $\Delta f = 0$ is also plotted in the figure. One can see that the individual realizations do indeed appear to be converging to the ensemble averaged function although any particular realization may deviate as Δt increases.

This M path channel model provides a simulation of a channel with an exponential delay spread profile and a uniformly distributed incident angle for the transmission paths. For typical urban (TU) propagation, the mean delay spread σ_d is equal to 1 μs. The value of the maximum Doppler shift depends on the vehicle velocity. The value of 160 Hz depicted in figure 3-3 corresponds to a vehicle velocity of 115 km/hr for DAB mode IV.

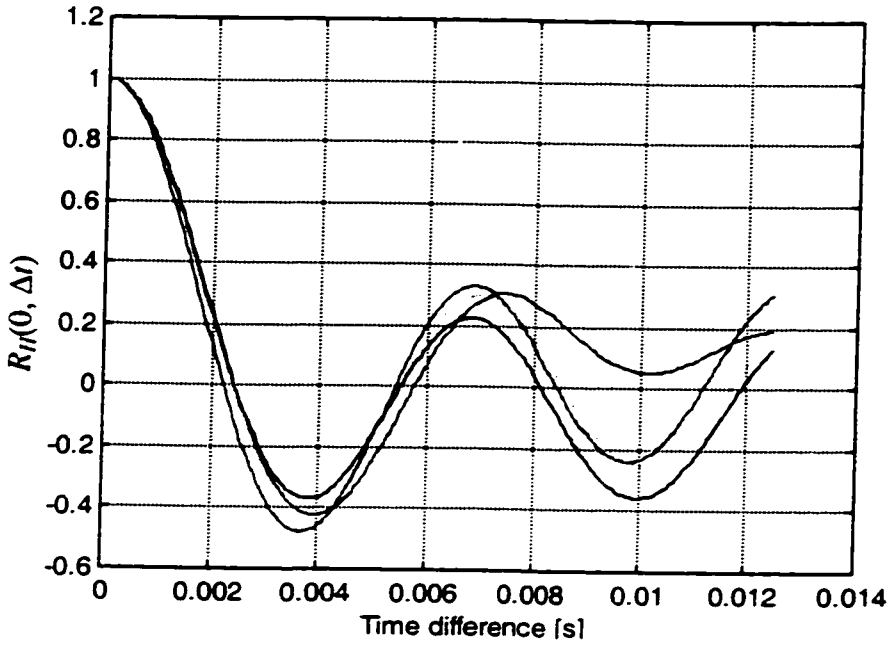

Figure 3-3 Autocorrelation function for three realizations of 40 path random delay random Doppler shift channel model (solid lines) and ideal channel (dashed line), both with f_d= 160 Hz.

3.2.3 Flat and frequency selective fast Rayleigh fading

In the previous section, it was shown that the lowpass equivalent of a multipath channel consisting of a large number of random paths can be described by a zero mean complex Gaussian random process. The received signal will be a linear transformation of this process and will thus itself be a zero mean Gaussian random process. Such a process has a modulus which follows a Rayleigh distribution. Thus the magnitude of the received signal will follow a Rayleigh distribution. At some points in time it will be very small and at others it will be very high. The situation when the signal strength is low is referred to as a fade and thus the channel is called a *Rayleigh fading* channel. Physically this type of channel occurs when there are many scattered paths between the transmitter and receiver but no line of sight path.

The fading rate of a wireless channel is a measure of how often the magnitude of the received signal falls below a certain threshold in a given time period. The exact value of this parameter depends on the nature of the transmitted signal and the fade threshold value. For a sinusoidal signal passing through a Rayleigh fading channel, it can be shown [33], [45] that the fading rate

is directly proportional to the Doppler spread f_d of the channel. Since f_d is proportional to $1/\Delta t_c$, one can also say that the fading rate is proportional to the inverse of the coherence time.

For wireless communication, one generally differentiates between two situations: fast and slow fading. With slow fading, the channel coherence time is much longer than the symbol period and the related fading rate is much lower than the symbol rate. The ratio of the symbol duration to the channel coherence time $T_S/\Delta t_c = f_d T_S$ is a convenient parameter for describing the channel fading rate and therefore the condition for slow fading is $f_d T_S << 1$ [28]. This means that a receiver can use some sort of automatic gain control and/or carrier tracking loop and essentially operate as if the channel was unchanging. For fast fading, this is no longer the case and symbol detection must take account of the rapidly varying channel. Transmissions over mobile channels are typically differentially modulated and in this case demodulation only requires that the channel coherence time be larger than the duration of a few symbols. Analysis will show that for mode IV operation of the COFDM system used in DAB, a conventional differential detection receiver cannot achieve the required BER for values of $f_d T_S$ in excess of about 0.08.

For wideband transmit signals, different frequency components are affected differently by the channel and hence this channel condition is called frequency selective fading. The situation where the duration of the channel delay spread is low in comparison to the duration of the transmit signal pulse or, equivalently, when the coherence bandwidth of the channel is large in comparison to the transmit signal bandwidth is called flat or frequency non-selective fading. In this case, all frequency components of the transmit signal will be affected similarly by the channel. For a flat fading channel, the received signal can be expressed as $y(t) = x(t)h(t)$. The received signal is obtained by multiplying the transmit signal by a time varying gain factor. For practical values of the channel delay spread the signal transmitted on each subcarrier of the OFDM signal can be viewed as a narrowband signal passing through a flat fading channel. In the next chapter, this fact will be used to adapt techniques developed for frequency non-selective fast fading channels to the OFDM signal.

3.2.4 Diversity combining

For fading channels the technique called diversity combining refers to an attempt to decrease the probability of a decision error by observing several random variables which are related to the

symbol value. For example, if a replica of a symbol delayed by a length of time longer than the channel coherence time is transmitted, the two received copies of the symbol will be uncorrelated. It is unlikely that both copies will be in the midst of a deep fade and therefore a proper combination of the two will result in a lower overall error probability. This would be called taking advantage of the time diversity of the channel. For frequency selective fading channels, one can also take advantage of frequency diversity to obtain an improvement in the BER.

The time and frequency interleaving specified for a COFDM system are attempts to take advantage of the time and frequency diversity in the mobile channel. The convolutional coding of the message sequence creates a string of coded bits having some dependence on a given information bit. The time and frequency interleaving then disperses this string across time and on several subchannels. The hope is that in this way, a fair percentage of the coded bits related to the value of a given information bit are likely to be detected reliably and therefore it can be decoded correctly. The depth of time interleaving needed to ensure the necessary time diversity is related to the coherence time of the channel which is related to the vehicle velocity. The breadth of frequency interleaving required to achieve the necessary frequency diversity is related to the delay spread of the channel.

3.3 OFDM Transmission over Time Varying Multipath Channel

3.3.1 OFDM guard interval function for wireless channels

The delay spread profile for a time varying WSSUS channel (3.7) is given by $R_h(\tau) = E\{|h(\tau,t)|^2\}$. This function is negligible for τ greater than the channel delay spread. This means that the random variable $h(\tau, t)$ takes a value that is close to zero with high probability for $\tau > \tau_m$. This in turn means that any sample function $h(\tau, t)$ will take on negligible values for $\tau > \tau_m$. Equation (3.1) then indicates that any input occurring at time $t < t_1 - \tau_m$ has negligible effect on the output occurring at time $t > t_1$. This leads to the conclusion that if the OFDM guard interval is larger than the channel delay spread, the intersymbol interference is negligible.

Typical urban wireless channels have delay spreads of less than 10 μs [5]. From table 2-1 the guard interval for mode IV DAB operation is 123 μs, one fifth of the total symbol duration. This is larger than required for typical values of delay spread. However, this relatively long guard interval allows broadcasters to use multiple transmission antennas to cover a wider area. As long as the time between the reception of the first signal from the nearest tower and the reception of the last signal from the furthest tower does not exceed the guard interval, there will be no ISI. Since mode IV has the longest guard interval of the modes being considered for use in Canada, it allows the widest spacing of transmit towers. This provides economic benefits to broadcasters and is thus the preferred mode of operation.

3.3.2 Discrete channel model for OFDM signal

Consider now the system depicted in the block diagram of figure 2-2 with the deterministic channel replaced with the M path model depicted in figure 3-2. It is useful to develop an expression similar to (2.26) for this revised model. As discussed in section 2.1.3, it is valid to add an equivalent AWGN component to the DFT outputs. This portion of the model will be unchanged from the earlier discussion.

To begin, consider the response through one of the M paths. The transmitted OFDM signal is given by (2.8). Each path adds a phase shift, a fixed attenuation, a Doppler shift and a delay to the transmitted signal

$$h_i(\tau,t) = e^{j\phi_i}\delta(\tau-\tau_i)e^{j2\pi f_i t} \tag{3.34}$$

An expression for the received signal valid over the useful symbol intervals is

$$y_i(t) = \sqrt{\frac{2E_U}{MT_U}}e^{j\phi_i}\sum_n \sum_{k=1-N/2}^{N/2} c_{k,n}e^{j2\pi k f_U(t-nT_S-\tau_i)}e^{j2\pi f_i t} \tag{3.35}$$

providing that the delay τ_i is less than the duration of the guard interval. Again it is assumed that the anti-aliasing filter cutoff frequency is larger than the signal bandwidth so that the expression for the sampled receive signal from the n^{th} useful symbol interval is

$$y_i(nT_S + lT_U/\hat{N}) = \sqrt{\frac{2E_U}{MT_U}}e^{j\phi_i}\sum_{k=1-N/2}^{N/2} c_{k,n}e^{j2\pi k\left(\frac{l}{\hat{N}}-\frac{\tau_i}{T_U}\right)}e^{j2\pi f_i(nT_S+lT_U/\hat{N})},\ l=0,1,\cdots,\hat{N}-1 \tag{3.36}$$

This is then passed through a DFT to get

$$y_{n,m}^{(i)} = \frac{1}{\hat{N}} \sum_{l=0}^{\hat{N}-1} y_i(nT_S + lT_U / \hat{N}) e^{-j2\pi \frac{lm}{\hat{N}}}$$
$$= \sqrt{\frac{2E_U}{MT_U}} e^{j\phi_i} e^{j2\pi f_i n T_S} \sum_{k=1-N/2}^{N/2} c_{n,k} z_{k,m}(\tau_i, f_i), \quad m = 1 - N/2, 2 - N/2, \cdots, N/2 \tag{3.37}$$

The ICI function $z_{k,m}(\tau_i, f_i)$ gives the effect of the transmitted symbol from the k^{th} subcarrier on the detected symbol from the m^{th} subcarrier. The output of a DFT is normally indexed from 0 to $\hat{N} - 1$, but because of the periodic property of the DFT it is valid to run the index as shown in the above expression. The ICI function is

$$z_{m,k}(\tau_i, f_i) = e^{-j2\pi k f_U \tau_i} e^{j\pi(1-1/\hat{N})(f_i T_U + k - m)} \frac{1}{\hat{N}} \frac{\sin[\pi(f_i T_U + k - m)]}{\sin\left[\frac{\pi}{\hat{N}}(f_i T_U + k - m)\right]} \tag{3.38}$$

The magnitude of the ICI function is plotted in figure 3-4 for the case of $\hat{N} = 8$ and $f_i T_U = 0.1$. Notice that it is periodic with period $\hat{N}$. The implication of this is that the transmitted symbol $c_{n,1-N/2}$ can have an ICI effect on the detected symbol $y_{n,N/2}$ despite the fact that these subcarriers are widely separated in frequency. This is an artifact of the sampling process and can be avoided by making $\hat{N}$ significantly larger than the number of subcarriers. The points plotted with circles on figure 3-4 are at integer values of k-m. If the Doppler shift for the i^{th} path f_i was equal to zero, the curve plotted with the dotted line would shift to the right and the ICI function would be zero for $k \neq m$. The parameter $f_i T_U = f_i / f_U$, the ratio of the Doppler shift to the carrier spacing, determines how much the curve plotted with the dotted line shifts and therefore the magnitude of the ICI component.

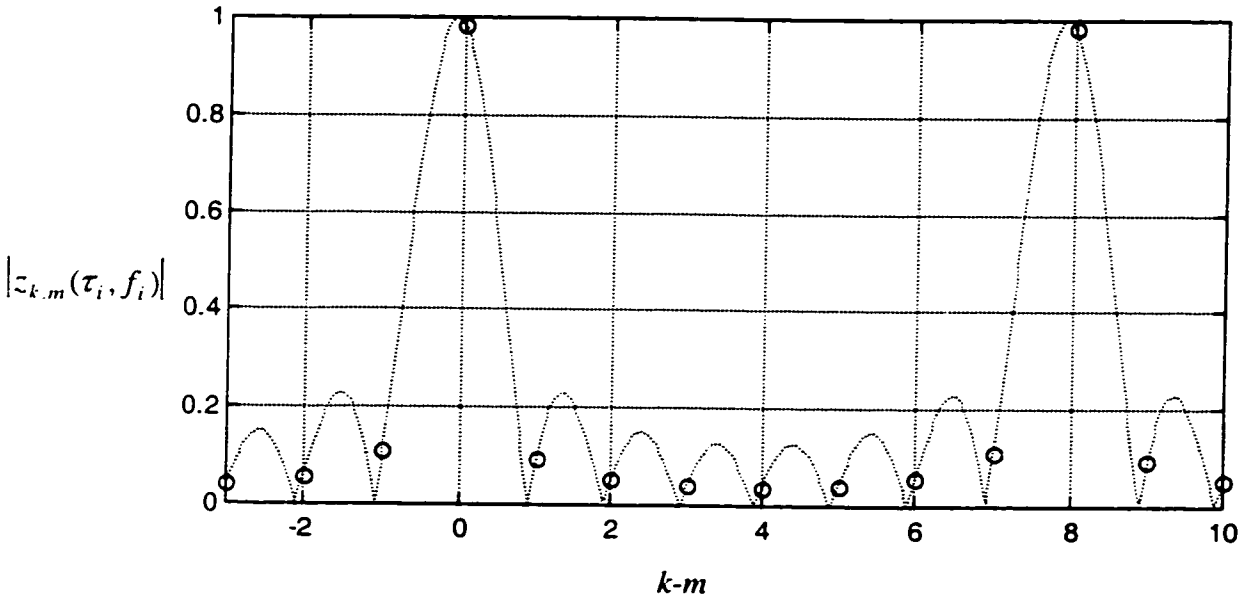

Figure 3-4 Magnitude of ICI function for $f_i T_U = 0.1$. Circles are plotted an integer values of k-m.

To proceed further, let the phase shift, delay and Doppler shift for path i be random variables with the density functions specified in (3.25) and (3.26). The expression for $y_{n,m}^{(i)}$ is then separated into a desired and an ICI component

$$y_{n,m}^{(i)} = H_{n,m}^{(i)} c_{n,m} + n_{n,m}^{(i)} \tag{3.39}$$

where

$$H_{n,m}^{(i)} = \sqrt{\frac{2E_U}{MT_U}} e^{j\Phi_i} e^{j2\pi F_i n T_S} e^{-j2\pi m f_U T_i} e^{j\pi(1-1/\hat{N})F_i T_U} \frac{1}{\hat{N}} \frac{\sin(\pi F_i T_U)}{\sin\left(\frac{\pi}{\hat{N}} F_i T_U\right)} \tag{3.40}$$

is the equivalent discrete time varying transfer function and

$$n_{n,m}^{(i)} = \sqrt{\frac{2E_U}{MT_U}} e^{j\Phi_i} e^{j2\pi F_i n T_S} \sum_{\substack{k=1-N/2 \\ k \neq m}}^{N/2} c_{n,k} e^{-j2\pi k f_U T_i} e^{j\pi\left(1-\frac{1}{\hat{N}}\right)(F_i T_U + k - m)} \frac{1}{\hat{N}} \frac{\sin \pi(F_i T_U + k - m)}{\sin \frac{\pi}{\hat{N}}(F_i T_U + k - m)} \tag{3.41}$$

is the ICI component for the m^{th} carrier.

For sufficiently large N, the summation above results in $n_{n,m}^{(i)}$ being a discrete Gaussian random process. For an exact mathematical treatment of the problem, one should calculate the second

order statistics of this process. However, a simplified analysis will result from treating $n_{n,m}^{(i)}$ a white random process. That is, the ICI contribution from any DFT output is uncorrelated with the ICI contribution from any other DFT output. Consequently the random process can be specified knowing only its variance. This variance will be different for different subcarriers since those near the edge of the band have fewer interfering subchannels. However, a worst case estimate occurs when $N = \hat{N}$, in which case the summation in the above expression is equal for all values of m due to its cyclic nature.

The easiest way to compute the variance of (3.41) is to compute the variance of the combined random variable (3.39) and then subtract the variance of the desired component. It can be shown that the variance of the received symbols is

$$E\{|\, y_{n,m}^{(i)}\,|^2\} = \frac{2E_U}{MT_U} \tag{3.42}$$

One can then compute the variance of the desired component by making some simplifications that are valid when the normalized Doppler spread f_d/f_U is less than about 0.2. The result is

$$E\{|\, H_{n,m}^{(i)} c_{n,m}\,|^2\} = \frac{2E_U}{MT_U}(1-(f_d T_U)^2) \tag{3.43}$$

giving the result for the variance of the ICI component

$$E\{|\, n_{n,m}^{(i)}\,|^2\} = \frac{2E_U}{MT_U}(f_d T_U)^2 \tag{3.44}$$

One may now sum (3.39) over the M independent paths which will just remove the factor of $1/M$ from the variance expressions. Finally adding an AWGN component and normalizing the expression as in section 2.1.3 gives

$$y_{n,m} = H_{n,m} c_{n,m} + n_{ICI} + n_w \tag{3.45}$$

where n_{ICI} represents the ICI component having variance

$$\sigma_{ICI}^2 = (f_d T_U)^2 \tag{3.46}$$

and n_w represents the AWGN component having variance.

$$\sigma_w^2 = N_0 / E_U \tag{3.47}$$

This is the discrete channel model that will be used for analysis of the detection problem in chapters 4 and 5.

To complete the statistical characterization of the channel, it is necessary to calculate the correlation function for the discrete time variant transfer function.

$$\begin{aligned} R_H(\Delta k, \Delta n) &= E\{H_{n+\Delta n,k+\Delta k} H_{n,k}^*\} \\ &= E\left\{ e^{j2\pi F_i \Delta n T_S} e^{-j2\pi \Delta k f_U T_i} \left(\frac{1}{\hat{N}} \frac{\sin(\pi F_i T_U)}{\sin\left(\frac{\pi}{\hat{N}} F_i T_U\right)} \right)^2 \right\} \end{aligned} \tag{3.48}$$

This calculation can be simplified by assuming that the product $f_d T_U$ is small enough that the $\sin(x)/\sin(x/N)$ factor in the above simplifies to $\hat{N}$ resulting in

$$\begin{aligned} R_H(\Delta k, \Delta n) &= E\{e^{j2\pi F_i \Delta n T_S} e^{-j2\pi \Delta k f_U T_i}\} \\ &= \frac{J_0(2\pi \Delta n f_d T_S)}{1 + 2\pi \Delta k f_U \sigma_d} \end{aligned} \tag{3.49}$$

This is just the result for the continuous spaced-time spaced-frequency correlation function (3.29) sampled at the symbol rate and at the subcarrier spacing.

3.3.3 Theoretical BER for differential detection of 4-DPSK OFDM

The decision variables $y_{n,k}$ given by (3.45) appear in the receiver at the output of the DFT. For a conventional differential detector (CDD) the decision on the bit values is based on the real and imaginary parts of $y_{n,k} y_{n-1,k}^*$. Using results in [26] and [28] one can write an expression for the probability of bit error in this case.

$$P_e = \frac{1}{2}\left(1 - \frac{\mu_1}{\sqrt{2\left(1 + \sigma_w^2 + \sigma_{ICI}^2\right)^2 - \mu_1^2}} \right) \tag{3.50}$$

where μ_1 is the correlation between subsequent DFT outputs on a subchannel

$$\mu_1 = R_H(0,1) = J_0(2\pi f_d T_S) \tag{3.51}$$

Figure 3-5 shows a plot of this function for DAB mode IV at various values of the normalized Doppler spread. The parameter E_b refers to the energy per information bit over the entire symbol interval. N_0 is the power spectral density of the AWGN process. For a rate 1/2 code there are two coded bits for each information bit. Each symbol comprises two coded bits so there is one symbol for each information bit. The useful signal interval is 4/5 of the entire interval so $E_U = 4E_b/5$. Simulation results agreeing with the theory are also plotted in the figure. The Matlab program used to generate these results will be discussed in chapter 5.

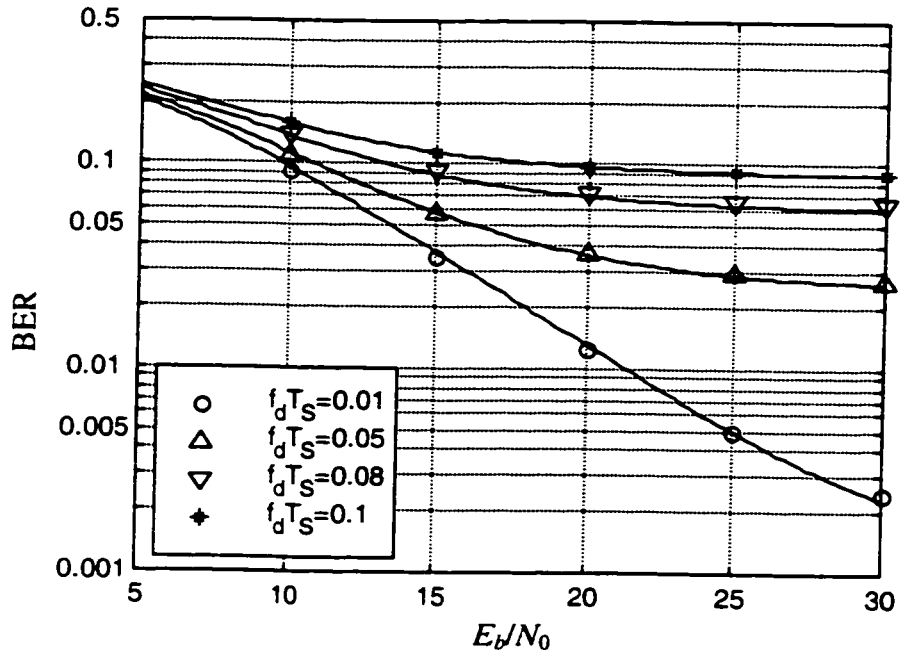

Figure 3-5 Theoretical BER as a function of E_b/N_0 for a conventional differential detector operating on the decision variables given by equation (3.45).

A primary goal of the DAB service is to achieve compact disk quality sound. It has been demonstrated [12] that this requires a decoded sequence bit error rate of 10^{-4} or lower. This must be achieved at a practical value of E_b/N_0 which is in the range of 15 to 20 dB. It is not possible to provide an exact analytical expression for the decoded BER but the simulation results from chapter 5 indicate that a coded sequence BER of about 0.07 or less is required to achieve a decoded BER less than 10^{-4}. From figure 3-5 one sees that this value is just reached in the required range of E_b/N_0 for a normalized Doppler spread of $f_dT_S = 0.08$ but not for higher values

of $f_d T_S$. A normalized Doppler spread of 0.08 translates into a vehicle speed of about 92 km/hr and one would expect significant deterioration of sound quality when the vehicle velocity exceeds this Doppler limit. Since speed limits in Canada are higher than this limit, DAB mode IV cannot be used with a CDD. One alternative is to use other DAB modes having shorter symbol duration and thus higher Doppler limits. However, one would like to be able to use mode IV because of the economic benefits related to the longer guard interval (see section 3.3.1). This motivates the search for OFDM demodulation techniques that will provide better performance than a conventional differential detector at higher values of $f_d T_S$. It would be possible to improve the performance by taking advantage of the RCPC code to achieve a lower code rate but this has not been considered because the resulting decrease in capacity is not acceptable. Also the use of a rate 1/2 code with a longer constraint length is not considered because it would no longer be compliant with the DAB specification.

3.4 Summary

A brief review of the theory of time varying linear systems was presented in this chapter. This was followed by a more in-depth discussion of the theory of randomly time varying linear systems which are usually used to model mobile wireless channels. It was seen that in the general case, the channel transfer function is treated as a random process indexed by two continuous time variables. As a result, the second order characterization of these systems requires an autocorrelation function of four variables. However, one usually applies the WSSUS assumption allowing the autocorrelation to be written as a function of a delay variable τ and a time difference Δt.

Alternate characterizations of the WSSUS channel obtained by Fourier transforming the random process in one or both of the time variables were discussed and the corresponding correlation functions analyzed. Of particular importance is the channel scattering function which indicates the time and frequency dispersion properties of the channel.

Several important parameters used to characterize WSSUS channels were introduced. The delay spread τ_m provides a measure of how an input impulse function is spread over time by the channel. This parameter is important for OFDM because if the guard interval is longer than the delay spread there can be no ISI. The Doppler spread f_d indicates how much an input sinusoid is

spread over frequency by the channel. For OFDM, this parameter determines the amount of ICI caused by the Doppler frequency shifting. Other related parameters are the coherence time Δt_c and the coherence bandwidth Δf_c. The coherence time is a measure of how long some level of correlation will be maintained in the output signal. Input signals with frequency components separated by more than the coherence bandwidth will emerge uncorrelated from the channel.

Physically, a mobile channel comprises many scattered paths between the transmitter and the receiver, and the received signal is the superposition of the signal propagating along these paths. If the number of paths is large enough, the low pass equivalent of the received signal can be characterized very well as a complex Gaussian random process. Periods of time when the modulus of a sample function of this process is much lower than the RMS value are referred to as fades. The average time between fades is proportional to the coherence time of the channel. Fast fading channels have a coherence time and consequently an average time between fades that does not greatly exceed the symbol duration for the digitally modulated transmit signal. Coherent detection of signals over fast fading channels presents difficulties because the received signal loses coherence over the span of several symbols. Differential encoding of the data symbols helps to mitigate this effect but will exhibit a bit error rate floor when detected with a conventional differential detector.

The concepts of time and frequency diversity were introduced and it was shown how the COFDM system used in the DAB attempts to take advantage of both time and frequency diversity to improve performance over fading channels.

A multipath mobile channel model that is easily adaptable to computer simulations was discussed. The model consists of the summation of equally weighted propagation paths with randomly chosen delay and Doppler shift. Analysis of this model showed that as the number of paths becomes large, the random process describing the time varying transfer function is an ergodic Gaussian random process. The spaced time spaced frequency correlation function and the scattering function for the channel model was derived. It was shown that the scattering function of the channel has the same shape as the density functions governing the delay and Doppler shift of the propagation paths.

The channel model was analyzed for its effects on an OFDM signal. It was shown that when the Doppler spread is small relative to the subcarrier spacing, the channel introduces an ICI component that can be modeled as a discrete white noise process added to the receiver output at each DFT tap. It was shown that the discrete outputs of the DFT taps can be modeled as a complex Gaussian random gain multiplied by the transmit symbol with two white Gaussian additive noise terms: one due to ICI and the other due to thermal noise. The correlation function for the random channel gain was derived as the continuous channel correlation function sampled at the subcarrier spacing and the symbol rate.

The chapter concludes with a discussion of the inadequacy of a receiver using a conventional differential demodulator for Mode IV DAB signals at highway vehicle speeds when typical urban propagation parameters are used for the channel model. The next chapter will discuss advanced demodulation techniques that can be used to solve this problem.

4

Advanced Demodulation Techniques for COFDM in Fast Fading Channels

Section 3.3.3 shows that using a conventional differential detector (CDD) to detect the symbol sequence does not provide adequate performance for a typical urban Rayleigh fading channel model at normalized Doppler spreads greater than about $f_d T_S$ = 0.08. However, differential detection does not make very good use of the statistical characterization that has been developed for the fading channel. This chapter investigates techniques for detection of differentially encoded PSK that perform significantly better and are appropriate when a channel model similar to equations (3.45) – (3.47) is valid.

For a DPSK modulation scheme transmitted over a flat fading channel, the BER performance can be improved by sampling the received signal more than once per symbol interval [6]. This might suggest a low complexity scheme for improving the performance of the CDD. However, the technique is not adaptable to an OFDM signal because it is not possible to separate the individual subchannels into signals that can be sampled more than once per symbol interval. Put another way, the retrieval of the transmitted sequence requires correlation with basis functions that last for the duration of the useful symbol interval. This situation cannot be remedied while maintaining the density $f_U T_U$=1 of the time-frequency lattice.

For the discrete channel model given by (3.45) the difficulty is that the discrete subchannel gain $H_{n,k}$ is a random quantity. If this parameter was known or could be estimated, one could solve for a noisy symbol value. Using the statistical model of the channel that has been developed, one can estimate the channel gain using linear minimum mean squared error techniques. The current gain is estimated by a linear combination of previous gain values. These can be calculated using previous decisions on symbol values. This decision feedback linear predictive technique [9], [34], [35] has been shown to improve BER performance for OFDM signals in fast fading channels.

Maximum likelihood sequence detection (MLSD) is a technique that chooses the most probable symbol sequence given the observed sequence of detection variables at the demodulator output. Based on the statistical channel model, one can write an expression for the multivariate probability density function for the receiver output sequence conditioned on the transmitted sequence, leading to ML detection [18]. This technique can reduce or even remove the BER floor that is evident in figure 3-5 for the CDD. It can also provide several dB of improvement at lower values of the signal to noise ratio E_b/N_0 before the error floor is reached. A direct implementation of the ML detection is computationally intensive because it requires a search over 4^N possible sequences to detect an N-symbol long transmitted word. A simplification results from using a linear predictive technique [23], [41], [42] which allows the use of the Viterbi algorithm to identify the ML sequence. This technique can be further developed [10] to perform a symbol by symbol MAP detection.

A somewhat different technique for detection in flat fading channels is to expand the fading process over a short time interval using a Karhunen-Loeve or a Taylor series. When the time interval in question is sufficiently small compared to the coherence time of the channel, it is valid to truncate the expansion to a few terms. Detection is then accomplished by using a filter bank where each filter is matched to a term of the series expansion [21]. The detection variables so produced can then be combined in various ways to make a decision on the transmitted symbol. This technique is capable of eliminating the BER floor associated with a conventional differential detector in a fast fading channel [38], [40], [43]. This technique will be discussed and shown to be inappropriate for OFDM because the filters that are matched to the higher order expansion terms introduce an unacceptably large ICI component into the output variable.

4.1 Decision Feedback Linear Prediction of Subchannel Gain

4.1.1 Decision feedback linear prediction detector for OFDM

From equation (3.45) the received symbols at the output of the DFT will be given by

$$y_{n,k} = H_{n,k} c_{n,k} + n_{n,k} \tag{4.1}$$

where $n_{n,k}$ is a discrete Gaussian random process that is the summation of the contributions from the ICI and the AWGN. The variance of $n_{n,k}$ is

$$\sigma^2 = \sigma_{ICI}^2 + \sigma_w^2 \tag{4.2}$$

Also the random process $n_{n,k}$ is white and independent of the process $H_{n,k}$. One would like to predict the channel gain $H_{n,k}$ for the n^{th} symbol based on the noisy channel gains $\tilde{H}_{n-l,k}$ from previous symbols. These noisy channel gains can be calculated by

$$\tilde{H}_{n-l,k} = y_{n-l,k} c_{n-l,k}^* = H_{n-l,k} + n_{n-l,k} \tag{4.3}$$

The true values of the $c_{n-l,k}$ are not known. However, one can adopt the standard technique of feeding back previous decisions to calculate $\tilde{H}_{n-l,k}$. An order L linear predictor for $H_{n,k}$ is given by

$$\hat{H}_{n,k} = \sum_{l=1}^{L} a_l \tilde{H}_{n-l,k} = \mathbf{a}^H \mathbf{u} \tag{4.4}$$

where $\mathbf{a}$ and $\mathbf{u}$ are $L\times 1$ matrices defined as follows

$$\begin{aligned} \mathbf{a}^H &= \begin{bmatrix} a_1 & a_2 & \cdots & a_L \end{bmatrix} \\ \mathbf{u} &= \begin{bmatrix} \tilde{H}_{n-1,k} & \tilde{H}_{n-2,k} & \cdots & \tilde{H}_{n-L,k} \end{bmatrix}^T \end{aligned} \tag{4.5}$$

The phase of $\hat{H}_{n,k}$ can then be used to estimate the current symbol value

$$\hat{c}_{n,k} = y_{n,k} \hat{H}_{n,k}^* / |\hat{H}_{n,k}| \tag{4.6}$$

The estimated information symbol $a_{n,k}$ is then obtained by comparing the phase of $\hat{c}_{n,k}$ with the phase of the previous symbol decision $c_{n-1,k}$.

One can apply standard linear prediction theory [15], [27] to determine the coefficients of the optimum L^{th} order linear predictor.

$$\mathbf{a} = \mathbf{R}^{-1}\mathbf{p} \tag{4.7}$$

where $\mathbf{R}$ is the correlation matrix for the fading process plus noise whose entries are given by

$$[\mathbf{R}]_{m,n} = R_H(0, m-n) + \sigma^2\delta_{m,n} \tag{4.8}$$

and

$$\mathbf{p} = \begin{bmatrix} R_H(0,-1) & R_H(0,-2) & \cdots & R_H(0,-L) \end{bmatrix}^T \tag{4.9}$$

is a $L\times 1$ matrix whose entries are the correlation between the current and previous channel gains. The mean squared error in the optimum linear predictor is given by

$$J_{\min} = E\{|H_{n,k} - \hat{H}_{n-k}|^2\} = 1 - \mathbf{p}^H\mathbf{R}^{-1}\mathbf{p} \tag{4.10}$$

for the normalized channel. The correlation between channel gains on different subchannels is given by equation (3.29) and it is possible to incorporate this in a prediction based on previous channel gain values from more than one subchannel. This is a straightforward extension of the theory for a single channel. The predictor using K adjacent subchannels is equation (4.4) with $\mathbf{u}$ redefined as the $KL\times 1$ matrix

$$\begin{aligned} \mathbf{u} &= \begin{bmatrix} \mathbf{u}_{k+M} & \mathbf{u}_{k+M-1} & \cdots & \mathbf{u}_{k-M} \end{bmatrix}^T \\ \mathbf{u}_k &= \begin{bmatrix} \tilde{H}_{n-1,k} & \tilde{H}_{n-2,k} & \cdots & \tilde{H}_{n-L,k} \end{bmatrix} \end{aligned} \tag{4.11}$$

The parameter $M=(K-1)/2$ is the number of subchannels on either side that are used for the prediction. The correlation matrix $\mathbf{R}$ is now given by

$$\mathbf{R} = E\{\mathbf{u}\mathbf{u}^H\} \tag{4.12}$$

and $\mathbf{p}$ is

$$\mathbf{p} = E\{\mathbf{u}H_{n,k}^*\} \tag{4.13}$$

The mean squared predictor error is still as given by equation (4.10).

Direct evaluation of the prediction coefficient matrix **a** involves the computation of the inverse of the correlation matrix **R**. For typical mobile channel correlation functions, this matrix may be nearly singular for small values of σ^2 and direct evaluation of the predictor coefficients by means of (4.7) is not possible. In this case one can resort to an alternate technique such as singular value decomposition [11].

A drawback of the decision feedback LP approach is that it initially requires N previous known symbol values. For the DAB signal, every subchannel transmits one reference symbol per frame. A simple way to initialize the LP detector would be to use a CDD for the N-1 symbols following the reference symbol providing the initial N decisions to feed back to the channel estimator. A related technique would be to detect the symbol following the reference symbol with an N=1 LP detector (equivalent to a CDD), then detect the next symbol with a N=2 detector, and so on until the required number of previous decisions are available.

4.1.2 Theoretical probability of bit error for perfect decision feedback

It is not difficult to calculate the theoretical error probability when all of the fed back decisions are correct. In this case each error in the decision of the current value of the transmitted symbol translates into an error in the differentially encoded symbol. Therefore the BER for the 4-DPSK symbols is equal to that for demodulation of 4-PSK with a noisy channel estimate. In appendix C of [28], an expression for the theoretical error probability for M-PSK in a slowly fading Rayleigh channel with a channel gain estimate is developed. The formula for 4-PSK is

$$P_e = \frac{1}{2}\left(1 - \frac{\mu}{\sqrt{2-\mu^2}}\right) \tag{4.14}$$

and μ is a correlation coefficient between the channel estimate and the actual noisy channel gain defined as

$$\mu = \frac{E\{\tilde{H}_{n,k}\hat{H}^*_{n,k}\}}{\sqrt{E\{|\tilde{H}_{n,k}|^2\}E\{|\hat{H}_{n,k}|^2\}}} \tag{4.15}$$

Since the prediction error is uncorrelated with the estimate, $E\{\tilde{H}_{n,k}\hat{H}^*_{n,k}\} = E\{|\hat{H}_{n,k}|^2\}$. The variance of the gain estimate is given by the variance of the channel gain minus the mean squared error (4.10) so the correlation coefficient evaluates to

$$\mu = \sqrt{\frac{\mathbf{p}^H \mathbf{R}^{-1} \mathbf{p}}{1+\sigma^2}} \tag{4.16}$$

Equation (4.14) provides a lower bound on the BER because errors in the fed back decisions will cause larger errors in the channel gain estimates and thus more errors in the symbol decisions. The actual error probability in this case is very difficult to calculate and is best determined by simulations.

4.1.3 Application to COFDM

Figure 4-1 shows a plot of the theoretical BER as a function of E_b/N_0 for the case of perfect decision feedback at various values of the normalized Doppler spread. The BER reaches 0.07 at E_b/N_0 =15 dB for f_dT_S = 0.1. Section 3.3.3 indicates that for soft Viterbi decoding of a CDD output, a BER of 0.07 can be improved to the target BER value of 10^{-4}. If a similar improvement can be obtained with soft Viterbi decoding of the LP detector outputs, then the target BER could be met for E_b/N_0 over 15 dB with normalized Doppler spreads in excess of 0.1.

In the simulation results presented in chapter 5, it will be shown that the actual performance of the LP detector is significantly worse than the idealized performance due to fed back errors and as a result the target BER cannot be met. To achieve a BER closer to the theoretical lower bound, the error rate in the fed back decisions needs to be reduced significantly. An obvious way to do this is to feed back the Viterbi decoded decisions rather than the LP detector output decisions. This immediately suggests an iterative receiver structure as shown in figure 4-2 (a). If convergence is achieved, the fed back error rate will tend to decrease with each successive iteration and thus the BER at the LP detector output will approach the curves in figure 4-1. This in turn suggests that it would be possible to meet the target BER for the decoded sequence in the required range of E_b/N_0.

The alternative iterative receiver depicted in figure 4-2 (b) solves problems related to the initialization of the LP detector. The first iteration of the receiver is done with a CDD requiring

only the one reference symbol for initialization. Subsequent iterations are done using just decoded decisions from the previous iteration and thus require no special initialization considerations.

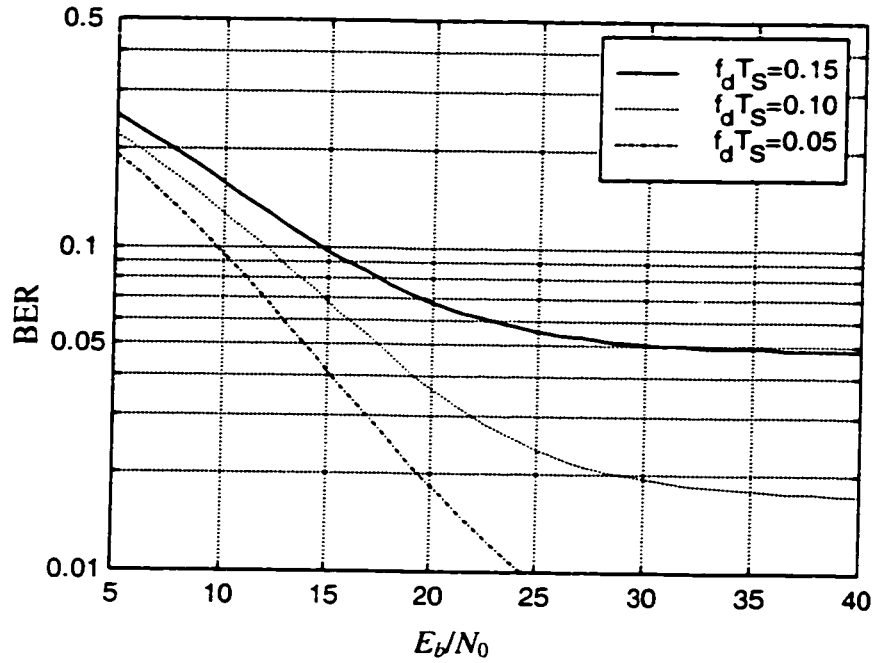

Figure 4-1 Linear prediction detector theoretical BER when there are no errors in the decision feedback. The linear predictor used N=5 previous channel gain values and K=1 subchannel.

4.1.4 Estimation of channel correlation function

The above discussion assumes a channel model given by (3.45) with an autocorrelation function (3.49). To calculate the optimum linear predictor, the receiver must know the normalized maximum Doppler spread, the channel delay spread and the noise variance. The DAB specification calls for one null symbol at the start of each frame. During this symbol, no signal is transmitted on any of the OFDM subcarriers. This provides a convenient opportunity for the receiver to measure the level of the additive noise.

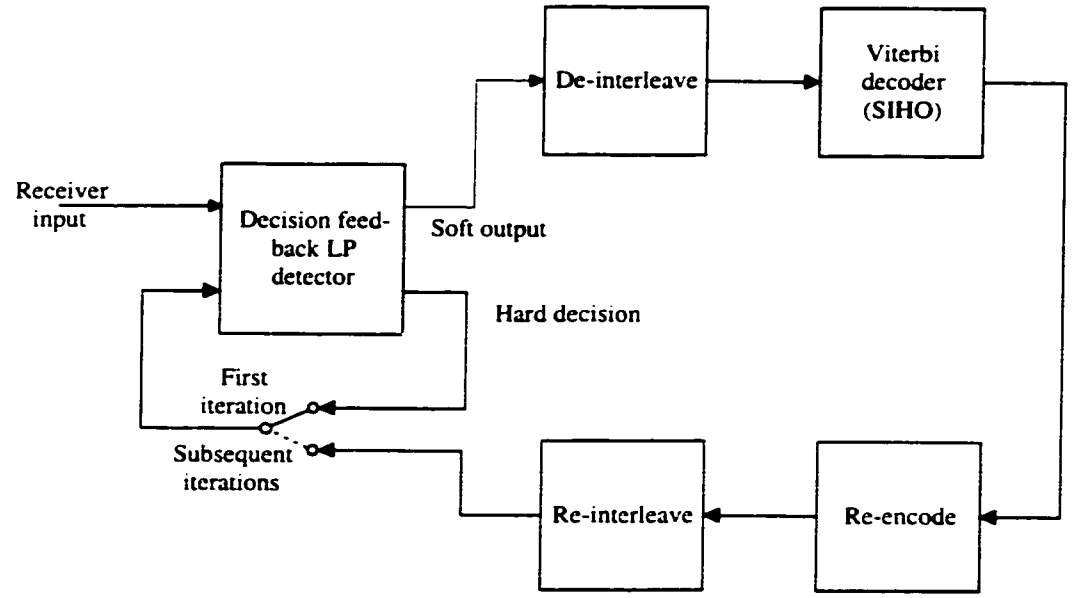

(a) Iterative decision feedback LP receiver

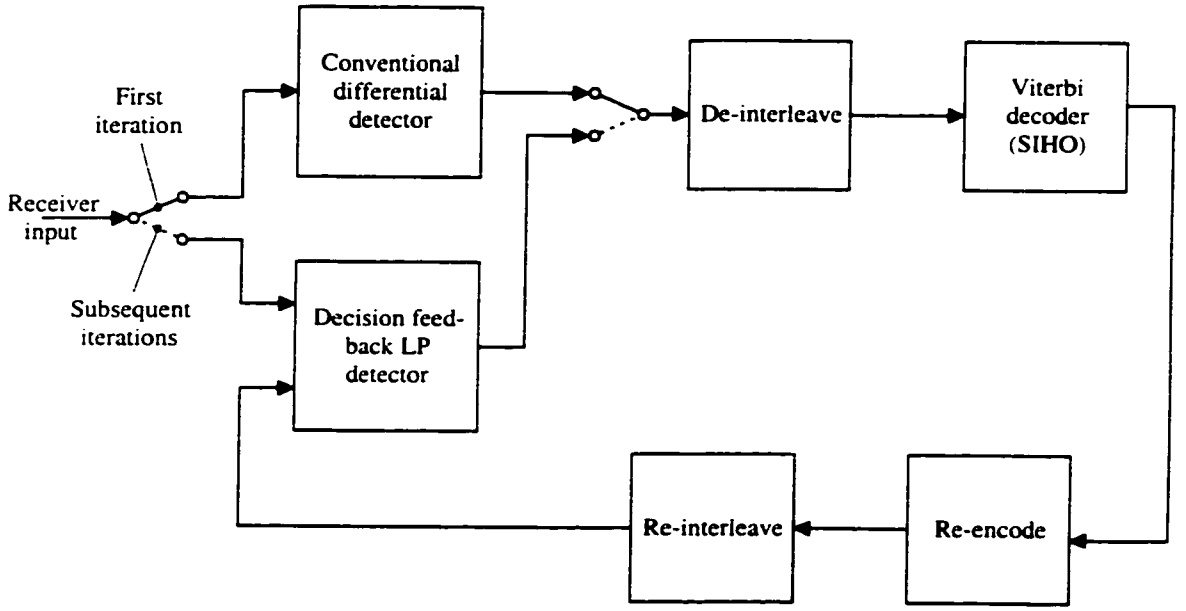

(b) Iterative decision feedback LP receiver with CDD for first iteration

Figure 4-2 Block diagram of iterative decision feedback LP receiver.

One technique for estimating the maximum Doppler spread is to count the number of times the modulus of the received signal crosses a certain level in a second. This parameter, referred to as the level crossing rate, can be related to the maximum Doppler frequency by [45]

$$r_c = \sqrt{2\pi} f_d \frac{\rho}{\sqrt{2}\sigma} e^{-\frac{1}{2}\left(\frac{\rho}{\sigma}\right)^2} \tag{4.17}$$

where ρ is the crossing threshold and $\sqrt{2}\sigma$ is the root mean squared value of the received signal modulus. To estimate the level crossing rate one can simply count the number of times the modulus of the received signal on a certain subchannel or collection of subchannels crosses the threshold in a certain time interval and then divide by this time interval. The channel delay spread is only of interest when one wants to use more than one subchannel in the linear prediction. This could be estimated by a dual process of that used for estimating f_d consisting of counting level crossings in the frequency domain: that is, observe how many times the modulus of the received sequence $y_{n,k}$, k=1-N/2, 2-N/2, ..., N/2 crosses a certain threshold level.

The expression for the discrete spaced frequency, spaced time correlation function $R_H(\Delta k, \Delta n)$ (3.49) relies on certain assumptions about the channel model. The correlation function can be calculated without any such assumption (other than ergodicity) by taking time averages of the observed channel gain values. As discussed previously, these values are not known but may be calculated by decision feedback. If the error rate in the fed back sequence is small the correlation function calculated in this way will be close to the true correlation function. Using the iterative scheme of figure 4-2 (b) the channel estimation is not required for the CDD on the first iteration. During startup, the receiver could run for a certain amount of time using just the CDD and feed back decoded decisions to calculate an estimate of the channel correlation function.

If one only requires a linear prediction based on a single subchannel, then the theory of adaptive filtering can be readily applied. The well known least mean squares (LMS) and recursive least squares (RLS) adaptive filtering techniques [15] allow for the recursive updating of the linear predictor coefficients without the explicit calculation of the channel correlation function. To adapt these techniques to the prediction of the channel gain $H_{n,k}$ would require observations of this channel gain. However, one can only observe the noisy version of the channel gain $\tilde{H}_{n,k}$ (by decision feedback). To circumvent this, the adaptive filtering techniques can be used to form a linear predictor for the noisy channel gain. Because the additive noise is assumed white and independent of the channel gain, this predictor is exactly the same as the predictor for $H_{n,k}$. The iterative receiver of figure 4-2 (b) allows one to obtain the time series $\tilde{H}_{n,k}$ using the decoded

decisions from the CDD. On higher iterations, an LMS or RLS linear predictor could then be run using this sequence as the desired signal.

4.2 Maximum Likelihood Sequence Detection

4.2.1 Direct formulation

Maximum likelihood sequence detection selects an estimate of the transmitted symbol sequence based on the maximum likelihood criterion: choose the transmit sequence that maximizes the conditional probability density function for the received sequence. One means of adapting this technique to an OFDM signal is to perform a separate MLSD on the symbols from each subchannel. Accordingly, the following $N\times 1$ matrices whose entries are N consecutive transmit symbols and received variables are defined. At this point it is no longer necessary for the development to distinguish between subchannels, and therefore the subchannel subscript k is dropped.

$$\begin{aligned} \mathbf{y}_N &= [y_1 \quad y_2 \quad \cdots \quad y_N]^T \\ \mathbf{c}_N &= [c_1 \quad c_2 \quad \cdots \quad c_N]^T \end{aligned} \tag{4.18}$$

To perform MLSD one must determine the multivariate probability density function for the received sequence conditioned on the transmitted symbol sequence. The received random variables $y_{n,k}$ given by (3.45) are zero mean complex Gaussian and their joint probability density function is given by [27]

$$p(\mathbf{y}_N \,|\, \mathbf{c}_N) = \frac{1}{\pi^N \,|\mathbf{\Lambda}|} \exp(-\mathbf{y}_N^H \mathbf{\Lambda}^{-1} \mathbf{y}_N) \tag{4.19}$$

The notation $p(\mathbf{y}_N|\mathbf{c}_N)$ indicates the joint probability density function for the received sequence $y_1, y_2, \ldots, y_N$ conditioned on the transmitted sequence $c_1, c_2, \ldots, c_N$. The correlation matrix Λ is given by

$$\mathbf{\Lambda} = E\{\mathbf{y}_N \mathbf{y}_N^H\} = \mathrm{diag}(\mathbf{c}_N)\mathbf{R}^{-1}\mathrm{diag}(\mathbf{c}_N^*) \tag{4.20}$$

where the m,n^{th} entry in the matrix $\mathbf{R}$ is given by (4.8)

Because the PSK symbols have constant modulus, the determinant $|\Lambda|$ is independent of the symbol sequence sent. The density function (4.19) thus reaches its maximum value when the exponent takes the lowest value and therefore one must choose the transmitted sequence that minimizes the maximum likelihood metric

$$\Gamma_N = \mathbf{y}_N^H \mathrm{diag}(\mathbf{c}_N)\mathbf{R}^{-1}\mathrm{diag}(\mathbf{c}_N^*)\mathbf{y}_N \tag{4.21}$$

Conceptually this is quite simple. Substitute the observed values of the received sequence $y_{n,k}$ into (4.21), then evaluate Γ_N for every possible transmitted sequence $\mathbf{c}_N$. Choose the $\mathbf{c}_N$ that yielded the smallest value of Γ_N. The complexity of this approach increases exponentially with the sequence length N. The direct implementation of this approach is thus computationally infeasible.

4.2.2 Trellis based approach

Providing that the fading process $H_{n,k}$ of (3.45) can be approximated by an autoregressive process in the n index, of order L, it is possible to adopt a trellis based approach to the evaluation of the ML metric for a symbol sequence. The states of the trellis represent the L most recent transmitted symbols c_n, c_{n-1}, ..., c_{n-L+1}. The branches of the trellis emerging from each state correspond to the possible information symbols transmitted. For $\pi/4$-shift 4-DPSK there are 8 possible transmit symbols at time n. For each of these symbols there are 4 possible symbols at time n-1 and so on. There are therefore $2(4^L)$ trellis states. Four branches corresponding to the four possible information symbols emerge from each state.

The development of the trellis based approach starts with theorem 1 in [23]. This says that the inverse correlation matrix in (4.20) may be factored as follows:

$$\mathbf{R}^{-1} = \mathbf{U}^H \mathbf{D} \mathbf{U}$$

$$= \begin{bmatrix} 1 & -a_{1,1}^* & -a_{2,2}^* & & -a_{N-1,N-1}^* \\ 0 & 1 & -a_{2,1}^* & \cdots & -a_{N-1,N-2}^* \\ 0 & 0 & 1 & & -a_{N-1,N-3}^* \\ & \vdots & & \ddots & \\ 0 & 0 & 0 & & 1 \end{bmatrix} \begin{bmatrix} 1/J_0 & 0 & 0 & & 0 \\ 0 & 1/J_1 & 0 & \cdots & 0 \\ 0 & 0 & 1/J_2 & & 0 \\ & \vdots & & \ddots & \\ 0 & 0 & 0 & & 1/J_{N-1} \end{bmatrix}$$

$$\begin{bmatrix} 1 & 0 & 0 & & 0 \\ -a_{1,1} & 1 & 0 & \cdots & 0 \\ -a_{2,2} & -a_{2,1} & 1 & & 0 \\ & \vdots & & \ddots & \\ -a_{N-1,N-1}^* & -a_{N-1,N-2} & -a_{N-1,N-3} & & 1 \end{bmatrix} \tag{4.22}$$

where $a_{i,j}$ is the j^{th} coefficient of the i^{th} order linear predictor for the fading process $H_{n,k}$ based on the observed process $H_{n,k}+n_{ICI}+n_w$. If the process $H_{n,k}$ is autoregressive of order L or if it can be approximated by an autoregressive process of order L, then all entries in the matrix $\mathbf{U}$ that are located L or more positions to the left of the diagonal can be set to zero. Also the mean squared predictor errors J_n will be equal for $n \geq L$. When this is done, the matrix product (4.22) can be arranged in the following recursive form (leaving out the constant factor $1/J_L$)

$$\begin{aligned} \Gamma_n &= \Gamma_{n-1} + (y_n^* c_n - a_{L,1}^* y_{n-1}^* c_{n-1} - a_{L,2}^* y_{n-2}^* c_{n-2} - \cdots - a_{L,L}^* y_{n-L}^* c_{n-L}) \\ &\qquad (y_n c_n^* - a_{L,1} y_{n-1} c_{n-1}^* - a_{L,2} y_{n-2} c_{n-2}^* - \cdots - a_{L,L} y_{n-L} c_{n-L}^*) \\ &= \Gamma_{n-1} + \left| y_n - c_n \sum_{i=1}^{L} a_{L,i} y_{n-i} c_{n-i}^* \right|^2 \end{aligned} \tag{4.23}$$

The product $y_{n-i}c_{n-i}^*$ in the above is equal to the channel gain during interval n-i given that c_{n-i} was transmitted. The summation in (4.23) is thus an L^{th} order linear prediction $\hat{H}_{n,k}$ of the channel gain $H_{n,k}$ given that the previous L symbols were c_{n-1}, c_{n-2}, ..., c_{n-L}. The product $c_n \hat{H}_{n,k}$ is thus the prediction of the received signal given that the symbol c_n was transmitted in the current symbol interval. Therefore it can be seen that each update to the metric is the squared Euclidean distance between the received value and the predicted received value. The ML sequence is thus the one that for each symbol minimizes the Euclidean distance between the actual received value and the L^{th} order linear prediction of that received value. Thus the ML detector is equivalent to the decision feed back LP detector discussed previously, except that one

searches for the minimum Euclidean distance over all possible previous L symbol sequences rather than using the symbol by symbol decisions on the previous L symbols.

The complexity of the trellis based approach is still quite high. For instance, supposing that the predictor order is as low as 2, one would still have to compute $4\times2\times4^2=128$ branch metrics for each new symbol.

4.2.3 Application to COFDM

It is conceptually possible to do a ML sequence detection for the COFDM system: take every possible information sequence, convolutionally encode it, interleave it, differentially encode it and substitute it into the ML metric (4.21). Choose the information sequence that yields the lowest value of this metric. If every possible information sequence is equally probable, and the channel model is valid, this process will minimize the probability of a sequence error. This is obviously not feasible in practice.

A suboptimal but computationally feasible procedure is to perform the MLSD, then de-interleave the sequence and perform Viterbi decoding. As mentioned in section 3.3.3, soft Viterbi decoding of a CDD output with a BER of about 0.07 will meet the target BER of 10^{-4}. The linear predictive ML technique with predictor order L=2 has been shown to achieve a BER of 0.07 at an equivalent E_b/N_0 of about 18 dB for a Doppler spread of $f_dT_S = 0.1$ [41]. The problem here is that hard Viterbi decoding of the detected sequence will not provide the same error rate improvement as soft Viterbi decoding of the CDD output. However, if the hard decisions are weighted by some measure of how confident one is in these decisions, the Viterbi decoder will perform much better and may be expected to achieve the same improvement in error rate as the soft Viterbi decoder operating on CDD output. One could argue that when the channel is in a fade, the noise component of the receiver outputs is more likely to make the metric update in (4.8) smaller for the incorrect symbol value and thus we are likely to make a mistake in this case. Thus a simple weighting factor to use on the Viterbi decoder inputs would be the modulus squared of the received signal.

4.3 Series Expansion of Time Varying Channel

4.3.1 Double filtering approach for flat fading

For time invariant AWGN channels, matched filtering is achieved by correlating the received signal with the complex conjugate of the received signaling pulse. In fact, the DFT processing of the OFDM signal is essentially a discrete implementation of a filter matched to the OFDM rectangular pulse shape. The output of the matched filter is a random variable that can be further processed to make an optimum decision on the transmitted symbol. With a flat fast fading channel this presents a problem because the received signal pulse shape varies with time and matched filtering would require time varying filters. To avoid this the fading process can be expanded in a series and the received signal can be filtered with a bank of time invariant filters, each matched to one of the terms in the series.

If the coherence bandwidth of the time varying channel is sufficiently large then the time variant transfer function $H(f,t)$ is essentially constant over the bandwidth occupied by one OFDM subchannel. In this case the received signal for the k^{th} OFDM subchannel is (see table 3-1, row 2)

$$y_k(t) = \sqrt{\frac{2E_U}{T_U}} H(kf_U, t) \sum_n c_{n,k} e^{j2\pi k f_U (t - nT_S)} p_S(t - nT_S) + n(t) \tag{4.24}$$

The time varying gain $H(kf_U, t)$ is a complex zero mean Gaussian random process with an autocorrelation function given by (3.29) with Δf=0. In [40] the authors demonstrate that when the normalized Doppler spread of the channel satisfies $f_d T_S < 0.2$, it is valid to truncate the Taylor series expansion of the fading process over symbol interval n to two terms:

$$H(kf_U, t) \cong H_{n,k}(0) + H_{n,k}(1)\left(\frac{t - nT_S - T_U/2}{T_S}\right) \tag{4.25}$$

where the $H_{n,k}(i)$ are zero mean complex Gaussian random variables having correlation

$$E\left\{H_{n+l,k}(i) H^*_{n,k}(j)\right\} = \frac{(-1)^j T_S^{i+j}}{i!\, j!} \left.\frac{d^{i+j}\left(R_H(0,\tau)\right)}{d\tau^{i+j}}\right|_{\tau = lT_S} \tag{4.26}$$

Substituting (4.25) into (4.24) produces the following expression for the received signal which is valid over useful symbol interval n

$$y_{n,k}(t) = \sqrt{2E_U}\left[H_{n,k}(0)\varphi_{n,k}^{(0)}(t) + \frac{T_U}{\sqrt{12}T_S} H_{n,k}(1)\varphi_{n,k}^{(1)}(t) \right] c_{n,k} + n(t) \tag{4.27}$$

The normalized expansion functions $\varphi_{n,k}^{(0)}(t)$ and $\varphi_{n,k}^{(1)}(t)$ are defined as

$$\varphi_{n,k}^{(0)}(t) = \frac{p_U(t - nT_S)}{\sqrt{T_U}} e^{j2\pi k f_U (t - nT_S)} \tag{4.28}$$

$$\varphi_{n,k}^{(1)}(t) = \sqrt{\frac{12}{T_U^3}} (t - nT_S - T_U/2) e^{j2\pi k f_U (t - nT_S)} p_U(t - nT_S) \tag{4.29}$$

where $p_U(t)$ is a unit pulse function that is zero outside the interval $[0,T_U]$. Thus the received signal can be approximated over one useful symbol interval by a linear function plus noise. Both the slope and intercept of the linear function are Gaussian random variables. For each symbol interval the double filtering technique requires that the received signal be processed by a filter matched to a constant rectangular pulse and one matched to a linear pulse. This filtering is equivalent to correlating with the complex conjugate of the expansion functions (4.28) and (4.29).

The series expansion technique for multicarrier modulation requires that the expansion functions (4.28), (4.29) satisfy [21]

$$\int_{-\infty}^{\infty} \varphi_{n,k}^{(i)}(t) \left(\varphi_{n,l}^{(j)}(t)\right)^* dt = 0 \tag{4.30}$$

for all $k \neq l$ and $i \neq j$. That is, the expansion functions for the received random process must be orthogonal at the different OFDM sub-carrier frequencies. In standard frequency division multiplexing systems, this is ensured by spacing the channels far enough apart that there is little or no overlap between occupied frequency bands. If condition (4.30) was fulfilled, the output of the two filters would be

$$y_{n,k}^{(0)} = \sqrt{2E_U}\,H_{n,k}(0)c_{n,k} + n_{n,k}$$
$$y_{n,k}^{(1)} = \frac{T_U}{T_S}\sqrt{\frac{E_U}{6}}H_{n,k}(1)c_{n,k} + n_{n,k} \tag{4.31}$$

The decision variables consist of a random channel gain multiplied by the transmitted symbol plus a noise term. This is similar to the situation for the standard OFDM receiver represented by (3.45) except that now there are two decision variables for each symbol interval. The statistics of the channel gain processes are given by (4.26) so it is possible to adopt an optimal or sub-optimal decision strategy for each OFDM subchannel based on the observables. For example, one could develop an expression for the multivariate density function for the observed random variables and then base a MLSD on this.

In [40] a maximum likelihood decision procedure for 4-DPSK based on the observation of two subsequent symbols is developed. For $E_b/N_0 > 20$ dB, the BER of this detector is less than the BER of the MLSD discussed in section 4.2.3. This MLSD based its decision on the observation of the current received symbol and two previous received symbols, a total of one more than for the double filtering technique. This is a good indication that the extra information gained by the observation of the linear term improves performance. The same sort of performance enhancement can be obtained by doing a MLSD based on observations of the received signal more that once per symbol interval. However, as discussed in the introduction to this chapter, it is not possible to do this for OFDM. In the range of E_b/N_0 of interest (15-20 dB), the performance is comparable to the MLSD.

4.3.2 ICI for double filtering technique applied to OFDM

Based on the discussion above, the double filtering technique would appear to be promising for COFDM demodulation. However, the discussion above is only valid if condition (4.30) is fulfilled. Unfortunately for an OFDM signal, this is not the case and the output of the filter that is matched to the linear series expansion term has ICI components that are large enough to make it essentially useless. Defining the ICI function as:

$$z_{k,l}^{(i,j)} = \left\langle \varphi_{n,k}^{(i)}(t) \middle| \varphi_{n,l}^{(j)}(t) \right\rangle \tag{4.32}$$

one can evaluate

$$z_{k,l}^{(1,0)} = z_{l,k}^{(0,1)} = \begin{cases} 0 & k = l \\ \dfrac{j\sqrt{3}}{\pi(l-k)} & k \neq l \end{cases}$$
$$z_{k,l}^{(1,1)} = \begin{cases} 1 & k = l \\ \dfrac{6}{\pi^2(l-k)^2} & k \neq l \end{cases} \tag{4.33}$$

and the true expressions for the decision variables are

$$y_{n,k}^{(0)} = \sqrt{2E_U}\left(H_{n,k}(0)c_{n,k} + \frac{T_U}{\sqrt{12}T_S}\sum_{l} z_{l,k}^{(1,0)} H_{n,l}(1)c_{l,k} \right) + n_{n,k} \tag{4.34}$$

$$y_{n,k}^{(1)} = \sqrt{2E_U}\left(\frac{T_U}{\sqrt{12}T_S} H_{n,k}(1)c_{n,k} + \sum_{l} z_{l,k}^{(0,1)} H_{n,l}(0)c_{l,k} + \frac{T_U}{\sqrt{12}T_S}\sum_{l\neq k} z_{l,k}^{(1,1)} H_{n,l}(1)c_{l,k} \right) + n_{n,k} \tag{4.35}$$

The second term in (4.34) corresponds to the ICI term in equation (3.45) for the standard OFDM detection technique. It has been shown that this term is manageable for normalized Doppler spreads around $f_d T_S$ = 0.1. However, the second and third terms in (4.35) are quite large in relation to the first term which is the desired term. This can be seen by referring to figure 4-3 which is a plot of the ICI functions for k-l varying between 0 and 10 subchannels. In fact the

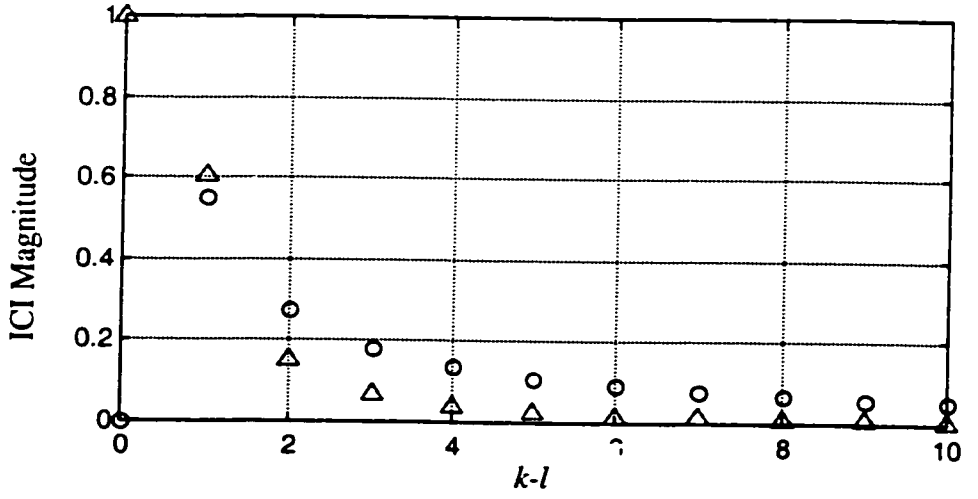

Figure 4-3 Magnitude of ICI functions $z_{k,l}^{(1,0)}$ (circles) and $z_{k,l}^{(1,1)}$ (triangles) as a function of k-l.

variance of $H_{n,l}(0)$ is considerably larger than the variance of $H_{n,k}(1)$ so the ICI represented by the second term of (4.35) is larger than the desired signal. This level of ICI renders the decision variable of no use in improving the detection performance for the OFDM signal

.4.4 Iterative Soft Decision Feedback

4.4.1 Symbol by symbol MAP demodulation of OFDM signal

In section 4.2 it was shown that a trellis structure could be used to realize a ML sequence detection for each subchannel of the OFDM signal. In [10] this technique is extended to allow for symbol by symbol MAP detection of a CPM or DPSK signal over a fast fading channel. The extension is basically analogous to the generalization of the Viterbi algorithm to a forward and backward recursion to achieve MAP decoding of convolutional codes [1], [16]. The MAP detection alone does not provide significant performance improvement over a MLSD. The advantage of MAP decoding is that it allows for the use of a-priori symbol probabilities and outputs conditional a-posteriori symbol probabilities. For the COFDM system, these output probabilities could be de-interleaved and used as the soft input to a Viterbi decoder or another MAP decoder. This would definitely perform better than a hard input Viterbi decoding of the MLSD outputs but may not be better than soft input Viterbi decoding using MLSD decisions and channel state information. The greatest potential advantage of the MAP detector occurs when there is some knowledge of the a-priori symbol probabilities. Such knowledge is available for coded sequences and it can be practically obtained using fed back soft decisions as discussed in the next section.

4.4.2 Iterative receiver structure with soft decision feedback

In the block diagram of figure 4-2, the Viterbi decoder is labeled as a soft input hard output (SIHO) device. That is, it operates on the soft output sequence from the LP detector and produces hard decisions that are fed back for a subsequent iteration of the LP detector. This hard decision feedback entails a loss of information. If the Viterbi decoder was replaced with soft input soft output (SISO) device such as a MAP or soft-output Viterbi algorithm (SOVA) decoder, this loss could be avoided and the soft decisions fed back would be suitable for use as the a-priori probability inputs to the MAP demodulator discussed above. Therefore, by replacing

the LP detector in figure 4-2 with a MAP demodulator and replacing the Viterbi decoder with a soft-in soft-out decoder, one obtains an iterative soft decision feedback detector. This type of iterative structure is similar that used for so called "turbo" decoding of serial concatenated codes [16] which achieves a significant performance advantage at the expense of an increase in computational complexity.

Recently published results for such a demodulation technique [19] show that this iterative technique provides a significant performance improvement over MAP or ML detection followed by a decoder at a normalized Doppler spread of $f_dT_S = 0.01$. Unfortunately, there was only a marginal improvement at $f_dT_S = 0.05$ and this finding is likely to carry over to higher values of normalized Doppler spread. The modulation scheme used in this reference was a single carrier 4-DPSK with the same rate 1/2 convolutional code used in our simulations. Considering this result, and the complexity of the iterative soft decision feedback scheme, it is deemed to be a marginal candidate as an advanced demodulation technique for COFDM in fast fading conditions.

4.5 Conclusion

In chapter 3, it was concluded that a COFDM receiver using a conventional differential detector for the first stage was unsuitable for mode IV DAB applications at normalized Doppler spreads of $f_dT_S > 0.08$. This chapter has discussed four advanced techniques that appear in the literature and could potentially be adapted to remedy this. All of these techniques use statistical information about the time varying channel to improve the error rate in the demodulated sequence prior to decoding. They are:

- A decision feedback linear predictive OFDM subchannel gain estimation technique.
- A maximum likelihood sequence detection technique that uses a simplified ML metric derived from OFDM subchannel gain linear predictive coefficients. The connection between this and the decision feedback technique was discussed.
- A double filtering approach based on expanding the OFDM subchannel fading process in a Taylor series truncated to two terms and detecting with filters matched to each term. This technique was shown unsuitable for OFDM because the filter matched to the higher order series term is not matched to the OFDM rectangular pulse shape and thus produces large ICI.

- A symbol by symbol MAP detector that on its own is not substantially better than the MLSD but when used in an iterative soft decision feedback (turbo) receiver could produce a significant performance enhancement. However, recently published results indicate that the improvement due to the iterative processing is not likely to be significant at high values of Doppler spread.

In addition to the review of the literature on detection of PSK and DPSK in fast fading, an iterative hard decision feedback receiver structure that works in conjunction with the decision feedback LP detector is proposed. The idea of using decoded decisions to improve the performance of decision feedback systems is not new. However, it has not previously been applied in an iterative fashion to COFDM systems. It provides an alternative to a MLSD followed by a Viterbi decoder and is simpler than an iterative soft decision feedback receiver. Much of the next chapter will be devoted to evaluating the performance of this receiver using simulations.

5

Simulation Results

As discussed in previous chapters, the ultimate goal of a DAB receiver is to produce CD quality sound and this can be achieved with a BER of 10^{-4} in the decoded bit sequence. It has been demonstrated that a conventional differential detector (CDD) based receiver cannot achieve this for mode IV DAB operation at normalized Doppler spreads greater than 0.08. It was shown in chapter 4 that there are several advanced demodulation techniques that should be able to achieve a lower BER than a CDD based receiver. We are particularly interested in evaluating the performance of the iterative linear prediction receiver depicted in figure 4-2 since this type of receiver structure has not, to our knowledge, previously been applied to demodulation of COFDM over fading channels. Since an exact BER expression for this technique is difficult to develop, we have resorted to computer simulations.

The simulations were written using the Matlab software package [25]. The channel model discussed in chapter 3 was used with the number of $M = 40$ distinct propagation paths. This number of paths, used in [36], achieves a realistic simulation while keeping reasonable simulation times. To speed up the simulations, an extremely fast commercially available software package [39] was used to do the convolutional encoding and Viterbi decoding. Appendix C contains a detailed description of the Matlab routines.

As discussed in section 2.2.2, the mode IV DAB signal is sectioned into transmission frames that are 77 symbols long and start with a null and reference symbol. Many of the simulations discussed here are done using a COFDM system that dispenses with the null and reference symbols. This will be referred to as a "generic" COFDM system. When the null and reference symbols are included, it will be termed a "practical" COFDM system.

The first simulation results presented here are for a conventional differential detector (CDD) based receiver. Simulations were performed for an ideal AWGN channel and for the 40-path fading channel model discussed in chapter 3. These results were compared to previously published results [36] to serve as a benchmark for the simulation. Another set of simulations was run for the decision feedback linear prediction detector based receiver without the iterative decision feedback. These results were compared to the theoretical expressions developed in section 3.1.2 and also to published results [9]. Lastly, the iterative decision feedback LP detector based receiver was simulated. Results are presented both for a COFDM system having no null or reference symbols and for a system using one null and one reference symbol per 77 symbol long frame as specified for DAB (see section 2.2.2).

5.1 Differential Detection Receiver

5.1.1 AWGN channel

The simulation was performed for a COFDM system similar to mode IV DAB but without a null or reference symbol. The following simulation parameters were used.

Number of frames:	40
Number of symbols per frame:	77
Number of subcarriers:	768
Number of information bits per frame:	59,136
Useful symbol interval duration:	500 μs
Guard interval duration:	123 μs
Code rate:	1/2
Code constraint length:	7
Code generating sequences (octal, right justified):	$g_0^{(0)} = 133,\ g_0^{(1)} = 171$

Table 5-1 List of simulation parameters.

The convolutional encoding for this and subsequent simulations was done on a frame by frame basis using a "tail biting" rather than a zero forcing technique [24]. For the zero forcing technique, 6 zeros would be appended to the information sequence to force the encoder back to the zero state at the end of the frame. With tail biting, the encoder is initialized using the last 6 information bits in the frame so that it starts and ends in the same state. This provides benefits when the frame length is small and the fractional rate loss due to the appended all zero sequence would be significant. We used this technique because it was simpler to program a simulation where the coded sequence was exactly twice the length of the information sequence. For the frame length used in the simulation the difference in performance between tail biting and zero forcing is negligible.

For this and all subsequent simulations, soft Viterbi decoding is performed. For differential detection, the decision variables input to the Viterbi decoder were the real and imaginary parts of the decision variable given by (2.40) or (2.41).

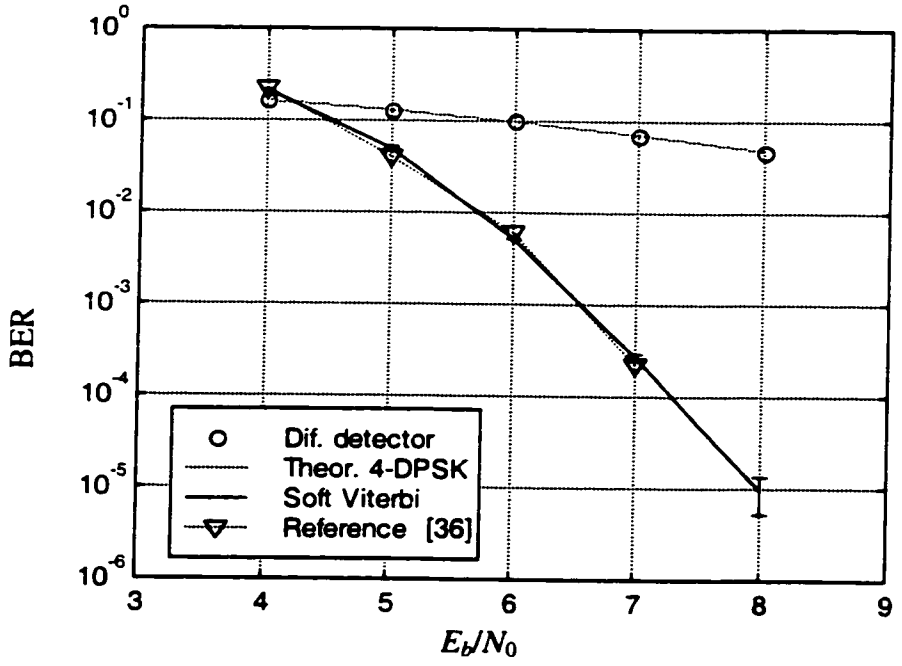

Figure 5-1 BER as a function of E_b/N_0 for generic COFDM system transmitted over ideal AWGN channel.

The Viterbi decoded BER as a function of E_b/N_0 is plotted in figure 5-1. The parameter E_b is the received energy per information bit over the entire symbol interval. The decoded sequence BER

is nearly identical to the results presented in [36]. Also the BER at the output of the differential detector compares well with the theoretical expression for 4-DPSK over an AWGN channel [28]. This provides a measure of confidence in the coding and modulation portions of the simulation.

In this simulation, there were 40 frames of data with 59,136 information bits in each frame. At a BER of 10^{-4} this translates to about 240 error events in the simulation. For a simulation where error events are independent, an interval estimate of the BER is given as [20]

$$\theta_{1,2} = \frac{n}{N}\left[1 + \frac{d_\alpha^2}{2n}\left(1 \mp \sqrt{\frac{4n}{d_\alpha^2} + 1}\right)\right]$$
$$1 - \alpha = \frac{2}{\pi}\int_0^{d_\alpha/\sqrt{2}} e^{-x^2}\,dx \tag{5.1}$$

where N is the total number of bits in the simulation, n is the number of error events and the probability that the actual BER falls between θ_1 and θ_2 is equal to 1-α. For n = 240 and $\alpha = 0.1$ this gives $\theta_1 = 0.9\times10^{-4}$ and $\theta_2 = 1.1\times10^{-4}$. Thus at the most critical value of BER, the 90% confidence interval is about ±10% of the computed BER. Actually, the error events are not independent since they will tend to appear in groups after an incorrect trellis branch is selected in the Viterbi decoder. This would tend to expand the confidence interval somewhat. For the remainder of the simulations in this chapter, the confidence interval is not computed but the number of frames and simulation repetitions is selected so that there are at least 240 error events at a BER of 10^{-4}.

5.1.2 Multipath channel

The multipath channel was modeled as shown in figure 3-2 with the number of paths M = 40 and the delays and Doppler shifts drawn randomly from the density functions given by (3.25) and (3.26). The mean delay spread was set to $\sigma_d = 10^{-6}$ seconds which is appropriate for typical urban propagation. Other simulation parameters were as listed in table 5-1 except that the duration of each simulation was 80 frames rather than 40. Each curve is the average of the BER obtained for 5 different realizations of the channel. A realization of the channel is obtained by a particular random choice of the 40 delays and Doppler shifts. The Viterbi decoder output BER as a function of E_b/N_0 is plotted in figure 5-2. Agreement between these results and those published in

[36] for the same channel model is satisfactory. This provides a level of confidence in the channel model and the interleaving portion of the COFDM simulator.

It is also of interest to observe the BER in the demodulated sequence prior to Viterbi decoding. This and the decoded BER is plotted in figure 5-3. Simulation parameters other than the normalized Doppler frequencies are the same as in figure 5-2.

It can be seen that the target decoded BER of 10^{-4} is achieved when the BER in the differentially detected sequence is less than about 0.07. This provides a rule of thumb that was used in the previous chapter for identifying demodulation techniques that might be suitable for achieving the target BER of 10^{-4} in the range of E_b/N_0 between 15 and 20 dB.

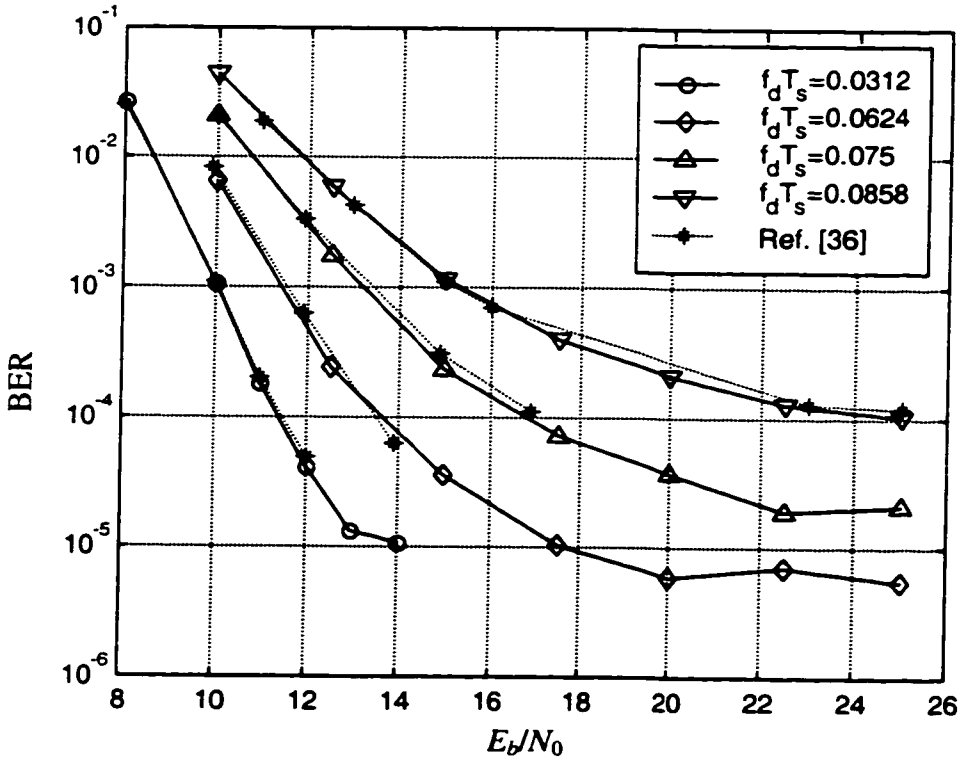

Figure 5-2 Viterbi decoded BER as a function of E_b/N_0 for generic COFDM signal transmitted over 40 path typical urban channel model.

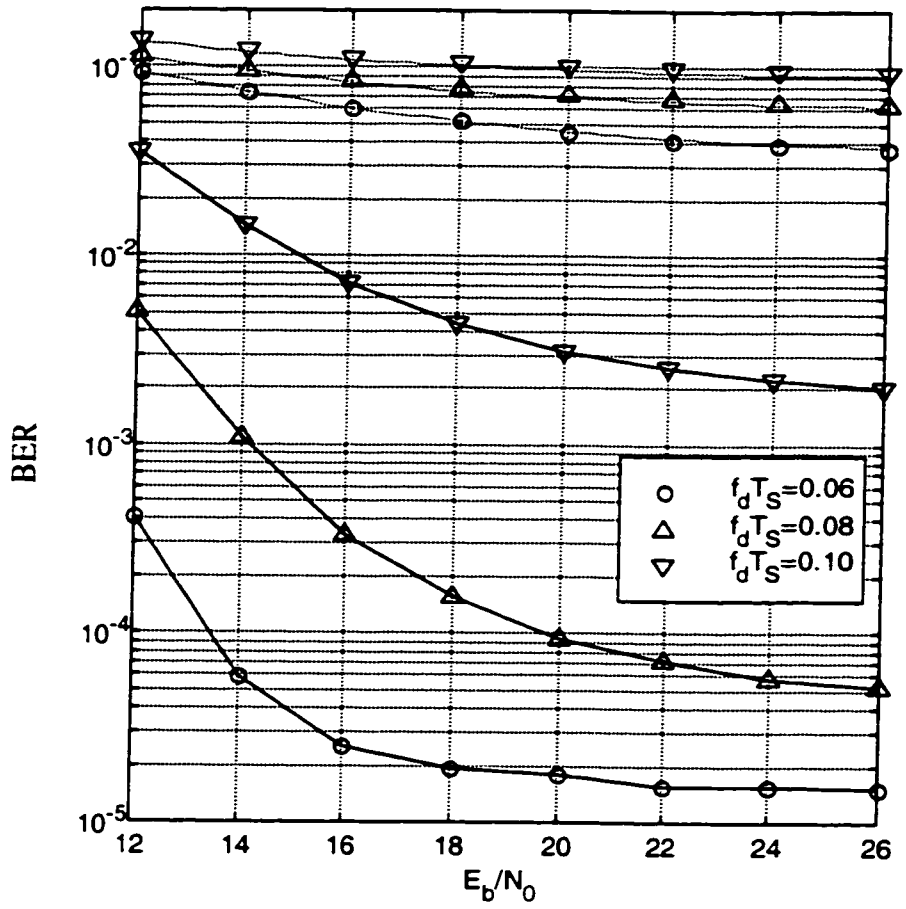

Figure 5-3 Differentially detected (dotted line) and Viterbi decoded (solid line) BER as a function of E_b/N_0 for generic COFDM signal transmitted over 40 path typical urban channel model.

5.2 Decision Feedback LP Receiver

5.2.1 Linear predictive detector for ordinary 4-DPSK

Simulation results for uncoded 4-DPSK signals are compared to the theoretical curves and to results published in [9]. The simulation parameters listed in table 5-2 were used. Figure 5-4 shows the bit error rate as a function of signal to noise ratio for various values of the predictor order when correct decisions were fed back and the normalized Doppler spread was $f_dT_S = 0.1$. Ordinary 4-DPSK as in equation (2.36) was used to encode the symbols. Also shown in the figure are the curves for the theoretical BER as derived in section 4.1.2. The predictor order is indicated by the parameters N representing the number of previous OFDM symbols and K

representing the number of subchannels used in the linear predictor. Although the simulation is done for the LP detector only, E_b is still defined to be $E_b = 5E_U/4$ as discussed in section (3.3.3). This facilitates direct comparison between the BER curves in the coded and non-coded cases.

Number of frames:	5
Number of symbols per frame:	77
Number of subcarriers:	768
Number of bits per frame:	118,272
Useful symbol interval duration:	500 μs
Guard interval duration:	123 μs
Channel mean delay spread σ_d:	10^{-6} s
Number of channel realizations	10

Table 5-2 List of simulation parameters.

It can be seen that when correct decisions are fed back, the BER is improved by using a higher order predictor. Also it can be seen that there is a BER floor starting to appear even with the use of higher order predictors. This is due to the ICI term in the noise variance which is independent of E_b/N_0. It is also apparent that the simulated BER is slightly higher than the theoretical. This is because the treatment of ICI in the model as a white Gaussian process with variance $(f_d T_U)^2$ is only an approximation. The BER floor was not apparent in the results presented in [9] because the channel model used in this reference produced no ICI. As shown in figure 5-5, when ICI is removed by the artifice of transmitting non-zero symbols only on every 20th subchannel, the BER floor is eliminated and the simulation results match the theoretical expression exactly.

From figure 5-4 one can see that with the higher order predictors, it is possible to achieve a BER of 0.07 in the desired range of E_b/N_0. This indicates that it should be possible to reach the desired decoded BER.

As one would expect, the BER increases when actual decisions are used to direct the linear predictive detector. This is shown in figure 5-6 where the actual detector decisions are fed back. Otherwise the simulation is unchanged from figure 5-4. Using more than one subchannel for the linear predictor results in poorer performance than using only one subchannel. This is because of the error multiplying effect associated with feeding back incorrect decisions. An error fed back in one channel can now cause an error in an adjacent channel. At some point, this effect

outweighs the benefit gained from using a higher order predictor. At lower values of f_dT_S, there is a decrease in BER obtained from using adjacent channels in the predictor, however in this case the target BER can be easily reached using a single channel or even a CDD so this does not interest us.

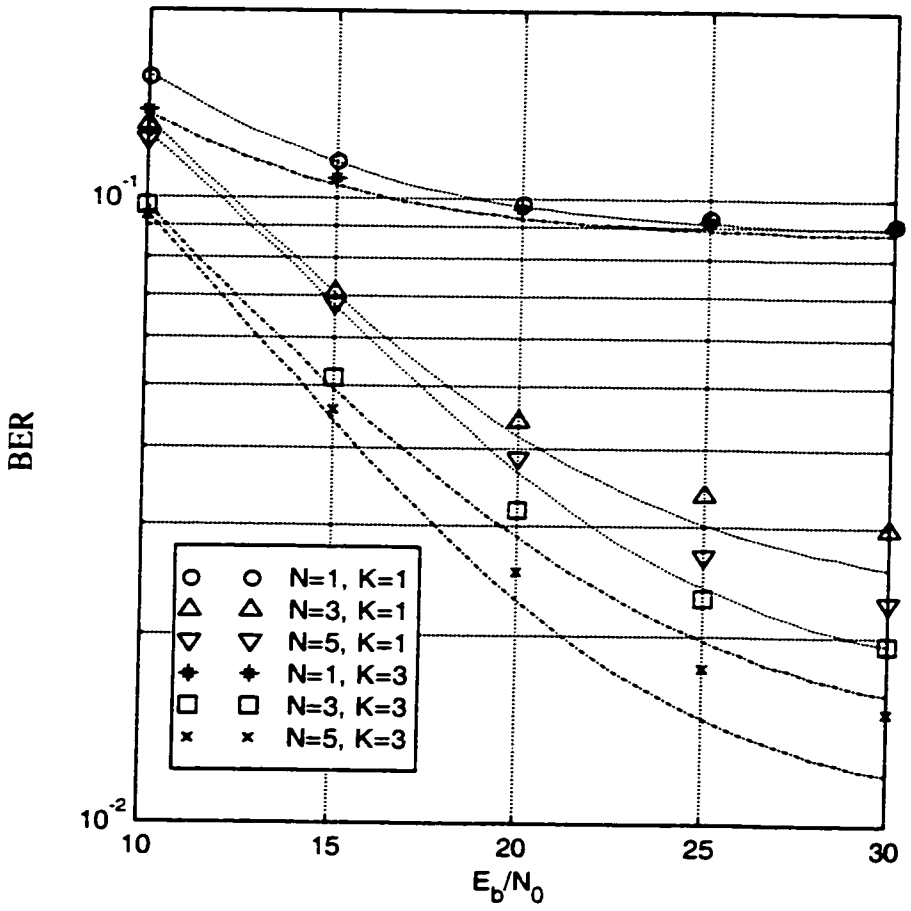

Figure 5-4 Simulated BER vs. E_b/N_0 for decision directed linear prediction detector operating with normalized Doppler f_dT_S=0.1 and using correct fed back decisions. Theoretical BER is plotted with dashed line for K=1 and dash-dot line for K=3. E_b/N_0 is defined as if the bits were encoded with a rate 1/2 code prior to transmission and E_b is the energy per information bit.

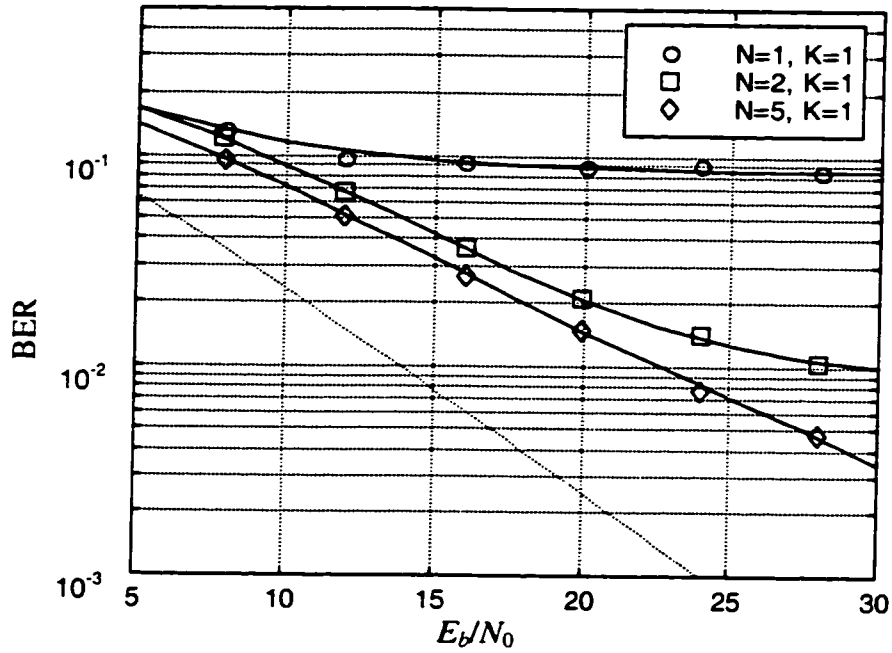

Figure 5-5 Theoretical (solid lines) and simulated BER with no ICI and when correct previous decisions are used for channel prediction. f_dT_S=0.1. Dashed line shows BER when current channel gain is also known. E_b/N_0 is defined with $E_b = 5E_U/8$ being the energy per encoded bit.

Another effect that occurs due to fed back errors is a phase offset in the previous subchannel gain values that are used to predict the current channel gain. The previous subchannel gain estimates are given by

$$H_{n-i,k} = y_{n-i,k}c^*_{n-i,k} \tag{5.2}$$

where $c_{n,k}$ is the decision made on the symbol from time interval n and subchannel k, and $y_{n,k}$ is the corresponding received signal value. For ordinary 4-DPSK, the symbol decisions $c_{n,k}$ may have a phase error that is a multiple of $\pi/2$ resulting in a previous gain estimate with a similar phase error. The result is that when an error is fed back, all of the subsequent decision directed subchannel gain estimates may end up having a phase error that is a multiple of $\pi/2$. When only one subchannel is used in the predictor, the receiver just carries on working on the rotated signal constellation and there are no errors in the differentially decoded symbols. The same is true when more than one subchannel is used in the predictor provided that all subchannels have the same phase offset. However, there will be some cases where adjacent subchannels are offset by a different multiple of $\pi/2$ resulting in a higher probability of making an error when a decision is

made based on the predicted channel gain. It has been observed that when a reference symbol is used to periodically correct the phase offsets, the performance of the multiple subchannel LP detector can be improved. However, for $f_dT_S = 0.1$ and a reference symbol that is available only every 77th symbol as in mode IV DAB, the improvement is not enough to outperform a single subchannel predictor.

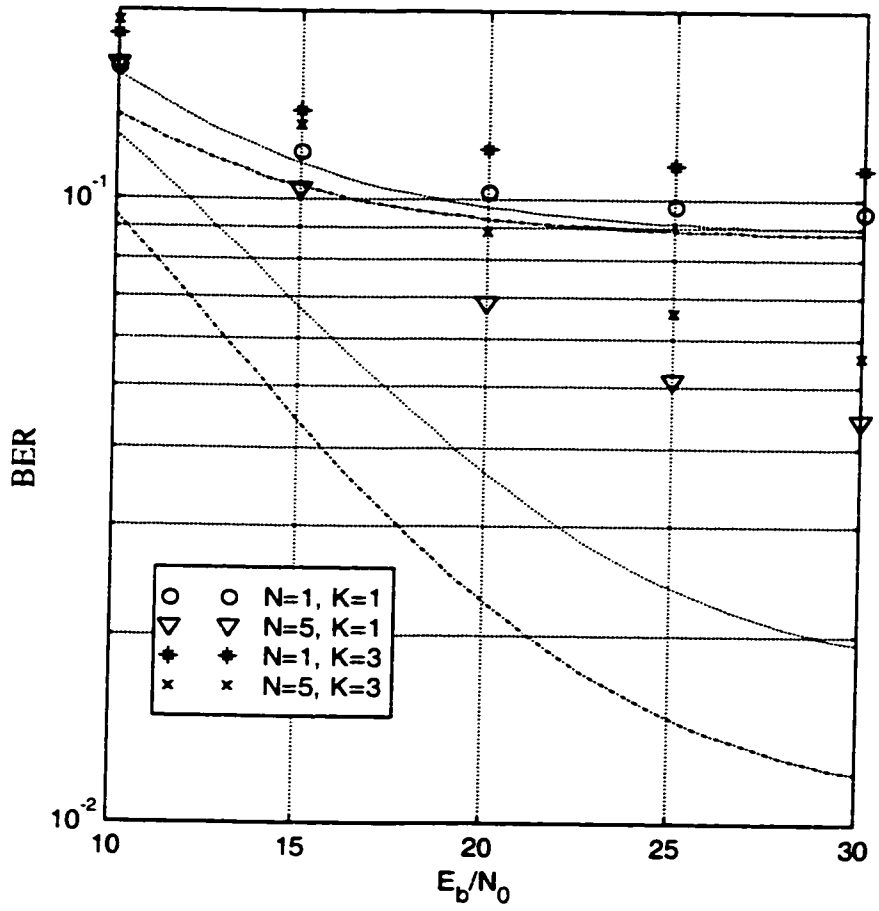

Figure 5-6 Simulated BER vs. E_b/N_0 for decision directed linear prediction detector operating with normalized Doppler f_dT_S=0.1 and using actual fed back decisions. Theoretical BER with no fed back decision errors is plotted with dashed line for K=1 and dash-dot line for K=3. E_b/N_0 is defined as if the bits were encoded with a rate 1/2 code prior to transmission and E_b is the energy per information bit.

5.2.2 Linear predictive detector for π/4-shift 4-DPSK

Figure 5-7 shows what happens when the LP detector is used on a π/4-shift 4-DPSK signal where the differential encoding is performed according to (2.37). Simulation parameters here were the same as in table 5-2. For a normalized Doppler spread of f_dT_S = 0.1, the use of a predictor of order higher than one results in a higher BER for E_b/N_0 less than 20 dB. The reason is that the transmitted symbols now form an 8-PSK constellation and therefore the probability of making an erroneous decision on the transmitted symbol is higher than for the 4-PSK constellation associated with ordinary 4-DPSK. This higher fed back error rate results in the deterioration in performance observed in figure 5-7 as compared to figure 5-6. When correct decisions are fed back, the performance of the LP detector on π/4-shift 4-DPSK is equivalent to ordinary 4-DPSK. For lower values of Doppler spread, higher order predictors will tend to show improved performances at lower values of E_b/N_0.

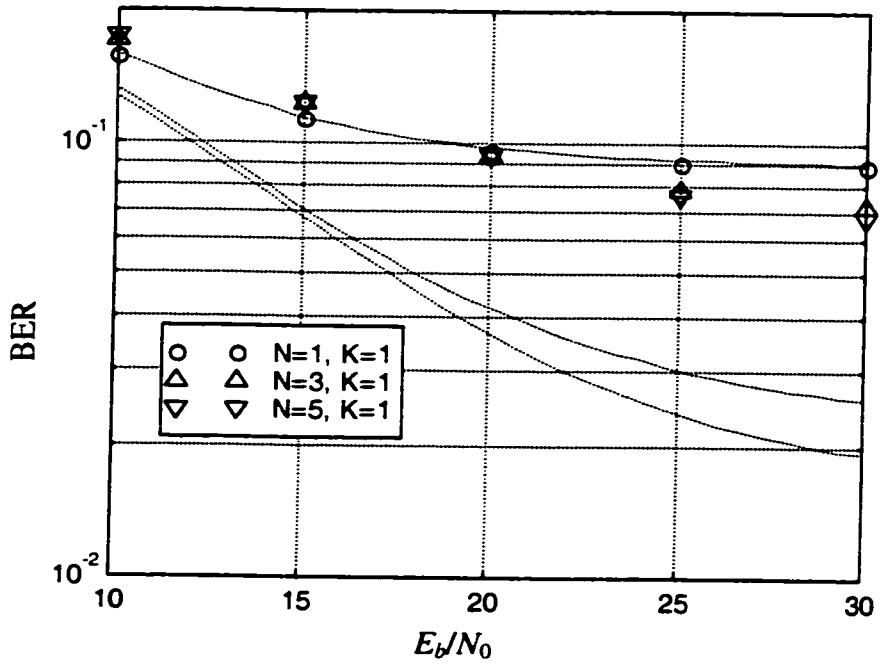

Figure 5-7 Simulated BER vs. E_b/N_0 for decision directed linear prediction detector with π/4-shift 4-DPSK and normalized Doppler $f_dT_S = 0.1$. Theoretical BER is plotted with dashed line. E_b/N_0 is defined as if the bits were encoded with a rate 1/2 code prior to transmission and E_b is the energy per information bit.

5.2.3 Linear predictive receiver for COFDM

The above discussion indicates that for the $\pi/4$-shift 4-DPSK modulation used in COFDM, a decision feedback LP detector followed by a de-interleaver and Viterbi decoder has no hope of achieving the target BER in the desired range of E_b/N_0. However, when the LP detector operates on correct fed back decisions, the uncoded BER is well below the figure of around 0.07 required for a CDD to meet a BER of 10^{-4} after decoding. The question is whether soft Viterbi decoding of the LP detector outputs obtained with correct fed back decisions can provide a similar BER improvement. As a first step, one needs to determine a suitable soft output of the LP detector. By analogy with the soft decision output of the CDD we have used the real and imaginary parts of

$$a_{n,k} = y_{n,k} \frac{\hat{H}^*_{n,k}}{|\hat{H}_{n,k}|} c^*_{n-1,k} |y_{n-1,k}| \tag{5.3}$$

where $y_{n,k}$ is the receiver DFT output, $\hat{H}_{n,k}$ is the LP gain estimate, and $c_{n-1,k}$ is the previous symbol decision. The soft decision is determined by rotating the current received value by the angle of the subchannel gain estimate, further rotating by the angle of the previous symbol decision (to differentially demodulate), and then weighing by the magnitude of the previous received value.

The BER obtained from soft Viterbi decoding of this LP detector output in the ideal case of no errors in the fed back decision sequence is as shown in figure 5-8. Simulation parameters here were identical to those listed in table 5-1 except that the simulation duration was 80 frames. The BER was averaged over 5 channel realizations. This curve shows the target decoded BER of 10^{-4} being achieved at $E_b/N_0 = 15$ dB for the normalized Doppler spread equal to 0.1. By feeding back decoded decisions to the LP detector in an iterative fashion as discussed in section 4.1.3 the receiver should be able to approach the performance in figure 5-8.

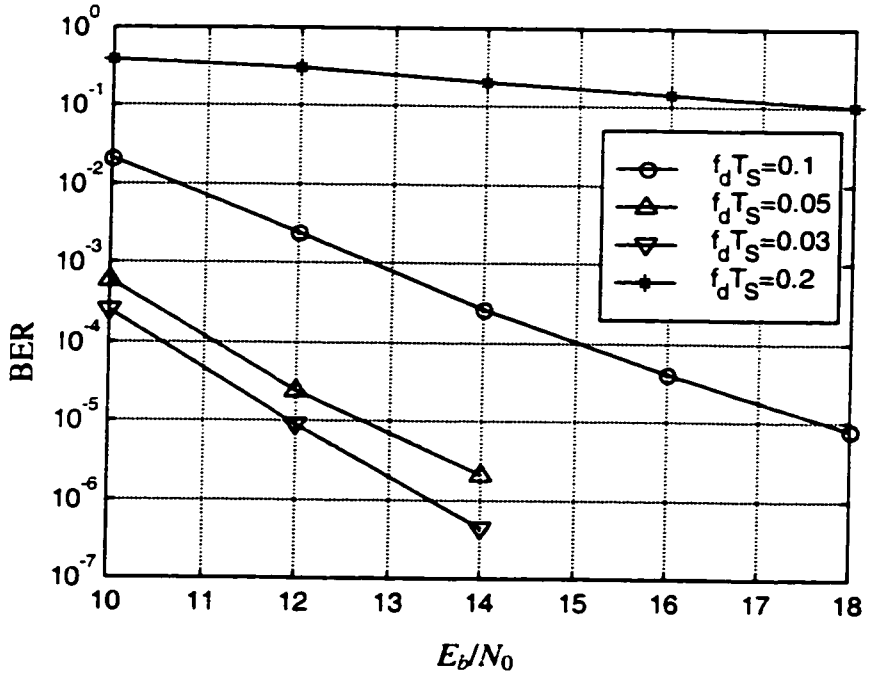

Figure 5-8 Simulated lower bound on BER of COFDM receiver using decision directed LP detector with no errors in fed back decisions. $N = 5$ previous symbols and $K = 1$ subchannel used for LP detector. Mean channel delay spread $\sigma_d=10^{-6}$ s.

5.3 ITERATIVE DECISION DIRECTED LP RECEIVER

5.3.1 Generic COFDM system

The term "generic" COFDM is used to refer to a system that doesn't make use of the null or reference symbols specified for the COFDM system used in DAB. Matlab routines (see appendix C) were written to simulate the iterative decision feedback COFDM receiver depicted in figure 4-2 b. Figure 5-9 shows the BER performance as a function of E_b/N_0 after the third iteration of the algorithm. The simulation parameters listed in table 5-3 were used. For $f_dT_S = 0.1$ it can be seen that the required BER of 10^{-4} is achieved at about $E_b/N_0 = 15.6$ dB. This can be compared with the conventional COFDM receiver depicted in figure 5-3 where at the same Doppler spread, the required BER cannot be achieved at any value of E_b/N_0. On the other hand, one can compare with the ideal case depicted in figure 5-8 where the LP detector used correct fed back decisions: for a normalized Doppler spread of $f_dT_S = 0.1$ there is only about 0.6 dB performance loss at a BER of 10^{-4}. At lower values of f_dT_S, this performance loss is even less.

Number of frames:	80
Number of symbols per frame:	77
Number of subcarriers:	768
Number of information bits per frame:	59,136
Useful symbol interval duration:	500 μs
Guard interval duration:	123 μs
Channel mean delay spread σ_d:	10^{-6} s
Number of channel realizations	5
Code rate:	1/2
Code constraint length:	7
Code generating sequences (octal, right justified):	$g_0^{(0)} = 133,\ g_0^{(1)} = 171$

Table 5-3 List of simulation parameters.

Number of iterations In figure 5-10 the error rate at the end of each of the three algorithm iterations is plotted for $f_dT_S = 0.1$. There is a significant improvement with each iteration. The decoded error rate decreases and the performance can approach the case of no fed back error. Although not shown, it has been observed that further iterations of the algorithm provide only marginal improvement.

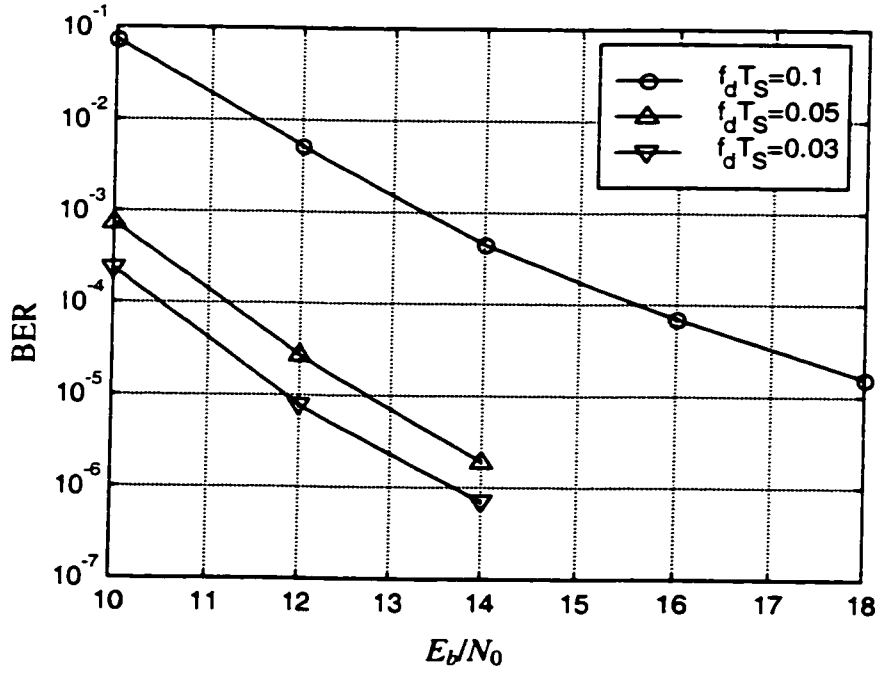

Figure 5-9 BER at Viterbi decoder output after 3rd iteration. $N = 5$ previous symbols and $K = 1$ subchannel used in linear predictor.

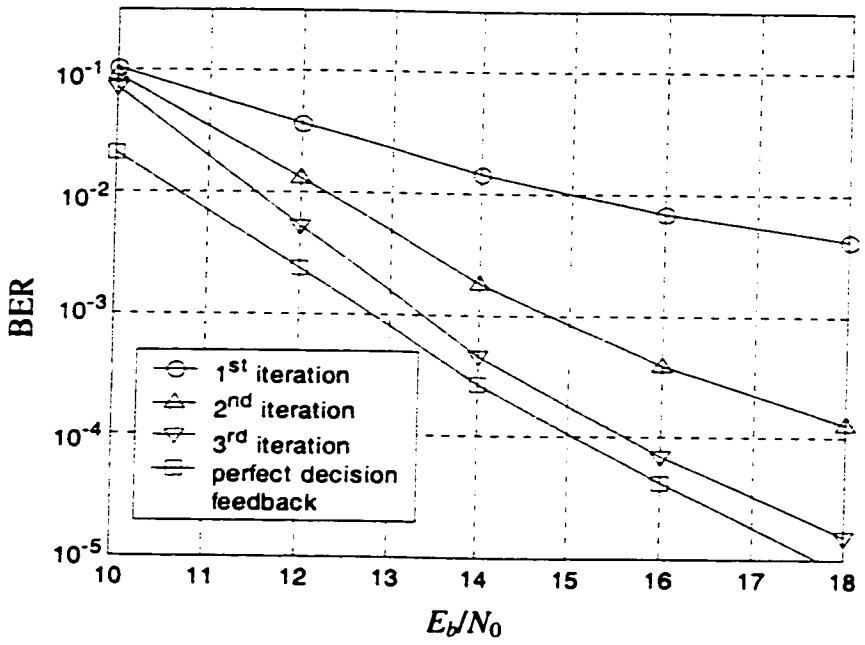

Figure 5-10 BER at Viterbi decoder output one to three iterations with f_dT_S = 0.1. First iteration uses CDD. N = 5 previous symbols and K = 1 subchannel used in the linear predictor.

Linear predictor order The effects of varying the order of the predictor can be seen in figure 5-11 where the decoded BER after the third iteration is plotted as a function of E_b/N_0. Here the simulation parameters listed in table 5-3 were used again. For f_dT_S = 0.1, this figure actually shows an improvement in the result with N = 3 previous samples used for the predictor over the result with N = 5. This is believed to be a statistical effect that would disappear with longer simulations and averaging over more channel realizations. One would expect improved performance with a higher order predictor since it has a lower mean squared error.

Simulations were run using more than one subchannel in the predictor (i.e. K > 1) but these did not converge at a sufficiently low BER. The reason is that at high values of f_dT_S, the LP detector using more than one subchannel requires a very low error rate in the fed back decision sequence to provide a reasonable output BER. One possible strategy would be to use a single subchannel predictor for the first few iterations of the algorithm and then switch to several subchannels. This was simulated for several values of Doppler spread and the results indicate that any improvement can only be obtained after the decoded BER for the iterations with a single channel had already

reached the required 10^{-4}. It may however be useful for applications requiring a lower BER than DAB.

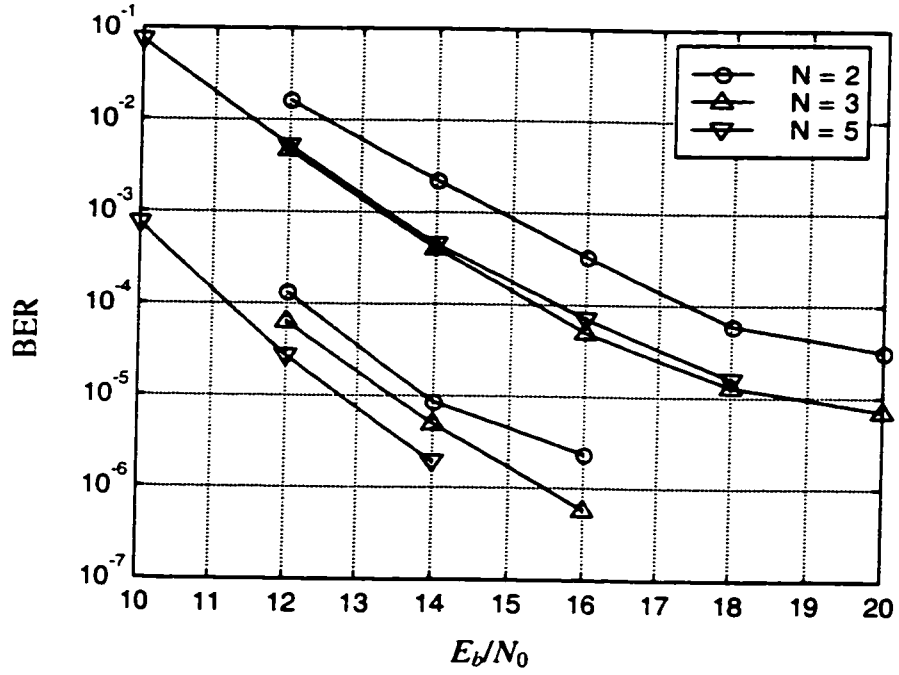

Figure 5-11 BER at Viterbi decoder output after 3rd iteration for various predictor orders. Upper set of points for $f_dT_S = 0.1$, lower set of points for $f_dT_S = 0.05$. $K = 1$ subchannel used in all cases.

Performance at higher Doppler spreads For the channel model used here, the normalized Doppler spread of $f_dT_S = 0.1$ corresponds to a vehicle velocity of 115 km/hr. Drivers have been known to exceed this velocity so it is of interest to see how the iterative receiver performs at larger Doppler spreads. Figure 5-12 shows the BER for normalized Doppler spreads up to 0.15. The other simulation parameters were the same as listed in table 5-3. It can be seen that the receiver experiences difficulties in reaching the required BER of 10^{-4} for normalized Doppler spread of $f_dT_S > 0.125$ which corresponds to a vehicle velocity of 144 km/hr.

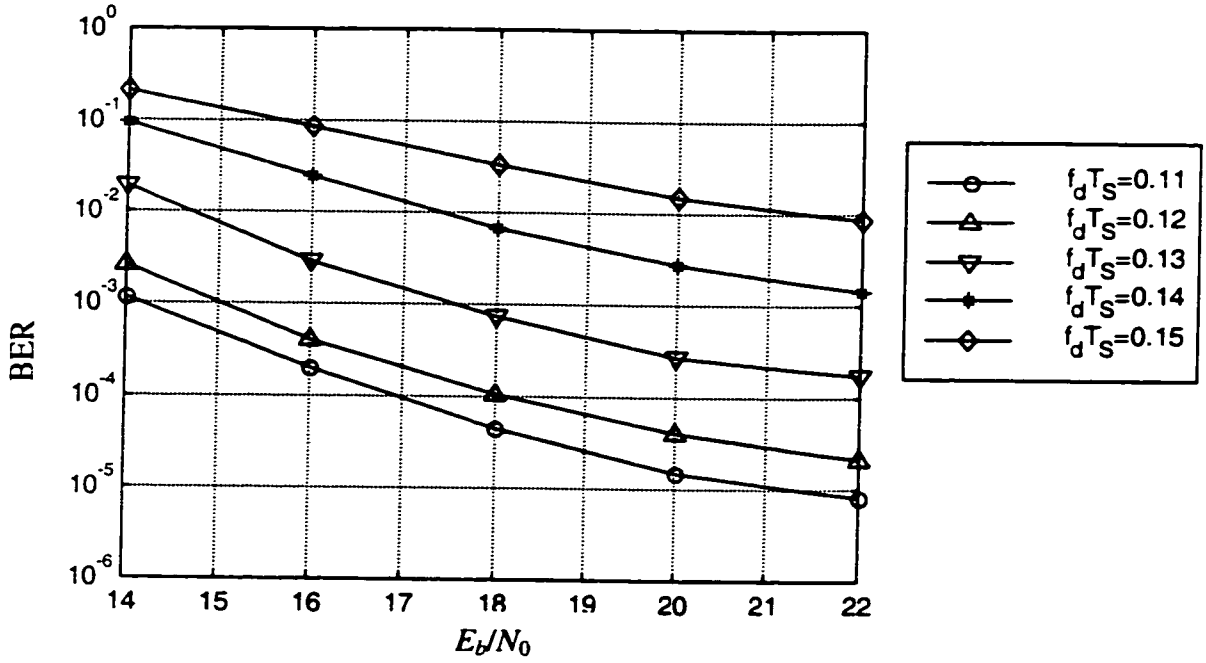

Figure 5-12 BER at Viterbi decoder output after 4th iteration. $N = 5$ previous symbols and $K = 1$ subchannel used in linear predictor.

Effects of errors in Doppler spread estimation The simulations performed up to this point have assumed that the receiver knows the Doppler spread of the channel. A technique for estimating this parameter based on the level crossing rate was discussed in section 4.1.4. There will always be some error in this estimation and one would like to quantify the effects of such an error. Figure 5-13 plots the simulated BER when the actual Doppler spread of the channel is $f_dT_S = 0.1$ but the value of Doppler spread used by the receiver varies between 0.05 and 0.2. Other simulation parameters were as listed in table 5-3. As expected, demodulation using an incorrect estimate of the Doppler spread results in a higher BER. The simulation results show that underestimating the Doppler spread by 30% causes about 2 dB poorer performance at a BER of 10^{-4} while overestimating it by 40% causes about 1.25 dB poorer performance. It seems to be better to overestimate than underestimate the Doppler spread and it may be possible to take advantage of this by choosing an estimator that is slightly biased on the high side.

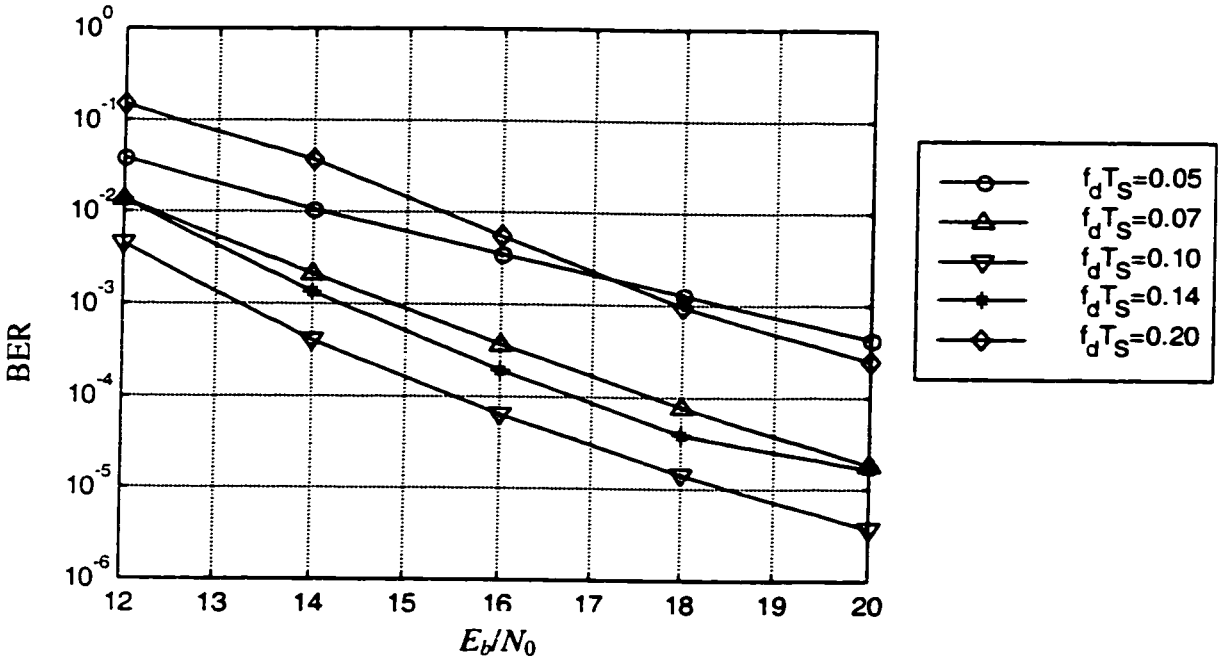

Figure 5-13 BER at Viterbi decoder output after 3rd iteration with with LP detector using mismatched estimate channel Doppler spread. Actual channel Doppler spread is $f_dT_S = 0.1$.

5.3.2 Practical COFDM system

As discussed in section 2.2.2 the COFDM signal used in DAB transmits a null and reference symbol at the start of each transmission frame followed by 75 data symbols. The presence of the null symbol presents a problem for the LP detector because there is now a symbol interval with no received signal on which to base the decision directed subchannel gain computation. This will affect the subchannel gain prediction for the next N OFDM symbols where N is the number of previous samples used in the linear predictor. Several schemes for dealing with this were investigated:

- using the computed subchannel gain from the previous symbol as the gain for the null symbol;

- using the predicted gain for the null symbol as the computed gain for the null symbol;

- using a single channel predictor of order 1 for the symbol immediately following the reference symbol, a predictor of order 2 for the symbol following this and so on up to some maximum predictor order (e.g. $N = 5$);

- using the optimum minimum mean squared error linear predictor coefficients for the case where one previous sample is missing. This requires $N+1$ different coefficient sets to be stored and used as appropriate. For instance, to form the linear predictor for the first data symbol requires a set of coefficients that are optimum when the missing sample occurred two symbols ago.

It has been determined through simulations that only the last of these above schemes provides satisfactory performance.

As discussed in section 5.2.1, the decision directed gain estimates used by the linear predictor can have a phase offset due to previous errors in the fed back decisions. The presence of a reference symbol offers an opportunity to correct this offset. This is done by comparing the phase of the subchannel gain prediction to the phase of the subchannel gain as determined by the reference symbol. However, with the null symbol occurring just prior to the reference symbol, there is a significant error in this gain prediction. This combined with the more closely spaced signal constellation for $\pi/4$-shift 4-DPSK may result in an error in the determination of the required phase correction. Because of this, it has been found that the simulations show slightly better results when no phase offset correction is done at the reference symbol.

Figure 5-14 shows the Viterbi decoded BER after three algorithm iterations. The simulation parameters here are as listed in table 5-3. For a normalized Doppler spread of $f_d T_S = 0.1$, the required BER is achieved at $E_b/N_0 = 16.4$ dB.

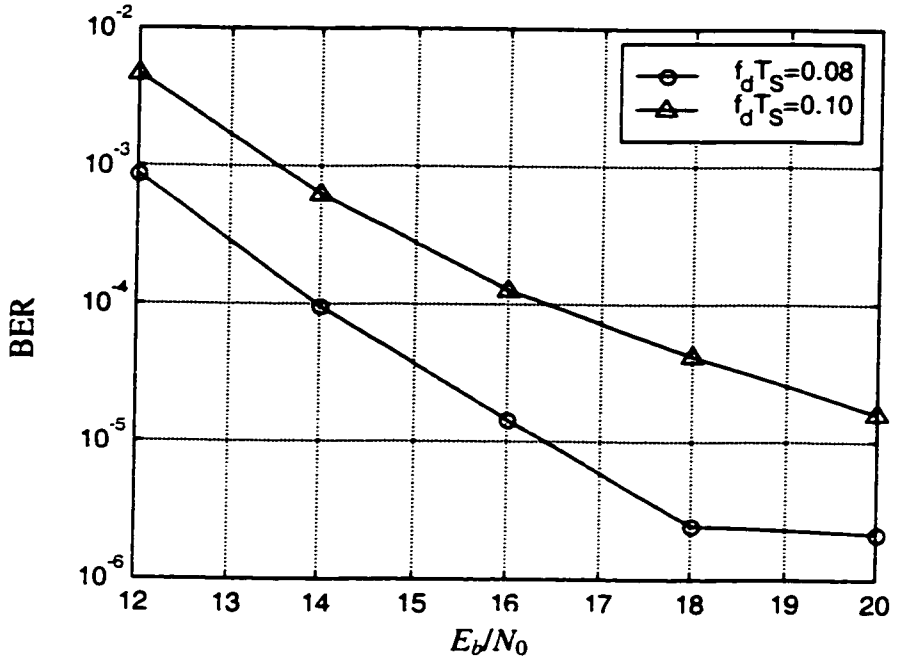

Figure 5-14 BER at Viterbi decoder output after 3rd iteration. $N = 5$ previous symbols and $K = 1$ subchannel used in linear predictor.

Effects of errors in Doppler spread estimation The effect of a mismatch in the receiver's estimate of Doppler spread is shown in figure 5-15. The actual channel Doppler spread was $f_dT_S = 0.1$ and the estimate used by the receiver varied from 0.05 to 2. The predictor used $N = 5$ previous symbols and $K = 1$ subchannel. Other simulations parameters were as listed in table 5-3. Here one sees approximately the same performance degradation as the corresponding result for the generic COFDM system plotted in figure 5-13.

Figure 5-16 also shows the effect of a mismatch in the value of Doppler spread that the receiver uses in the LP detector. For this figure, the receiver used a normalized Doppler spread of $f_dT_S = 0.1$ for all of the curves but the actual channel Doppler spread was varied. The importance of this result is that the receiver can achieve satisfactory performance up to a normalized Doppler spread of $f_dT_S = 0.1$ without doing any adaptive adjustment to the detection algorithm.

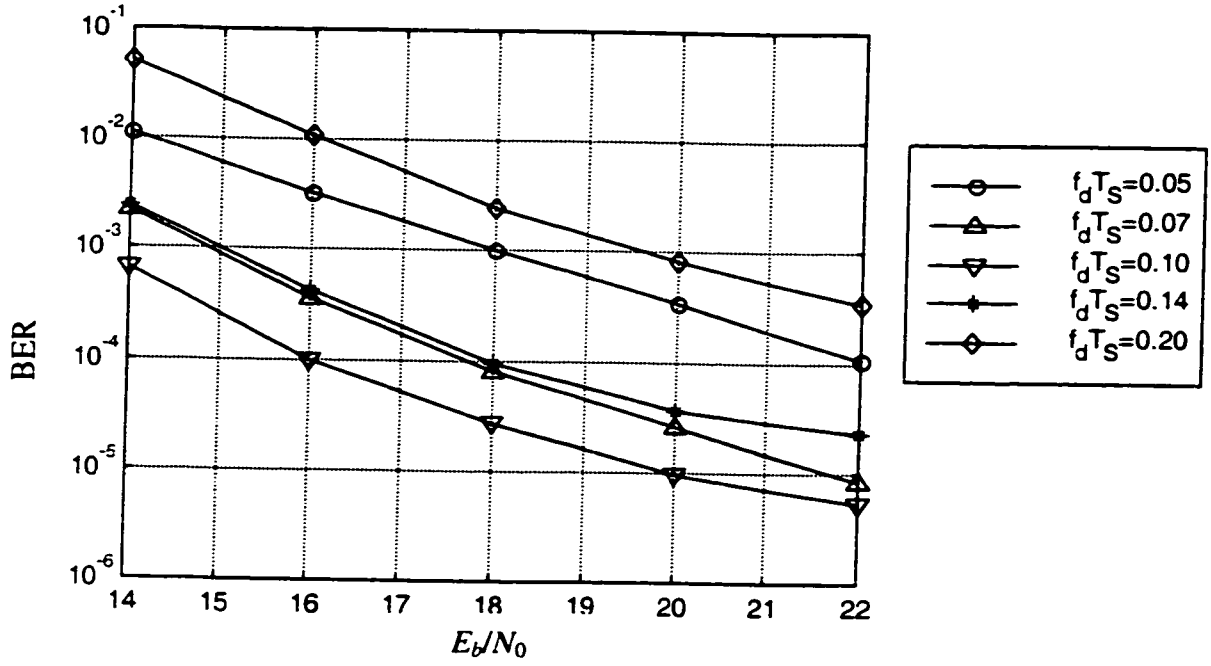

Figure 5-15 BER at Viterbi decoder output after 3rd iteration with the LP detector using a mismatched estimate channel Doppler spread. The actual channel Doppler spread is $f_dT_S = 0.1$.

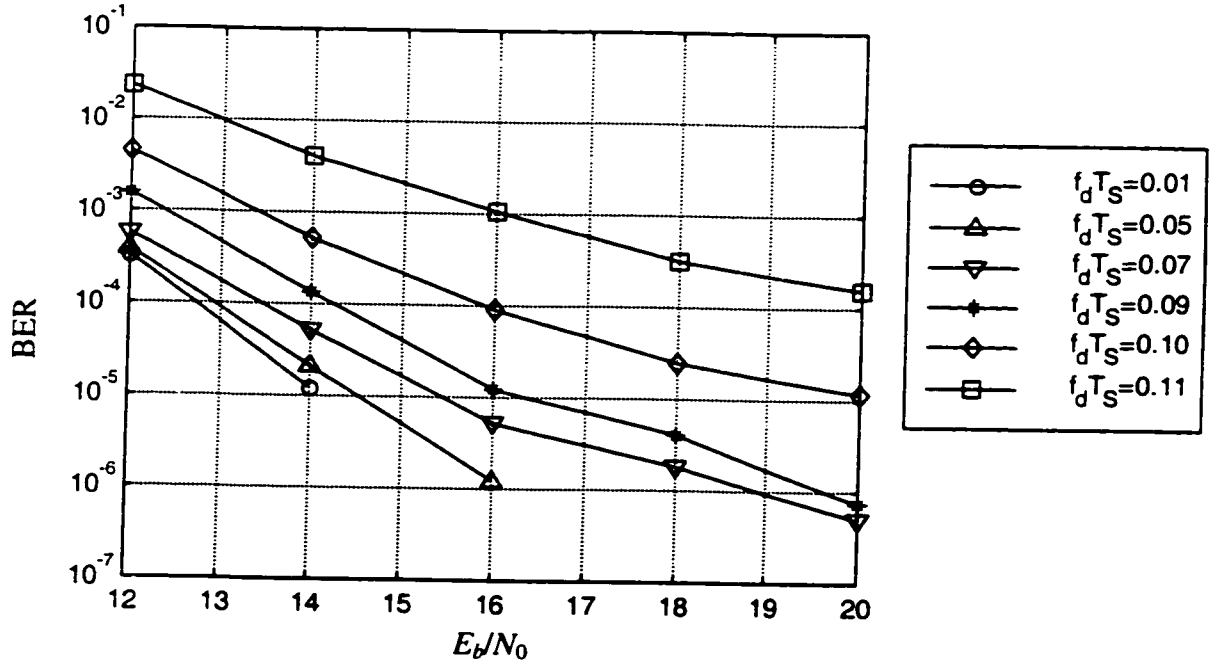

Figure 5-16 BER at Viterbi decoder output after 3rd iteration with the LP detector using $f_dT_S = 0.1$ for its estimate of the channel Doppler spread. The actual channel Doppler spread varies as indicated in the legend.

Linear predictor order One can observe the effects of varying the number of previous symbols used in the linear predictor in figure 5-17. The channel Doppler spread was $f_d T_S = 0.1$. $K = 1$ subchannel was used for the predictor and other simulation parameters were as lised in table 5-3. As expected, the BER performance shows a tendency to improve with higher order predictors. In chapter 6 it will be seen that implementing a higher order predictor requires only a marginal increase in the overall processing load.

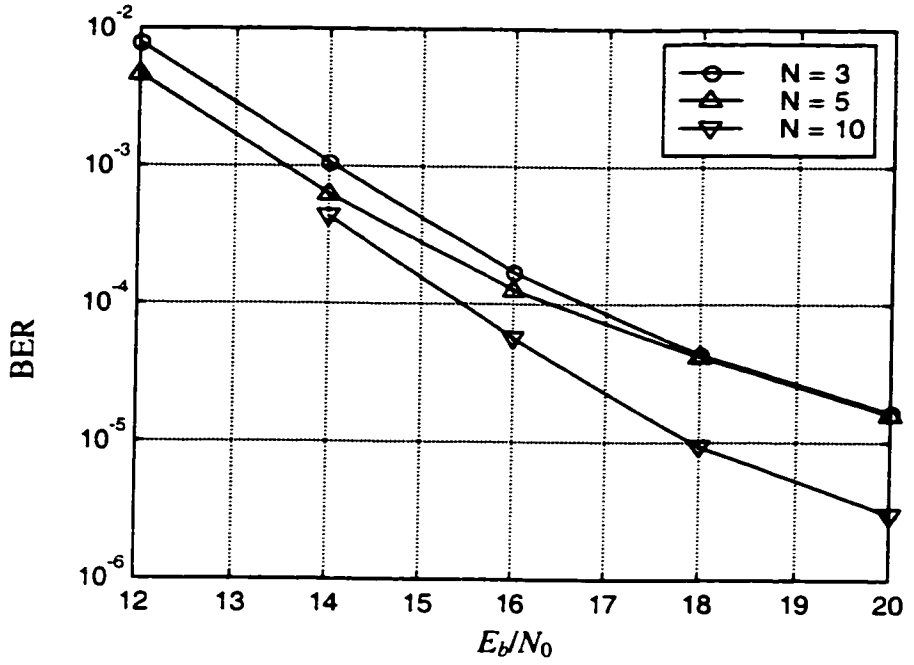

Figure 5-17 BER at Viterbi decoder output after 3rd iteration for various predictor orders. The normalized Doppler spread is $f_d T_S = 0.1$.

Mismatch in estimate of noise variance The simulation results plotted in figure 5-18 show that the receiver is relatively insensitive to an error in the estimation of the noise variance. The average performance is somewhat worse than in the previous figures due to one channel realization that resulted in particularly poor performance. However, the variation in performance due to noise mismatch for any particular channel realization was similar to that shown for the average.

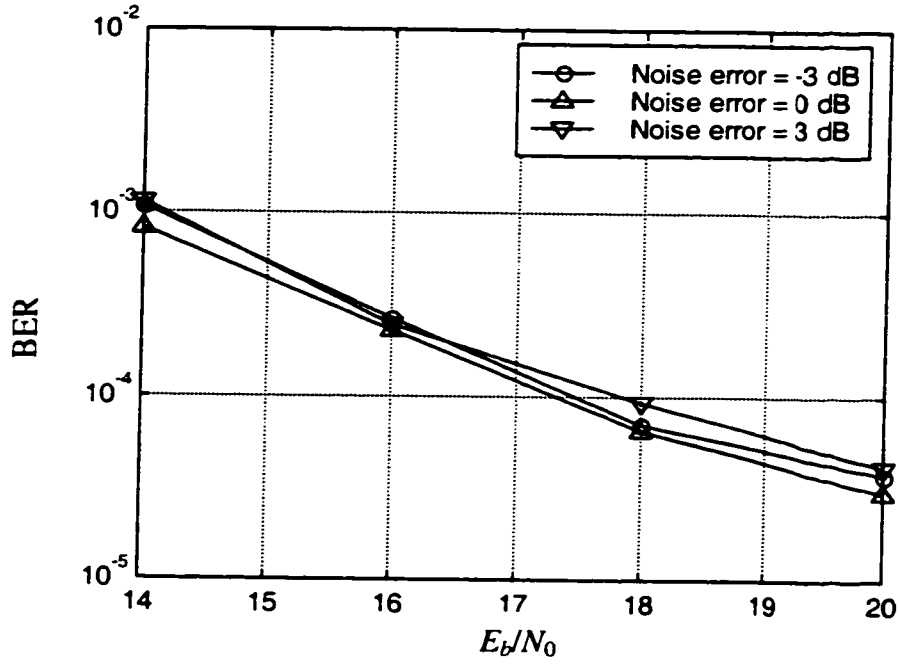

Figure 5-18 BER at Viterbi decoder output after 3rd iteration with the LP detector using a mismatched estimate of the noise variance. The normalized Doppler spread is $f_dT_S = 0.1$.

5.4 Conclusion

The performance objective for a DAB receiver is to achieve high channel reliability, i.e. CD quality sound at practical values of signal to noise ratio in the range of E_b/N_0 = 15-20 dB. This can be achieved if the decoded BER is lower than 10^{-4}. Conventional differential detector based receivers cannot achieve this BER in typical urban channel conditions with E_b/N_0 = 20 dB for a normalized Doppler spread exceeding f_dT_S = 0.08 corresponding to a vehicle velocity of 92 km/hr. The simulation results in this chapter have demonstrated an iterative decision directed linear predictive receiver that can significantly extend this performance limit. For the generic COFDM system operating under the same conditions, the Doppler spread can be increased to about $f_dT_S = 0.125$ corresponding to a velocity of 144 km/hr.

Other simulation results show that a decision directed linear predictive receiver operating in typical urban channel conditions can overcome the BER floor associated with a CDD, however another lower error floor associated with ICI effects appears. Another interesting result is that at the relatively high values of Doppler spread investigated here, there is a significant degradation

in actual performance of the LP detector over the theoretical performance of the ideal LP detector due to errors in the fed back decision sequence. For $\pi/4$-shift 4-DPSK, this degradation makes the performance worse than with a conventional differential detector. However, when Viterbi decoded decisions are used for the LP detector, a significant performance improvement can be obtained and this results in the success of the iterative technique.

The iterative decision feedback linear predictive receiver was simulated for the case of a generic COFDM system having no null or reference symbol and for a practical COFDM system having a null and a reference symbol. It was found that the presence of the null symbol resulted in the need for a slightly more complicated scheme for the LP detector and caused a slight deterioration in performance. However, the performance requirements for a DAB receiver were achieved in both cases.

Based on the simulation results one can conclude that the iterative decision feedback LP receiver is a promising technology for increasing the Doppler limit of Mode IV receivers. It should be noted however, that the simulations were done for a relatively limited range of conditions. Some suggestions for future simulations are:

- studying the effects of varying the channel delay spread profile including the effects of multiple active echoes resulting from multiple transmission towers;
- studying the effects of different channel models such as hilly and rural terrain;
- studying the effects of the fast information channel symbols. This will be discussed in more detail in chapter 6.

6

Receiver Implementation

The receiver simulations discussed in the previous chapter used a non real-time implementation of the iterative algorithm. Each step in the detection process was performed for the entire data file and the results stored on disk before proceeding to the next step. This allowed a considerable simplification of the simulation programming. This chapter provides a description of how to practically implement the iterative algorithm and presents a complexity estimate of this implementation.

One aspect of the COFDM specification used for DAB has not been taken into account in the simulations. This is that the three symbols following the null and reference symbols in the mode IV transmission frame comprise a fast implementation channel that is not time interleaved but is convolutionally encoded at a lower rate than the audio data. The effects of this on the receiver design are discussed.

6.1 Receiver Complexity Estimate

6.1.1 Real time receiver implementation

Figure 6-1 shows a schematic diagram of the receiver timing for the operations necessary in the iterative receiver. The first row in the figure represents a series of encoded data frames that will be interleaved and transmitted. The second row represents the interleaved data sequence at the output of the DFT. The first frame in this sequence is labeled 0-15 to indicate that it contains bits from frames 0 to 15 of the encoded data sequence. The diagram represents logical frames which for mode IV are half the length of the transmission frames (see section 2.2.2).

The first operation shown in the diagram is the differential detection. This can be performed on a symbol by symbol basis as the outputs from the DFT become available. The next step is frequency de-interleaving of the differential detector soft outputs. This can also be performed on a symbol by symbol basis. Next it is necessary to perform the time de-interleaving. This operation must be delayed for 16 frames because of the time interleaver latency. Viterbi decoding can then be performed on a frame of soft de-interleaved data. The fourth row of figure 6-1 shows the 15^{th} de-interleaved, decoded data frame being the first one available with valid data for subsequent processing. Furthermore, this frame is not available until the interleaved frame containing data from frames 15-30 has been differentially demodulated. The dependency of this frame on the previous 16 frames of differential detector output is shown by arrows on the diagram. This completes the processing necessary for the first receiver iteration.

Notice that in the receiver block diagram of figure 4-2, a Viterbi decoder followed by a sequence re-encoder is shown. The re-encoding process is not discussed here because the Viterbi decoder on all but the last iteration of the receiver can be designed to output the maximum likelihood decoded codeword rather than the decoded information sequence. This is done simply by saving the input trellis branch labels rather than the output branch labels.

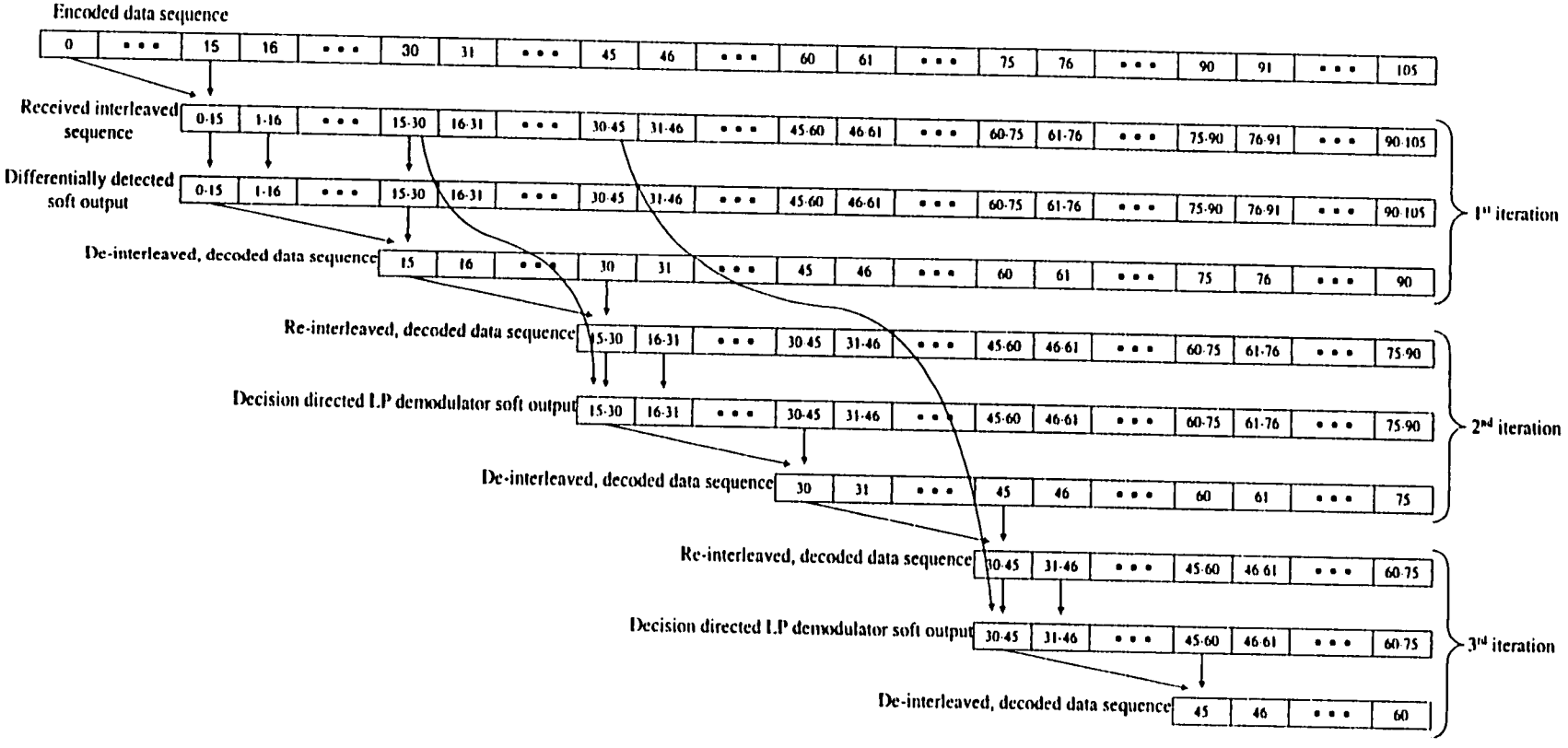

Figure 6-1 Diagram showing timing for 3 iteration receiver.

Before the corrected sequence can be used in the decision directed linear prediction detector it must be re-interleaved. This operation is depicted in figure 6-1 along with the associated delay. The first complete reinterleaved, corrected frame of data is available 31 frames after the receiver starts and it contains data from frames 15-30 of the encoded data sequence. The next operation is the decision directed linear predictive detector using the re-interleaved decoded data sequence for the decisions. This operates on the soft output of the DFT containing data from the same frames 15-30 of the encoded sequence. However, this frame arrived at the receiver 16 frames before. This illustrates a disadvantage of the iterative algorithm. Each successive iteration entails a cumulative delay equal to the interleaver depth and also requires a buffering of the input data equal to the interleaver depth.

The remaining steps of the algorithm are essentially a repetition of the steps after the differential demodulation in the first iteration. Notice that on the third iteration, the re-interleaved, decoded data sequence does not have valid data until 60 frames after the first received frame. This frame is then used for the decision directed LP detector but it is required to operate on the DFT output that arrived 31 frames before. Thus one sees that the receiver latency and buffer requirements are indeed increasing with more iterations. Simulations have shown that only marginal improvements in BER are obtained by going to more than three iterations of the algorithm. Consequently figure 6-1 shows only three iterations of the algorithm.

6.1.2 Receiver timing

The iterative receiver described in this thesis requires more than three times as many processing steps as a conventional differential detector based receiver. One would like to assess the feasibility of performing the additional processing in the allotted time with currently available technology. It is assumed that the receiver demodulates all of the DAB data. In an actual receiver, this would not always be necessary as several audio programs are multiplexed onto the COFDM signal. There are 75 OFDM data symbols in a mode IV transmission frame. There are 768 subcarriers and one frame is 48 ms in duration. This works out to a throughput requirement of 1.2 mega-symbols per second or 0.833 μs of processing time allowable for each symbol.

In the following, only the baseband processing steps are considered. It is assumed that there is a receiver front end that outputs samples of the real and imaginary samples of the lowpass equivalent received signal. This front end would have to perform the functions of down-conversion, synchronous quadrature demodulation and sampling of the in-phase and quadrature signals. In an actual system, it would require some feedback from the baseband processor to adjust for carrier shifts and symbol timing.

The operations necessary for a three iteration receiver are summarized in table 6-1. Each row of the table contains an estimate of the number of processing steps necessary to perform the operation on one QPSK symbol which is equivalent to one information bit (assuming a convolutional code rate of 1/2).

The estimated number of complex multiply-adds for the DFT is calculated assuming that a 1024 point FFT is used to extract the 768 subcarrier data symbols. On one particular DSP processor, a radix 2 FFT butterfly takes 11 instructions [37]. An N point FFT requires $(N/2)\log_2 N$ butterflies. This works out to about 80 instructions per symbol.

The differential detector can be performed with a minimum amount of processing: 2 loads and 2 stores plus a complex multiply – around 10 instructions per symbol.

The LP detector requires more processing steps than a CDD. It is assumed that the necessary predictor coefficients are stored in a lookup table that is indexed by the receiver's estimate of the Doppler spread. This avoids the substantial processing associated with matrix inversion or the less complex but still significant processing required by any adaptive filtering technique to adjust predictor coefficients. Also since the computer simulations showed that using more than one subchannel in the linear predictor did not have a beneficial effect, the complexity estimation assumes a one subchannel linear predictor implying that the predictor coefficients are real. The calculations required for the LP detector of order N are as follows.

- Compute the predicted subchannel gain. This is a FIR filtering operation on the real and imaginary parts of the previous channel gain decisions and should take about $2N$ instructions.

- Rotate the received sample by the angle of the predicted channel gain. This requires:
  - normalizing the predicted channel gain which should be done by a procedure that avoids divide and square root operations. Probably a table lookup would be accurate enough. About 10 instructions.
  - loading the current received value – 2 instructions.
  - multiplying by the conjugate of the normalized predicted channel gain – 6 instructions
- Rotate this result by the previous decision – 6 instructions
- Multiply by the previous received magnitude and store the results – 4 instructions
- Calculate the current channel estimate
  - load the current decision and convert to 4-DPSK – 10 instructions
  - multiply the current received value by the conjugate of the current decision – 6 instructions
  - store the current channel estimate – 2 instructions
- Calculate the current received magnitude – 2 instructions

Based on the above, the linear predictive receiver should take about 60 instructions per symbol for a predictor of order N=5.

The most time consuming operation is the Viterbi decoding. Based on the benchmarks given in [17] it would take about 200 instructions on a modern DSP processor to decode one symbol.

The de-interleaving and interleaving processing steps consist of data moves plus several instructions to compute the address offsets. This should require no more than 10 operations per symbol.

From the table, one sees that a total of 910 instructions on a DSP microcomputer would be required to produce one demodulated symbol. This estimate would vary somewhat depending on actual algorithm parameters used. For example, changing the predictor order by ΔN would add approximately $4\Delta N$ instructions. This is almost inconsequential compared to the total number of instructions. A rough estimate of the processing requirement is therefore 910 instructions/symbol $\times$ 1.2 Msymbol/s $\approx$ 1100 MIPS. This is achievable with the latest in DSP microcomputer

technology, however, the prices of these devices are currently fairly high (>$100 US per unit)

Receiver operation	Estimated number of instructions per symbol	Number of repetitions	Total instructions per symbol
Fast Fourier Transform	80	1	80
Differential detector	10	1	10
Frequency de-interleave	10	3	30
Time de-interleave	10	3	30
Viterbi decoder	200	3	600
Time re-interleave	10	2	20
Frequency re-interleave	10	2	20
Linear predictive detector	60	2	120
			Total = 910

Table 6-1 Estimated number of DSP microcomputer instructions required to implement the iterative LP receiver.

6.1.3 Memory requirement

The largest receiver memory requirement comes from the need to buffer large amounts of data due to the time interleaving latency. One frame of interleaved data contains bits from the previous 16 frames of the encoded sequence and therefore it is necessary to buffer 16 frames of interleaved data to produce one frame of de-interleaved data. For soft outputs it is assumed that one byte (8 bits) provides sufficient resolution. Studies have shown [36] that soft outputs of a CDD need only 4 bits of resolution for input to a Viterbi decoder so this is considered to be a safe assumption. One logical frame of data contains 56.25 kbits so the storage requirement for 1 frame of soft data is m_s=56.25 kbytes and for one frame of hard data is m_h=7.04 kbytes. The memory requirements are summarized in table 6-2. The total memory requirement is $83m_s+35m_h$ $\approx$ 5 Mbytes. Additional memory would be required for other functions but these should not take

more than 100 kbytes.

Data	Number of frames stored	Memory requirement
DFT output	32	$32m_s$
Differential detector soft output	16	$16\ m_s$
De-interleaved soft CDD output	1	m_s
First decoded hard output	16	$16m_h$
First re-interleaved hard output	1	m_h
First LP detector soft output	16	$16m_s$
First de-interleaved soft LP detector output	1	m_s
Second decoded hard output	16	$16m_h$
Second re-interleaved hard output	1	m_h
Second LP detector soft output	16	$16m_s$
Second de-interleaved soft LP detector output	1	m_s
Final decoded hard output	1	m_h

Table 6-2 Summary of memory requirements for iterative receiver.

6.2 Effect of Fast Information Channel

In section 2.2.2 it was indicated that the actual mode IV transmission frame included a Fast Information Channel (FIC) which is not time interleaved. The 77 OFDM symbols in the transmission frame actually consist of a null symbol followed by a reference symbol followed by 3 FIC symbols followed by 72 audio data symbols. The FIC is used to allow the receiver immediate access to multiplexing information about the audio programs in the following data symbols. To compensate for the loss in time diversity in the FIC, the data are protected with a

rate 1/3 convolutional code and include a cyclic redundancy code (CRC) frame check sequence (FCS). In this thesis, we have not simulated a COFDM system that includes the FIC symbols.

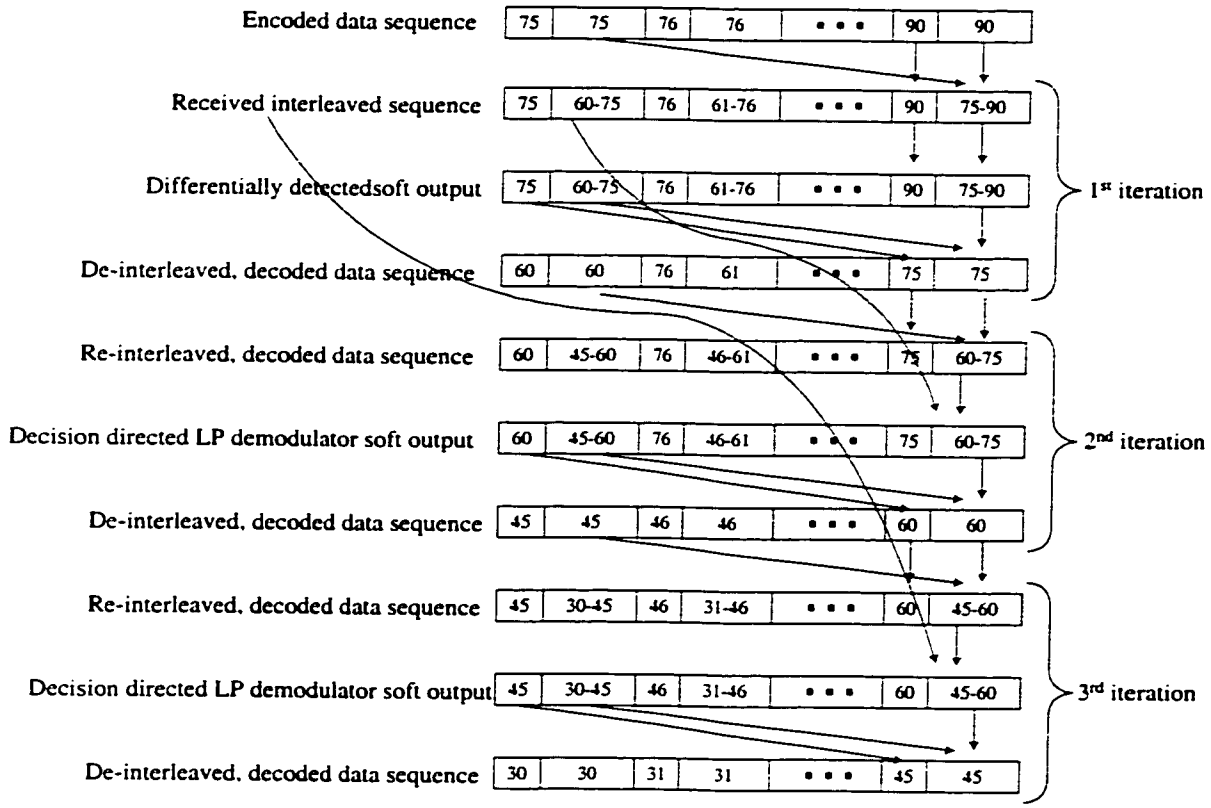

Figure 6-2 Modifications to receiver timing with FIC symbols.

The receiver can still operate in the presence of the FIC symbols. Figure 6-2 depicts the timing modification to the iterative decision directed LP receiver necessitated by the FIC. In this diagram, each frame is now split into a FIC and a data portion. The time de-interleaving and re-interleaving operations now need only be performed on the data portion of each frame.

The FIC data could still be used by the receiver after the first iteration. It would possibly have a relatively high error rate at this point, but any errors could be detected with high probability using the FCS and the receiver could wait for the reception of an error free frame before acting on the data. The primary purpose of the FIC data in higher algorithm iterations would be to provide the corrected symbols necessary to form the linear prediction of the subchannel gain for

the first few audio data symbols following the FIC symbols.

6.3 Conclusion

The iterative decision directed LP receiver entails a significant increase in complexity over a standard CDD based receiver. Rough complexity estimates are that the receiver would require a DSP microcomputer operating at 1100 MIPS to do the computations and that 5 Mbytes of memory would be required for buffering of the signals. This estimate includes the receiver operations from the FFT demodulation through the Viterbi decoding but does not include the decoding of the compressed audio signal and any further DSP operations required by this signal.

The iterative receiver also has the property of adding an additional delay equal to the interleaving latency of 384 ms for each additional iteration of the algorithm. Since 3 algorithm iterations is sufficient to achieve the required BER, there would be slightly more than one second of delay. This is not considered a severe problem for broadcasting applications.

7

Conclusion

7.1 Thesis Summary

The investigation described herein had the objective of developing a demodulation technique that would improve the performance of a digital audio broadcast (DAB) receiver in fast fading conditions. This investigation was accomplished by:

- studying the COFDM modulation technique used for the DAB signal,
- analyzing the transmission of the DAB signal through a mobile wireless channel model appropriate for propagation in a typical urban environment,
- studying published techniques for demodulation in fast fading conditions, and finally,
- proposing and simulating a COFDM receiver design.

The simulation results were encouraging so a complexity analysis of the proposed receiver

design was also performed to determine its practicality.

The receiver design is based on a decision directed linear predictive (LP) detector for the 4-DPSK signaling technique used by DAB. This detector is used with decoded decisions derived in an iterative fashion. It is shown that the proposed receiver structure provides a significant improvement over the BER performance of differential detector based receivers.

7.2 Thesis Contribution

It has been shown that a receiver based on conventional differential detection of the DPSK signal used for DAB cannot meet the bit error rate criterion of 10^{-4} at vehicle speeds exceeding 92 km/hr for mode IV operation in a typical urban propagation environment with signal to noise E_b/N_0 = 20 dB. Computer simulations have indicated that the proposed iterative decision directed LP receiver can extend this limit to 144 km/hr under the same conditions. This receiver design has not previously been applied to COFDM detection.

To operate effectively, the receiver requires an estimate of the channel Doppler spread but is relatively insensitive to errors in this estimation. In fact, the receiver can be designed for the maximum required vehicle velocity and its performance is still satisfactory at lower velocities but deteriorates rapidly at higher velocities.

The receiver design is based on an assumption of a particular propagation model. It has not been determined how well the design will perform if the actual propagation environment does not match this model. One step that could potentially deal with this is do adopt an adaptive filtering technique that would allow the receiver parameters to be recursively updated based on observations of the received signal. This was discussed briefly but not simulated in this thesis.

The proposed receiver design that achieves this reliability improvement is somewhat more complex than the standard differential detector based receiver. The standard receiver requires differential detection, de-interleaving and Viterbi decoding. The proposed design requires one iteration with the same processing as the standard receiver, then two subsequent iterations consisting of re-interleaving, decision directed LP detection, de-interleaving and decoding. It is

estimated that this design would require 1100 MIPS on a DSP microcomputer and approximately 5 Mbytes of memory. This is a significant processing load, probably requiring some operations to be implemented in hardware ASICs. Another effect is an additional delay equal to the interleaver latency for each algorithm iteration. This resulting delay of over 1 second is not critical for the broadcast application.

Other possible receiver designs that could potentially be useful for fast fading conditions but were not simulated here are a maximum likelihood sequence detector and an iterative soft decision feedback structure (turbo receiver). However, it is expected that the turbo receiver will only provide a marginal improvement in performance over the other feasible techniques. A technique based on a series expansion of the fading process (double filtering) was studied and found inappropriate for COFDM demodulation.

The channel model used in this study consists of a superposition of M independent propagation paths, each having a randomly determined delay and Doppler shift. Analysis shows that its spaced-frequency spaced-time correlation function matches ideal characteristics for isotropic reception and an exponentially decaying delay spread. Furthermore, as the number of paths becomes large, the time averaged correlation function for the channel model approaches the ensemble average. This is desirable since computer simulations must operate on a single realization of the channel model at a time. The computer implementation of the M path summation is also quite straightforward.

7.3 Future Work

The iterative decision directed LP receiver was simulated using a realistic channel model for a typical urban propagation environment. The results reported here are encouraging but it should be noted that they were observed over a relatively limited range of channel conditions. Some suggestions for future work are:

- Study the effects of varying the channel delay spread profile including the effects of multiple active echoes resulting from multiple transmission antennas.

- Study the effects of different channel models such as hilly and rural terrain.

- Study the effects of the fast information channel symbols. Based on the discussion in chapter 6, it is believed that the proposed receiver design could operate successfully when these symbols are included in the model. However, this needs to be verified by computer simulations.

- Run the simulations on field measured received signals.

If the further simulations listed above yield good results, the proposed receiver design should be considered as a candidate for a working mode IV DAB receiver. If its relative merits compared to other candidate designs appear superior, and if the market warrants, development of a working prototype should follow.

Appendices

A. DFT OF A WHITE GAUSSIAN PROCESS

Let $x_\nu[n]$ n=0, 1, ..., N-1 be the N samples of a complex, zero mean, wide sense stationary, discrete white Gaussian process in symbol interval ν. The DFT of this process is[1]

$$X_\nu[k] = \frac{1}{N}\sum_{n=0}^{N-1} x_\nu[n] e^{-j2\pi\frac{nk}{N}} \quad k = 0, 1, 2, \cdots, N-1 \tag{A.1}$$

which will also be a Gaussian process. The mean of the transformed process is

$$\begin{aligned} \eta = E\{X_\nu[k]\} &= E\left\{\frac{1}{N}\sum_{n=0}^{N-1} x_\nu[n] e^{-j2\pi\frac{nk}{N}}\right\} \\ &= \frac{1}{N} e^{-j2\pi\frac{nk}{N}} \sum_{n=0}^{N-1} E\{x_\nu[n]\} = 0 \end{aligned} \tag{A.2}$$

Also the autocorrelation of the transformed process is given by

[1] Here we multiply by the factor 1/N in the DFT rather than in the inverse DFT as is usually done.

$$R_X[\nu,\lambda,k,l] = E\{X_\nu[k]X_\lambda[l]\} = E\left\{\left(\frac{1}{N}\sum_{n=0}^{N-1}x_\nu[n]e^{-j2\pi\frac{nk}{N}}\right)\left(\frac{1}{N}\sum_{m=0}^{N-1}x_\lambda^*[m]e^{j2\pi\frac{ml}{N}}\right)\right\} \qquad (A.3)$$
$$= \frac{1}{N^2}\sum_{n=0}^{N-1}\sum_{m=0}^{N-1}e^{-j2\pi\frac{nk-lm}{N}}E\{x_\nu[n]x_\lambda^*[m]\}$$

Since the noise is white and the symbol intervals do not overlap, the expectation in the sum above is non-zero only when $\nu=\lambda$ and $n=m$. Consequently

$$E\{X_\nu[k]X_\nu[l]\} = \frac{1}{N^2}\sum_{n=0}^{N-1}e^{-j2\pi\frac{(k-l)n}{N}}E\{|x_\nu[n]|^2\}$$
$$= \frac{1}{N^2}E\{|x_\nu[n]|^2\}\sum_{n=0}^{N-1}e^{-j2\pi\frac{(k-l)n}{N}} \qquad (A.4)$$

The summation in the above is equal to

$$\frac{1-e^{-j2\pi(k-l)}}{1-e^{-j2\pi\frac{k-l}{N}}} = \begin{cases} N & k=l \\ 0 & k\neq l \end{cases} \qquad (A.5)$$

Therefore

$$R_X[\nu,\lambda,k,l] = E\{X_\nu[k]X_\lambda[l]\} = \frac{1}{N}E\{|x_\nu[n]|^2\}\delta_{\nu,\lambda}\delta_{k,l} \qquad (A.6)$$

This indicates that the N outputs of the DFT will be uncorrelated Gaussian random variables. There is also no correlation between DFT outputs from subsequent symbol intervals.

B. Calculation of Channel Correlation Function

The time variant transfer function for one path of the channel model is given by (3.27)

$$H(\omega,t) = e^{-j\Phi} e^{j\Omega t} e^{-j\omega T} \tag{B.1}$$

where $\Omega = 2\pi F$ and $\omega = 2\pi f$. The random variables F and T have density functions defined by (3.25) and (3.26) and Φ is uniformly distributed between $-\pi$ and π. For brevity, the subscript i indicating i^{th} path and the factor $1/\sqrt{M}$ will not be used in this development. The random variables Φ, Ω and T are independent. The real and imaginary parts of $H(\omega, t)$ are given by

$$\begin{aligned} X(\omega,t) &= \cos\Phi\cos\Omega t\cos\omega T + \cos\Phi\sin\Omega t\sin\omega T \\ &\quad - \sin\Phi\cos\Omega t\sin\omega T + \sin\Phi\sin\Omega t\cos\omega T \end{aligned} \tag{B.2}$$

$$\begin{aligned} Y(\omega,t) &= -\sin\Phi\sin\Omega t\sin\omega T - \sin\Phi\cos\Omega t\cos\omega T \\ &\quad + \cos\Phi\sin\Omega t\cos\omega T - \cos\Phi\cos\Omega t\sin\omega T \end{aligned} \tag{B.3}$$

The complex spaced-frequency spaced-time correlation function for the process is calculated as

$$\begin{aligned} R_H(\Delta\omega,\Delta t) &= E\{e^{j\Omega\Delta t}\}E\{e^{-j\Delta\omega T}\} \\ &= E\{\cos\Omega\Delta t\}E\{\cos\Delta\omega T\} - jE\{\cos\Omega\Delta t\}E\{\sin\Delta\omega T\} \\ &= \frac{J_0(\omega_d\Delta t)}{1+j\Delta\omega\sigma_d} \end{aligned} \tag{B.4}$$

The spaced-frequency spaced-time correlation function for the real part of the process is

$$R_X(\Delta\omega,\Delta t) = E\{X(\omega+\Delta\omega,t+\Delta t)X(\omega,t)\} \tag{B.5}$$

Substituting (B.2) into this and doing the necessary algebraic manipulation results in

$$R_X(\Delta\omega,\Delta t) = \frac{1}{2}E\{\cos\Omega\Delta t\}E\{\cos\Delta\omega T\} \tag{B.6}$$

A similar calculation for the spaced-frequency spaced-time cross correlation function between the real and imaginary parts of the process results in

$$R_{XY}(\Delta\omega,\Delta t) = \frac{1}{2}E\{\cos\Omega\Delta t\}E\{\sin\Delta\omega T\} \tag{B.7}$$

For any stationary complex process $H(\omega, t)$ one can show that

$$R_H(\Delta\omega,\Delta t) = R_X(\Delta\omega,\Delta t) + R_Y(\Delta\omega,\Delta t) - j\left(R_{XY}(\Delta\omega,\Delta t) - R_{YX}(\Delta\omega,\Delta t)\right) \tag{B.8}$$

From this combined with (B.4), (B.6) and (B.7) it can be deduced that

$$R_X(\Delta\omega,\Delta t) = R_Y(\Delta\omega,\Delta t) = \frac{1}{2}\frac{J_0(\omega_d\Delta t)}{1+(\Delta\omega\sigma_d)^2} \tag{B.9}$$

and

$$R_{XY}(\Delta\omega,\Delta t) = -R_{YX}(\Delta\omega,\Delta t) = \frac{1}{2}\frac{J_0(\omega_d\Delta t)\Delta\omega\sigma_d}{1+(\Delta\omega\sigma_d)^2} \tag{B.10}$$

If the factor $1/\sqrt{M}$ was included in the development, the correlation functions would be the same as above but multiplied by a factor of $1/M$. If M independent paths were then summed, the correlation functions for the resulting channel would be as shown above and the process would become Gaussian for large enough M. For a Gaussian process, the properties (B.9) and (B.10) are important because they allow one to write any finite order density function for the complex process knowing only the complex spaced-frequency spaced-time correlation function $R_H(\Delta\omega,\Delta t)$. This is not in general possible without knowing the four correlation functions for the real and imaginary parts of the random variable [27]. From (B.10) it is also evident that the real and imaginary parts of the channel function are independent for $\Delta\omega = 0$.

C. MATLAB SIMULATION ROUTINES

Three sets of simulation routines were written. The first simulates only the linear predictive detector. The second simulates a generic COFDM system that doesn't use a null or reference symbol and the third simulates a COFDM system that inserts a null and reference symbol every 77^{th} transmitted OFDM symbol. The COFDM simulations use a commercially available codec software package [39]. A rate 1/2 code is used for all of the simulations.

This appendix contains a brief description of the Matlab routines used in the simulations. More detailed documentation for each routine is contained in the comments which can be observed either by editing the file or by typing "help filename" from the Matlab command window.

All simulations operate in a non-real time mode where a number of operations are performed on all of the input data and intermediate results are stored on disk. There is a separate disk file for each transmission frame of data. The data file naming follows the following convention

filename.?xx

where "?" is a letter indicating the type of data in the file and "xx" is a two digit tag indicating the frame number. Frame numbering starts at 00. Data files contain either hard or soft data. For hard data, the bit stream is segmented into 16-bit words. These are converted to 16-bit unsigned integers and then stored in 16-bit unsigned integer format. Soft data are stored in Matlab float 32 format. Table C-1 indicates the letter designation for the various data file types. Simulation results are stored in the \results subdirectory in *.mat files. The format and naming of the result files varies and is detailed in the comments for each particular program.

The following sections provide a brief description of the routines used in the three simulations. Routine descriptions are indented to indicate that they are called by the routine described above with one less level of indentation.

File	Description	Data type
i	The information sequence input to the simulation	Hard
c	The convolutionally encoded data sequence	Hard
n	The interleaved, encoded data sequence	Hard
r	The channel output	Soft
w	The channel output with AWGN added	Soft
f	Soft detector output (either CDD of LP detector)	Soft
e	Hard detector output (either CDD of LP detector)	Hard
g	De-interleaved soft detector output	Soft
u	Viterbi decoded output sequence	Hard
v	Recoded output sequence	Hard
o	Re-interleaved, recoded output sequence	Hard

Table C-1 Letter designation used for simulation data files.

C.1 Linear predictive detector

All of the m-files should be loaded in the same directory and this directory should be the current directory. Subdirectories named "data" and "results" must exist to store the data and result files.

transmit.m This routine creates a series of binary data files that are used as input to the simulation.

rx_lp.m This is the main routine that does the linear predictive detector simulation.

chan.m This routine performs the OFDM modulation and demodulation and passes the data through the *M*-path channel model. The real and imaginary parts of the received values are stored on disk.

del_val.m Returns *M* random delay values to be used in the channel model. The delays are integer values that indicate the delay in sample intervals.

fdop.m Returns *M* random Doppler frequency shift values to be used in the channel model.

int2bin.m Used to convert the input data from 16-bit unsigned integer format to binary format.

gen_ofdm.m Generates the OFDM signal for one symbol interval.

mpath.m Passes the OFDM signal for one symbol interval through the M-path channel model.

demod.m Demodulates the OFDM signal after it has been passed through the channel model.

lmmse_fb.m This routine does the decision feedback linear predictive detection on the received data files.

plot_cor.m Calculates the linear predictor coefficients.

bin2int.m Converts the binary detected bits to 16-bit unsigned integer format prior to saving the results.

lmmse_fb_cor.m This routine simulates the LP detector for the ideal case when there are no fed back errors.

ber_count.m Counts the number of bit errors by comparing a series of result files to a series of input files. Also returns BER computed as the number of errors divided by the total number of bits.

C.2 Generic COFDM system

All of the m-files should be loaded in the same directory and this directory should be the current directory. Subdirectories named "data" and "results" should exist to store the data and result files.

transmit.m This routine creates a series of data files that are the information bits for the simulation. It also encodes these information bits and interleaves them.

ncode.m Creates the information bits and encodes them. Information and encoded bits are saved in a series of data files.

bin2int.m Converts the binary bits to 16-bit unsigned integer format prior to

saving the results.

vcmexenc.m Does convolutional encoding of information sequence. This is a commercially available routine [39].

intlv.m Does time and frequency interleaving on the encoded data.

int2bin.m Used to convert the input data from 16-bit unsigned integer format to binary format.

rx_soft_nc.m This is the main program for the iterative receiver simulation.

chan.m This routine performs the OFDM modulation and demodulation and passes the data through the *M*-path channel model. The real and imaginary parts of the received values are stored on disk.

del_val.m Returns *M* random delay values to be used in the channel model. The delays are integer values that indicate the delay in sample intervals.

fdop.m Returns *M* random Doppler frequency shift values to be used in the channel model.

gen_ofdm.m Generates the OFDM signal for one symbol interval.

mpath.m Passes the OFDM signal for one symbol interval through the M-path channel model.

demod.m Demodulates the OFDM signal after it has been passed through the channel model.

dif_det.m Performs differential detection on the received data for the first algorithm iteration. Saves soft and hard decision data.

ber_count.m Counts the number of bit errors by comparing a series of result files to a series of input files. Also returns BER computed as the number of errors divided by the total number of bits.

de_intlv.m De-interleaves the soft decision data from the differential detector or the LP detector.

dcode.m Does Viterbi decoding on the de-interleaved soft data.

vcmexdec.m . Does the Viterbi decoding. This is a commercially available routine

[39].

recode.m Re-encodes the Viterbi decoded sequence.

re_intlv.m Re-interleaves the re-encoded sequence.

lmmse_fb.m Performs the decision directed LP detection of the received data using the decoded data sequence. Outputs both soft and hard decisions.

plot_cor.m Calculates the linear predictor coefficients.

C.3 Practical COFDM system

All of the m-files should be loaded in the same directory and this directory should be the current directory. Subdirectories named "data" and "results" should exist to store the data and result files.

Most of the routines for this simulation have the same names as for the simulation of the generic system. Many of the routines are exactly the same. Chan.m is modified to insert a null and reference symbol. Dif_det.m is modified to work with the null and reference symbol. lmmse_fb.m is replaced with lp_01.m which uses predictors optimized for the existence of the null symbol.

transmit.m This routine creates a series of data files that are the information bits for the simulation. It also encodes these information bits and interleaves them.

ncode.m Creates the information bits and encodes them. Information and encoded bits are saved in a series of data files.

bin2int.m Converts the binary bits to 16-bit unsigned integer format prior to saving the results.

vcmexenc.m Does convolutional encoding of information sequence. This is a commercially available routine [39].

intlv.m Does time and frequency interleaving on the encoded data.

int2bin.m Used to convert the input data from 16-bit unsigned integer format to binary format.

rx_soft_nc.m This is the main program for the iterative receiver simulation.

chan.m This routine performs the OFDM modulation and demodulation and passes the data through the M-path channel model. The real and imaginary parts of the received values are stored on disk.

del_val.m Returns M random delay values to be used in the channel model. The delays are integer values that indicate the delay in sample intervals.

fdop.m Returns M random Doppler frequency shift values to be used in the channel model.

gen_ofdm.m Generates the OFDM signal for one symbol interval.

mpath.m Passes the OFDM signal for one symbol interval through the M-path channel model.

demod.m Demodulates the OFDM signal after it has been passed through the channel model.

dif_det.m Performs differential detection on the received data for the first algorithm iteration. Saves soft and hard decision data.

ber_count.m Counts the number of bit errors by comparing a series of result files to a series of input files. Also returns BER computed as the number of errors divided by the total number of bits.

de_intlv.m De-interleaves the soft decision data from the differential detector or the LP detector.

dcode.m Does Viterbi decoding on the de-interleaved soft data.

vcmexdec.m . Does the Viterbi decoding. This is a commercially available routine [39].

recode.m Re-encodes the Viterbi decoded sequence.

re_intlv.m Re-interleaves the re-encoded sequence.

lp_01.m Performs the decision directed LP detection of the received data using the decoded data sequence. This function does linear prediction based on only one subchannel. It also uses linear predictors that are optimum in the presence of the null symbol. Outputs both soft and hard decisions.

lp_coef_01.m Calculates the optimum linear predictor coefficients taking into

account the presence of the null symbol.

delrc.m Deletes a row and column from a matrix.

References

[1] L.R. Bahl, J. Cocke, F. Jelinek, J. Raviv, "Optimal Decoding of Linear Codes for Minimizing Symbol Error Rate", *IEEE Transactions on Information Theory*, 20(2), 284-287, March 1974.

[2] P.A. Bello, "Characterization of randomly time-variant linear channels", *IEEE Transactions on Communication Systems*, 11(4), 360-393, December 1963.

[3] J.A.C. Bingham, "Multicarrier Modulation for Data Transmission: An Idea Whose Time Has Come", *IEEE Communications Magazine*, 5-14, May 1990.

[4] R.W. Chang, "Synthesis of Band-Limited Orthogonal Signals for Multichannel Data Transmission", *Bell System Technical Journal*, 45, 1775-1796, December 1966.

[5] COST 207 Report, Digital Land Mobile Radio Communications, Commission of European Communities, Directorate General, Telecommunications, Information Industries and Innovation, Luxembourg, 1989.

[6] W.C. Dam, D.P. Taylor, "An Adaptive Maximum Likelihood Receiver for Correlated Rayleigh-Fading Channels" *IEEE Transactions on Communications*, 42(9), 2684-2692, September 1994.

[7] T. de Couason, R. Monnier, and J.B. Rault, "OFDM for digital TV broadcasting", *Signal Processing*, 39, 1-32, September 1994.

[8] European Telecommunications Standards Institute, "Radio broadcasting systems; Digital Audio Broadcasting (DAB) to mobile, portable and fixed receivers", ETS 300 401, Second Edition, June 1996.

[9] P.K. Frenger, A. Svensson, "Decision-Directed Coherent Detection in Multicarrier Systems on Rayleigh Fading Channels", *IEEE Transaction on Vehicular Technology*, 48(2), 490-

498, March 1999.

[10] M.J Gertsman, J.H. Lodge, "Symbol-by-Symbol MAP Demodulation of CPM and PSK Signals on Rayleigh Flat-Fading Channels", *IEEE Transactions on Communications*, 45(7), 788-799, July 1997.

[11] G.H. Golub, C.F. Van Loan, *Matrix Computations*, The Johns Hopkins University Press, 1983

[12] T. Grusec, L. Thibault, "MUSICAM Listening Tests Report", *CRC Report CRC-RP-91.001*, Communications Research Center, Ottawa, Canada, 1991.

[13] J. Hagenauer, "Rate-Compatible Punctured Convolutional Codes (RCPC Codes) and their Applications", *IEEE Transactions on Communications*, 36(4), 389-400, April 1988.

[14] J. Hagenauer, N. Seshadri, C.W. Sundberg "The Performance of Rate-Compatible Punctured Convolutional Codes for Digital Mobile Radio", *IEEE Transactions on Communications*, 38(7), 389-400, July 1990.

[15] S. Haykin, *Adaptive Filtering*, Third Edition, Prentice Hall, New Jersey, 1996.

[16] C. Heegard, S.B. Wicker, *Turbo Coding*, Kluwer Academic Publishers, Massachusetts, 1999.

[17] H. Hendrix, "Viterbi Decoding Techniques in the TMS320C54x Family", *Texas Instruments Application Note SPRA071*, June 1996.

[18] P. Ho, D. Fung, "Error Performance of Multiple-Symbol Differential Detection of PSK Signals Transmitted Over Correlated Rayleigh Fading Channels", *IEEE Transactions on Communications*, 40(10), 1566-1569, October 1992.

[19] P. Hoeher, J. Lodge, "Turbo DPSK: Iterative Differential PSK Demodulation and Channel Decoding", *IEEE Transactions on Communications*, 47(6), 837-843, June 1999.

[20] M.C. Jeruchim, P. Balaban, K.S. Shanmugan, *Simulation of Communication Systems*, Plenum Press, New York, 1992.

[21] R.S. Kennedy, *Fading Dispersive Communication Channels*, John Wiley and Sons, New York, 1969.

[22] B. Le Floch, M. Alard, C. Berrou, "Coded orthogonal frequency division multiplex", *Proceedings of the IEEE*, 83(6), 982-997, June 1995.

[23] J.H. Lodge, M.L. Moher, "Maximum Likelihood Sequence Estimation of CPM Signals Transmitted Over Rayleigh Flat-Fading Channels", *IEEE Transactions on Communications*, 38(6), 787-794, June 1990.

[24] H. Ma, J. Wolf, "On Tail Biting Convolutional Codes", *IEEE Transactions on Communications*, 34(2), 104-111, 1986.

[25] *Matlab*, The MathWorks Inc., 1998.

[26] A. Neul, "Bit error rate for 4-DPSK in fast Rician fading and Gaussian noise", *IEEE Transactions on Communications*, 37(12), 1385-1387, December 1989.

[27] A. Papoulis, *Probability, Random Variables, and Stochastic Processes*, Third Edition, McGraw Hill Inc., New York, 1991.

[28] J.G. Proakis, *Digital Communications*, Third Edition, New York: McGraw-Hill, 1995.

[29] C. Reiners, H. Rohling, "Multicarrier transmission technique in cellular mobile communications system", *Proceedings of the 44th Vehicular Technology Conference (VTC'94)*, 1660-1664, June 8-10, 1994, Stockholm, Sweden.

[30] B.R. Saltzberg, "Performance of an Efficient Parallel Data Transmission System", *IEEE Transactions on Communication Technology*, 15(6), 805-811, December 1967.

[31] K. Shenoi, *Digital Signal Processing in Telecommunications*, Prentice Hall, New Jersey,

1995.

[32] S.B. Slimane, "OFDM Schemes with Non-Overlapping Time Waveforms", *Proceedings of the 48th Vehicular Technology Conference (VTC'98)*, 2067-2071, May 18-21, 1998, Ottawa, Canada.

[33] G.L. Stuber, *Principles of Mobile Communication*, Kluiver Academic Publishers, Boston, 1996.

[34] A. Svensson, "1 and 2 Stage Decision Feedback Coherent Detectors for DQPSK in Fading Channels", *Proceedings of the 45th Vehicular Technology Conference (VTC'95)*, 644-648, July 1995, Chicago, USA.

[35] A. Svensson, "Coherent detector based on linear prediction and decision feedback for DQPSK", *Electronics Letters*, 30(20), 1642-1643, September 1994.

[36] L. Thibault, M.T. Le, "Performance evaluation of COFDM for digital audio broadcasting Part I: Parametric study", *IEEE Transactions on Broadcasting*, 43(1), 64-75, March 1997.

[37] *TMS320C54x DSP Reference Set, Volume 4: Applications Guide*, Texas Instruments, October 1996.

[38] M. Visintin, "A simple DPSK Receiver with improved asymptotic performance over fast Rayleigh-fading channels", *IEEE Communications Letters*, 1(4), 99-101, July 1997.

[39] *Viterbi Codec Library*, Communications Research Center (CRC), Ottawa, Canada, 1998.

[40] G.M. Vitetta, U. Mengali, D.P. Taylor, "Differential detection of PSK signals transmitted over linearly time-selective Rayleigh fading channels", *1998 International Conference on Communication (ICC '98)*, 433-437, June 1998, Atlanta, USA.

[41] G.M. Vitetta, D.P. Taylor, "Maximum Likelihood Detection of Differentially Encoded PSK Signals Transmitted over Rayleigh Frequency-Flat Fading Channels", *1994 International*

Conference on Communication (ICC'94), 1889-1893, New Orleans, USA.

[42] G.M. Vitetta, D.P. Taylor, "Maximum Likelihood Decoding of Uncoded and Coded PSK Signal Sequences Transmitted over Rayleigh Flat-Fading Channels", *IEEE Transactions on Communications*, 43(11), 2750-2758, November 1995.

[43] G.M. Vitetta, D.P. Taylor, U. Mengali, "Double-filtering receivers for PSK signals transmitted over Rayleigh frequency-flat fading channels", *IEEE Transactions on Communications*, 44(6), 686-695, June 1996.

[44] S.B. Weinstein, P.M. Ebert, "Data Transmission by Frequency-Division Multiplexing Using the Discrete Fourier Transform", *IEEE Transactions on Communications Technology*, 19(5), 628-634, October 1971.

[45] M.D. Yacoub, *Foundations of Mobile Radio Engineering*, CRC Press Inc., Florida, 1993.